SCATTERING BY BURIED OBSTACLES

K. K. Mei, et al

California University

Prepared for:

Army Mobility Equipment Research and Development Center

November 1974

SCATTERING BY BURIED OBSTACLES

A Final Report Submitted to MERDC for Research

done on the period 20 April 1971 - 31 July 1974

Contract DAAK02-71-C-0206

Submitted by K. K. Mei
W. C. Kuo
S. K. Chang

November 1974

ELECTRONICS RESEARCH LABORATORY
College of Engineering
University of California, Berkeley

SCATTERING BY BURIED OBSTACLES

by

K. K. Mei, W. C. Kuo, and S. K. Chang

Final Report

November 1974

ELECTRONICS RESEARCH LABORATORY

College of Engineering
University of California, Berkeley
94720

TABLE OF CONTENTS

Introduction

The purpose of this investigation is to find theoretical solutions to scattering of electromagnetic fields by buried obstacles. The fields are generated by wire antennas above the ground and the buried obstacles may be either conductor or dielectric bodies. The effort of this investigation is divided into three major parts as follows:

(I) Wire antennas above the lossy ground

(II) Scattering by a buried wire conductor

(III) 2-dimensional scattering by dielectric bodies.

The first part of the investigation is primarily concerned with the source problem of the scattering phenomena. It enables us to find the near fields of an antenna above a lossy ground and the near fields penetration into the ground, which are the primary fields to be scattered by the obstacles. In order to study that problem the Sommerfeld's integrals are extensively studied. The integrals, which are part of the classical solution to the Green's function of Maxwell's equations involving lossy half space, are useful to our problem only if they can be computed economically. Hence, the first part of this investigation is the extensive search for techniques which speed up the convergence of Sommerfeld's integrals.

The second part of the investigation involves some practical application of the results of the first part which have direct bearing on the "detectability" of buried obstacles. It may answer some fundamental questions relating the input power of the primary source to the scattered fields from a buried obstacle back to the air.

The third part of the investigation contains the preliminary work of

scattering by buried dielectric obstacles. Since the final objective of this research is the detection of buried dielectric bodies, the technique of computing dielectric scattering is of primary importance. Unfortunately, there has been no such work reported in the open literatures in field theories. Hence, we have to undertake the investigation of the most basic work in dielectric scattering problem here. Our work on "Uni-moment method"[1] has advanced the computational methods to include scattering by dielectric bodies. The application of the "Uni-moment method" to 2-dimensional scattering problems is presented in this report. It has demonstrated that the "Uni-moment method" indeed solves many dielectric scattering problems which are hitherto unsolvable. The work reported in this investigation has layed the ground work for further study of scattering by buried dielectric bodies. The prospect of solving a problem which has been thought to be untouchable, is better than ever.

"This research was supported by the Mine Detection Division, Countermine/Counter Intrusion Department, U.S. Army Mobility Equipment Research and Development Center, and by the National Science Foundation."

PART ONE

WIRE ANTENNA ABOVE THE LOSSY GROUND

PART TWO

SCATTERING BY A BURIED WIRE CONDUCTOR

I. Field Integrals and Antenna Integral Equations

Elementary field theory states that the electric field due to an infinitesimal current element oriented in the z-direction is[2]

$$d\bar{E}(\bar{r}) = I(\bar{r}') \left[\frac{1}{j\omega \epsilon} \nabla \frac{\partial}{\partial z} G(\bar{r},\bar{r}') - j\omega\mu G(\bar{r},\bar{r}')\hat{z} \right] \frac{d\ell'}{4\pi} , \tag{1-1}$$

where $G(\bar{r},\bar{r}') = \dfrac{e^{-jk|\bar{r}-\bar{r}'|}}{|\bar{r}-\bar{r}'|}$ for the free space,

and $\bar{r}'$, $\bar{r}$ are the position vectors of the source and field respectively. Thus, the electric fields of a linear antenna of length L is the integral of eq. (1-1),

$$\bar{E}(\bar{r}) = \frac{1}{4\pi} \int_L \left[\frac{1}{j\omega \epsilon} \nabla \frac{\partial}{\partial z} G(\bar{r},\bar{r}') - j\omega\mu G(\bar{r},\bar{r}')\hat{z} \right] I(\bar{r}')d\ell' . \tag{1-2}$$

Therefore, when the current I(z) on a linear antenna is known it is only necessary to carry out the integral of eq. (1-2) to find the electric fields everywhere in space. The fundamental problem in antenna theory is to find the current due to a specific excitation.

Eq. (1-2) is an integral representation of the electric fields in terms of the current. If we let $\bar{r}$ approach to the conducting surface of the antenna, where the tangential electric field $E_z(\bar{r})$ is known, i.e.,

$$E_z(\bar{r}) = - E_z^{inc}(\bar{r}) , \tag{1-3}$$

where $E^{inc}(\bar{r})$ is the incident electric field, eq. (1-2) becomes

$$\int_L \left[\frac{\partial^2}{\partial z^2} G(\bar{r},\bar{r}') + k^2 G(\bar{r},\bar{r}') \right] I(\bar{r}')d\ell' = - j\omega \epsilon E_z^{inc}(z). \tag{1-4}$$

The above equation is an integro-differential equation from which the

current $I(z')$ may be found.[3] Eq. (1-4) represents an antenna problem if $E_z^{inc}(z)$ is a localized field such as that produced by a generator, and it represents a scattering problem if $E_z^{inc}(z)$ is an illuminating field such as a plane wave.

The above brief discussion is limited to linear antenna or scatterer in open uniform space, because $G(\bar{r},\bar{r}')$, as given, is the solution of the scalar wave equation in an infinite uniform space. The method is readily extended to antennas or scatterers in or above a lossy half-space if the Green's function is replaced by the solution of a scalar wave equation satisfying the boundary conditions of the lossy half-space. Such Green's functions are known as the Sommerfeld's integrals[4] represented by $s(\bar{r},\bar{r}')$. The details of derivations of the Sommerfeld's integrals may be found in reference [4] and given in Appendix A, so we shall not rederive the integrals here.

In principle all one has to do is to substitute the proper Sommerfeld's formula in place of $G(\bar{r},\bar{r}')$ in (1-4) in order to find the current on a vertical or horizontal linear antenna above a lossy half-space. Such applications result in immediate difficulties because Sommerfeld's integrals converge very slowly. For instance, in order to solve a practical antenna problem, the Green's function $G(\bar{r},\bar{r}')$ has to be evaluated for different values of $\bar{r}$ and $\bar{r}'$ at least a few hundred times. The evaluation of any one of the Sommerfeld's integrals will require seconds for each pair of values of $\bar{r}$ and $\bar{r}'$, if we use a conventional integration routine. Thus, the application of the integral equation is economically unfeasible, unless we can increase the speed of computation of Sommerfeld's integrals. In the following chapter, we shall discuss several methods of approximation of Sommerfeld's integrals for fast convergence.

II. Approximation of Sommerfeld's Integrals for Fast Convergence.

Sommerfeld's integrals, the Green's functions of Maxwell's equations satisfying the boundary conditions of lossy half-space, were first derived by A. Sommerfeld in 1909. These integrals have since been extensively studied by many scientists in search for the ground waves. In the application of Sommerfeld's integrals to study the antennas over lossy ground, we are not so much interested in the physics of the problem as we do the mathematical or computational aspect of the integrals, which as we have shown in Chapter I is useful only if the integrals converge rapidly. Unfortunately, the integrals are oscillatory and slowly decaying type which are most time consuming to compute.

To concentrate our attention only to the study of the convergence of the Sommerfeld's integrals, we have left the derivation of the integrals in Appendix A. Only the derivation of the integrals for the horizontal dipole antennas are given in the Appendix, because the formulas of a vertical antenna are essentially contained in those of the horizontal ones.

The Sommerfeld's integrals of an horizonal dipole antenna are given by (A-11) - (A-16) of Appendix A, but are given in the following also for convenience:

$$\pi_x = \frac{e^{-jkR}}{R} - \frac{e^{-jkR'}}{R'} + 2\int_0^\infty J_0(\lambda r)e^{-\nu(z+h)}\frac{\lambda d\lambda}{\nu + \nu_E} \quad , \tag{2-1}$$

$$\pi_{xE} = \frac{2}{r}\int_0^\infty J_0(\lambda r)e^{\nu_E z - \nu h}\frac{\lambda d\lambda}{\nu + \nu_E} \quad , \tag{2-2}$$

$$\pi_z = -\frac{2}{k^2}\cos\phi\int_0^\infty J_1(\lambda r)e^{-\nu(z+h)}\frac{\nu - \nu_E}{\nu + \nu_E}\lambda^2 d\lambda \quad , \tag{2-3}$$

$$\pi_{zE} = -\frac{2}{k_E^2}\cos\phi\int_0^\infty J_1(\lambda r)e^{\nu_E z-\nu h}\frac{\nu-\nu_E}{\epsilon\nu+\nu_E}\lambda^2 d\lambda \quad . \tag{2-4}$$

where, the source is assumed to be in the air, π_x and π_z are respectively the x and z components of the Hertz potential measured [illegible], and π_{xE} and π_{zE} are the same components measured [illegible] the complex refractive index of the ground, and

$$\nu = \sqrt{\lambda^2 - k^2} \quad ,$$

$$\nu_E = \sqrt{\lambda^2 - k_E^2} \quad ,$$

$k^2 = \frac{\omega^2}{c^2}$ and $k_\Sigma^2 = \frac{\omega^2\epsilon}{c^2}$ are the wave numbers in air and earth respectively. The constant h is the height of the source location and the variable z is the height of the field location as shown in Fig. A-1.

When the source is located in the ground, we shall interchange π_x and π_{xE}, ν and ν_E, and replace k_E, $\frac{1}{\epsilon}$ for k, ϵ in (2-1) and (2-2), and similar modifications for (2-3) and (2-4).

The approximations we shall use take advantage of the decaying property of the exponential which is quite different for (2-1) and (2-2), and whether it is $e^{\nu(z+h)}$ or $e^{\nu_E(z+h)}$. Therefore, it is necessary that the approximation techniques are treated in 3 different cases, namely, (A) both source and observation locations above the ground ($h > 0$, $z > 0$), (B) source location above and observation location under the ground ($h > 0$, $z < 0$), and (C) both source and observation locations under the ground ($h < 0$, $z < 0$).

A. $(h > 0, z > 0)$[5]

The approximation techniques of this case are numerous. They are reported, for instance, in references [6] and [7]. They have assumed, however, the refractive index of the half-space to be large and the observation point to be far away from the interface. In this section we shall use an approximate boundary-condition technique to arrive to an approximation of Sommerfeld's integral, which is also valid for source or field points relatively close to the ground.

Approximate Boundary Condition

Consider the Hertz potential π_x(or π_z) over a small portion of air-earth interface. The dependence of all potential components on the radial direction may be described by

$$\pi = w \exp(-j(k_x x + k_y y)), \quad z \geq 0, \tag{2-5}$$

where w is the so called "attenuation factor" and is a function of position. It is assumed that the attenuation factor w does not vary too much over the range of a wave length λ_o in the air, or quantitatively,

$$\left| \frac{\lambda_o}{2\pi\omega} \frac{\partial w}{\partial x} \right| << 1; \quad \left| \frac{\lambda_o}{2\pi\omega} \frac{\partial w}{\partial y} \right| << 1. \tag{2-6}$$

This assumption is claimed valid[8] in most of the practical situations.

With equation (2-5) and (2-6), the solution of the wave equation

$$\nabla^2 \pi_E + k_E^2 \pi_E = 0 \text{ for } z \geq 0 \tag{2-7}$$

is obtained:

$$\pi_E(r,z) = \pi_E(r,0) \exp(j\sqrt{k_E^2 - k_\lambda^2}), \tag{2-8}$$

where π_E is the Hertz potential for the source in the air and observer in the ground, and $k_\lambda^2 = k_x^2 + k_y^2$. If equation (2-8) is substituted into the boundary condition for π at $z = 0$, (eq. (A-7) and (A-8)), we obtain a new set of boundary conditions valid for the solution in the region $z > 0$

$$\frac{\partial \pi_x}{\partial z} = jk\sqrt{\epsilon_1^o}\,\pi_x \text{ at } z = 0 ; \tag{2-9}$$

$$\frac{\partial \pi_z}{\partial z} - \frac{jk\pi_z}{\sqrt{\epsilon^o}} = \frac{1 - \epsilon}{\epsilon} \frac{\partial \pi_x}{\partial x} \text{ at } z = 0 , \tag{2-10}$$

where $$\epsilon_1^o = \epsilon - \cos^2\psi , \tag{2-11}$$

and $$\epsilon^o = \epsilon^2/\epsilon_1^o. \tag{2-12}$$

The ψ in eq. (2-10) is defined according to the propagation constant and is given by $\cos\psi = k_\lambda/k$. Since k is real, ψ is real and hereon will be considered equal to the angle that a wave is incident on the zeroth Fresnel's zone. The above assumption is justified by the following consideration. From the theory of wave propagron between transmitter and receiver above a ground plane, it is found that the wave which arrives at the receiver from the contribution of reflected wave is essentially from one direction. That is, there is only a certain limited area on the ground plane from which a reflected wave may reach the receiver. Usually, for practical applications, only a few Fresnel's zones are needed to be a good approximation. The only case when the wave zone covers a large area is when both the source and observer are very close to the ground. But for this case $\cos\psi$ is almost equal to 1. Therefore our assumption of optical reflection angle is practically valid.

The approximate boundary conditions of eq. (2-9) and (2-10) are similar to the impedance condition except that the "effective refractive indeces" are used here. With these boundary conditions, we obtain a set of solutions to the wave equation if we follow the similar procedure as that in Sommerfeld's treatment [4], [9]. The solutions are given by

$$\pi_x = \frac{e^{-jkR}}{R} - \frac{e^{-jkR'}}{R'} + \{2\frac{e^{-jkR'}}{R'} - 2jk\sqrt{\varepsilon_1^o}\int_0^\infty J_o(\lambda r)e^{-\nu(z+h)}\frac{\lambda}{\nu + jk\sqrt{\varepsilon_1^o}}\frac{d\lambda}{\nu}\} \tag{2-13}$$

$$\pi_z = \frac{-2}{k^2}\cos\phi\int_0^\infty J_1(\lambda r)e^{-\nu(z+h)}\frac{(\nu - jk\sqrt{\varepsilon_1^o})}{\varepsilon\nu + jk\sqrt{\varepsilon_1^o}}\lambda^2 d\lambda\ , \tag{2-14}$$

where $\cos\phi = x/r$, $R = \sqrt{r^2 + (z-h)^2}$, and $R' = \sqrt{r^2 + (z+h)^2}$. The integrals in the above formulas can be transformed to other integral forms which do not involve the Bessel's function. The detail of the transformation is given in reference [9]. In Appendix B, the integral in Eq. (2-13) is shown to be equivalent to the following integral,

$$-\int_{j\infty}^{z}\exp(-jk[R'_\xi + \sqrt{\varepsilon_1^o}\,(\xi - z)])d\xi/R'_\xi\ .$$

The Hertz potentials are then given by

$$\pi_x = \frac{e^{-jkR}}{R} - \frac{e^{-jkR'}}{R'} + \{2\frac{e^{-jkR'}}{R'} - 2jk\sqrt{\varepsilon_1^o}\int_z^{-j\infty} e^{-jk[[R'_\xi + \sqrt{\varepsilon_1^o}(\xi - z)]}\frac{d\xi}{R'_\xi} \tag{2-15}$$

$$\pi_z = \frac{2}{k^2}\frac{\partial}{\partial x}[I_A + I_B]\ , \tag{2-16}$$

where I_A and I_B are given by

$$I_A = \frac{-jk}{\sqrt{\epsilon^o}} \left[\frac{e^{-jkR'}}{R'} + \frac{jk}{\sqrt{\epsilon^o}} \int_{-j\infty}^{z} \exp\left(\frac{jk(\xi-z)}{\sqrt{\epsilon^o}} \right) \frac{e^{-jkR'_\xi}}{R'_\xi} d\xi \right] \tag{2-17}$$

$$I_B = \frac{-1}{\epsilon^o} \frac{\partial}{\partial z} \left[I_A / (jk\sqrt{\epsilon^o}) \right], \tag{2-18}$$

and $R'_\xi = \sqrt{r^2 + (h+\xi)^2}$. For the convenience of comparison let

$$U = 2 \frac{e^{-jkR'}}{R'} - 2jk\sqrt{\epsilon_1^o} \int_z^{-j\infty} e^{-jk[R'_\xi + \sqrt{\epsilon_1^o}(\xi-z)]} \frac{d\xi}{R'_\xi} , \tag{2-19}$$

$$V = 2 \frac{e^{-jkR'}}{R'} - \frac{2jk}{\sqrt{\epsilon^o}} \int_z^{-j\infty} e^{-jk[R'_\xi + \frac{(\xi-z)}{\sqrt{\epsilon^o}}]} \frac{d\xi}{R'_\xi} . \tag{2-20}$$

The equation U is corresponding to the integral term of Sommerfeld's formula in equation (A-11) i.e.

$$U_s = 2 \int_0^\infty J_o(\lambda r) e^{-\nu(z+h)} \frac{\lambda}{\nu + \nu_E} d\lambda. \tag{2-21}$$

The equation of V can be shown to be corresponding to the Sommerfeld's formula for the vertical dipole and is given by [3]

$$V_s = 2 \frac{e^{-jkR'}}{R'} + 2 \int_0^\infty J_o(\lambda r) e^{-\nu(z+h)} \frac{\nu_E}{\epsilon\nu + \nu_E} \frac{\lambda}{\nu} d\lambda . \tag{2-22}$$

Numerical Results

The integrals in U and V of eqs. (2-19) and 2-20) are computed by using the Simpson algorithm in a complex plane. The choice of integral path is rather arbitrary. We find that a straight line path extending

from $\xi = z$ to $\xi = z - j\infty$ is good enough.

The values of U and V are given in Figs. (2-1) to (2-6) for lossy tangent being .01 and 1 and different locations of observer and source. Values of U_s and V_s in Eqs. (2-21) and (2-22) are also computed and shown in these figures by dots. It is clear that the approximation given by U and V is accurate. The computational time we consume is of the order of 100 times less than that using U_s and V_s. Together in these figures the familiar approximations using the plane wave reflection coefficients are also presented. As expected, the plane wave approximation is not a good approximation where value of (h + z) is getting smaller.

Taylor's Expansion of ν_E

The approximation of (A-11) and (A-15) by (2-13) and (2-14), while physically justified in previous paragraphs, is mathematically amount to replacing ν_E by $jk\sqrt{\epsilon_1^o}$, which makes the transformation to the integrals of (2-15) and (2-16) possible. Approximating $\nu_E = \sqrt{\lambda^2-k_E^2}$ by $jk\sqrt{\epsilon_1^o}$, a constant, in an integrand must also be justified mathematically. Indeed, it can be and we shall show in the following.

$$\text{Let} \quad \nu_E = \sqrt{\lambda^2-k_E^2} = \sqrt{(\lambda^2-k^2) - (k_E^2-k^2)}$$

$$= \sqrt{\nu^2 - (k_E^2-k^2)} \quad . \tag{2-23}$$

The Taylor's expansion of (2-23) at $\nu = 0$ is

$$\nu_E \simeq j\sqrt{k_E^2-k^2} \quad (1 + (\sqrt{k_E^2-k^2})\nu^2 + \text{higher order terms})$$

$$= jk\sqrt{\epsilon_1^o}\,(1 - \frac{1}{2}\frac{\sin^2\psi}{\epsilon_1^o})\,[1 + k\sqrt{\epsilon_1^o}\,(1 - \frac{1}{2}\frac{\sin^2\psi}{\epsilon_1^o})\nu^2 + \cdots] \quad . \tag{2-24}$$

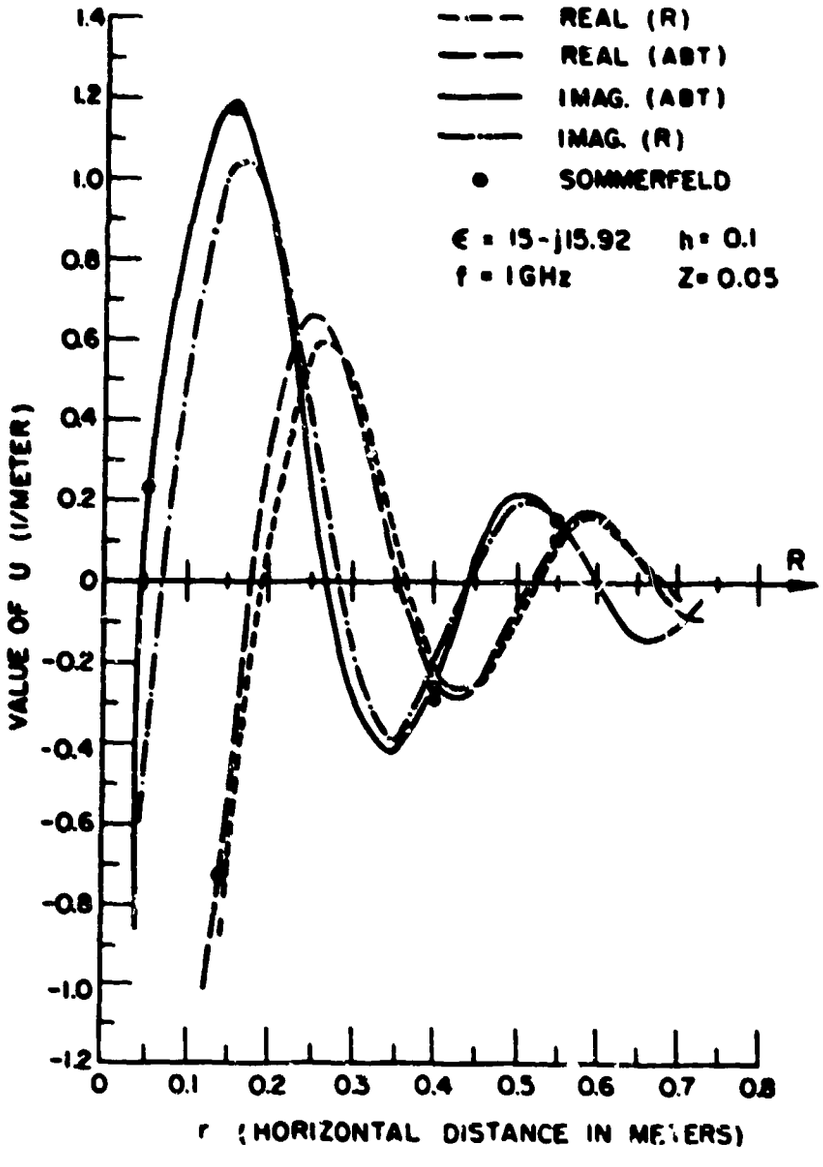

Fig. 2-1. Value of the U integral vs. horizontal range, h > 0 z > 0. Where R: plane wave approximation, ABT: approximate boundary value method.

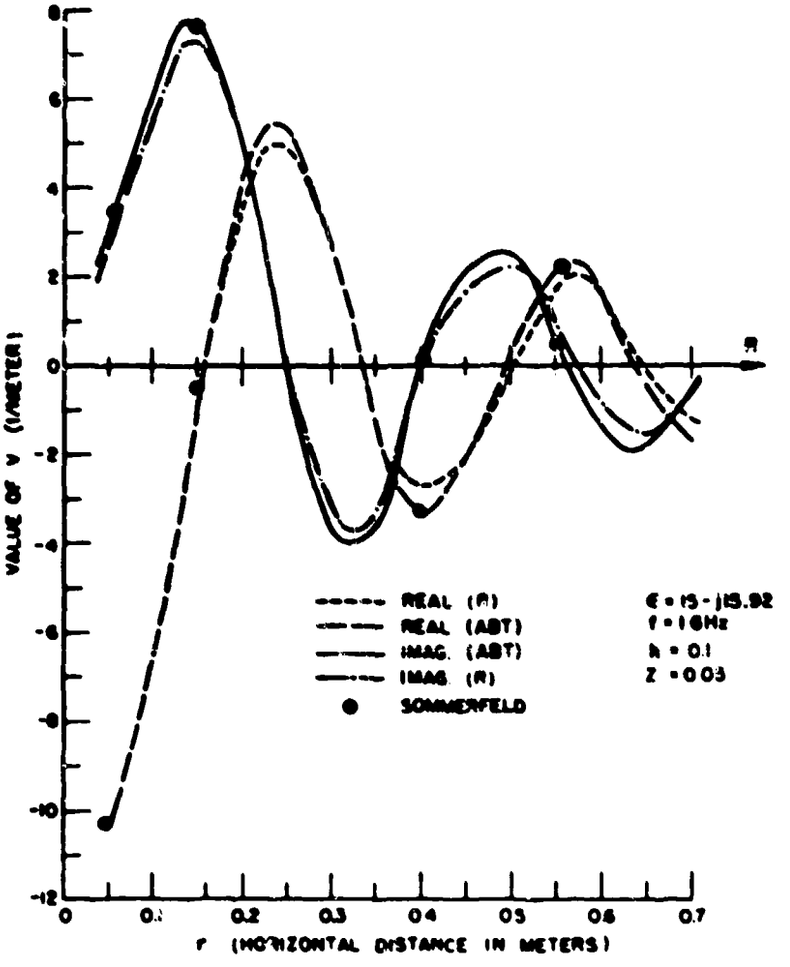

Fig. 2-2. Value of the V integral vs. horizontal range h > 0, z > 0. (R, and ABT, are defined in Fig. 2-1.)

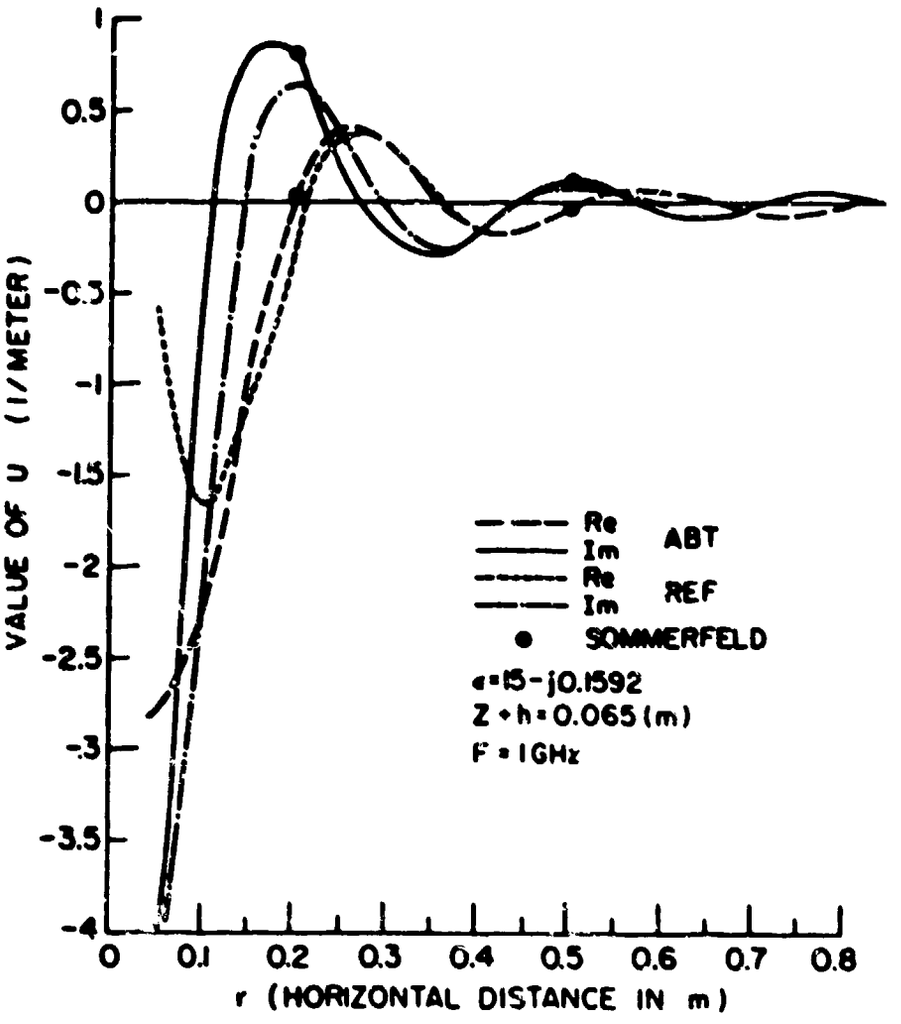

Fig. 2-3. Value of the U integral vs. horizontal range, h > 0, z > 0, (REF is equivalent to R, and R and ABT are defined in Fig. 2-1.)

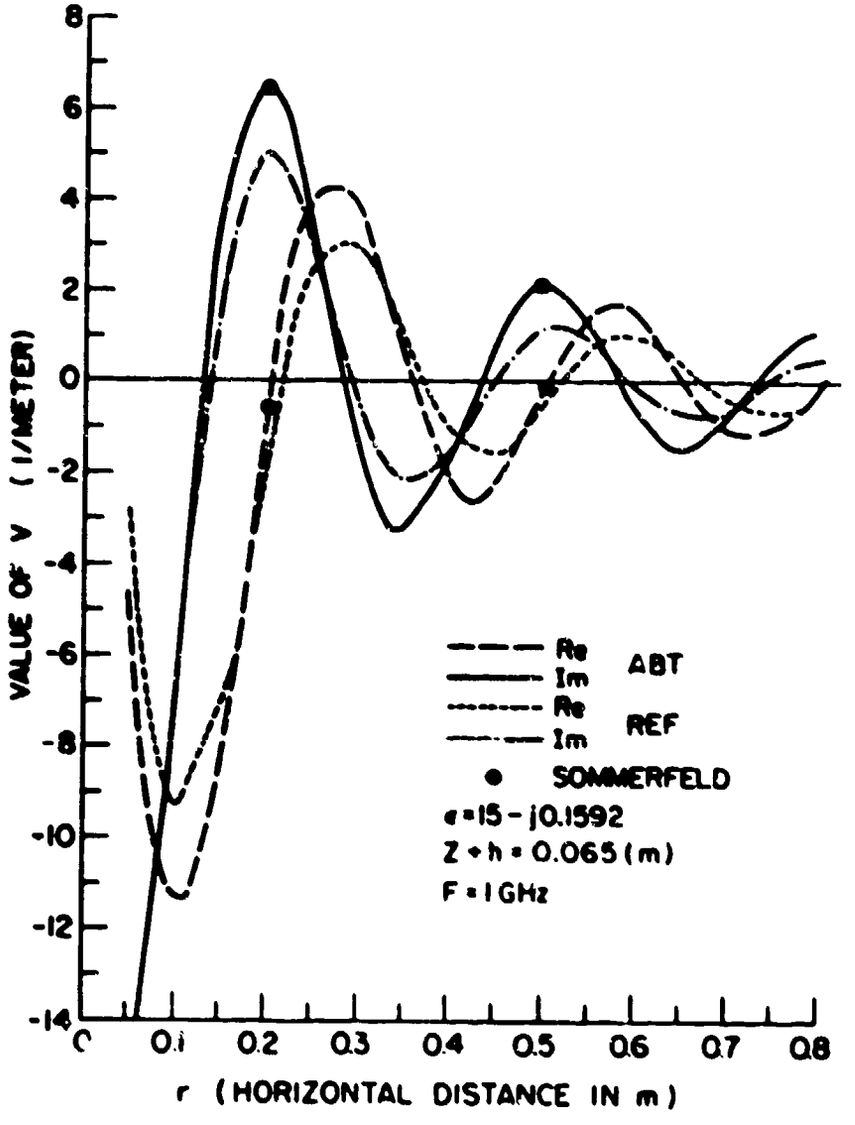

Fig. 2-4. Value of V integral vs. horizontal range h > 0, z > 0. (REF, ABT are defined in Fig. 2-3.)

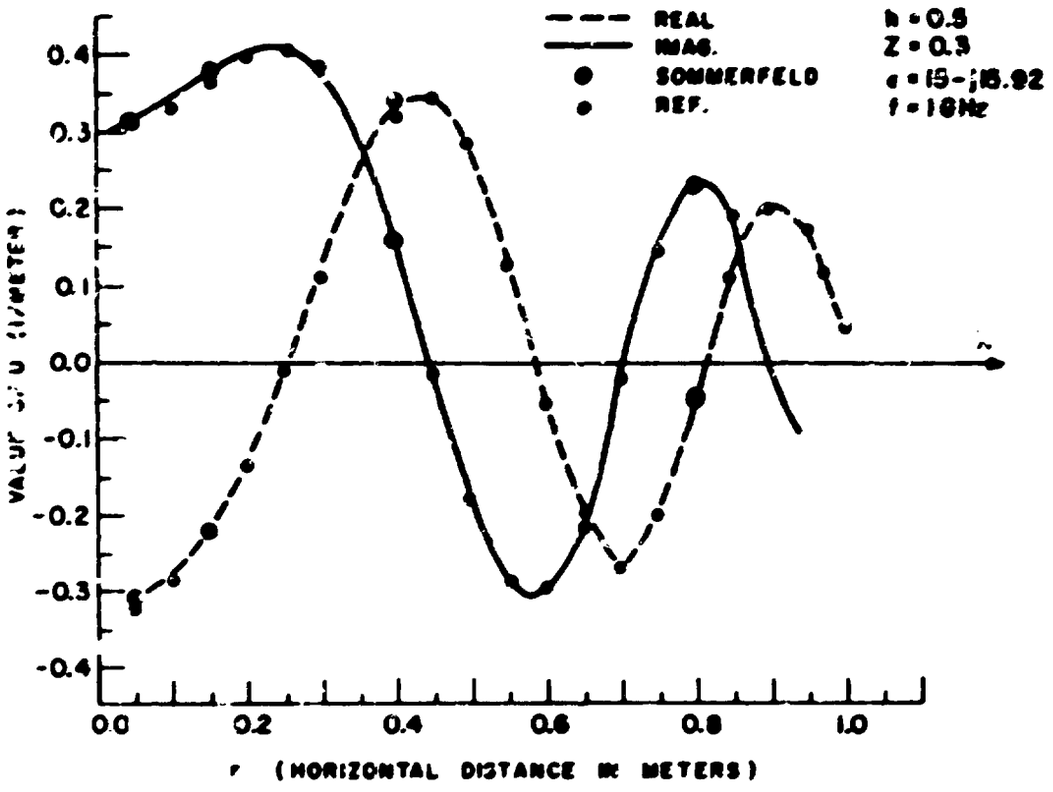

Fig. 2-5. Value of the U integral vs. horizontal range, h > 0, z > 0. (REF. is defined in Fig. 2-3.)

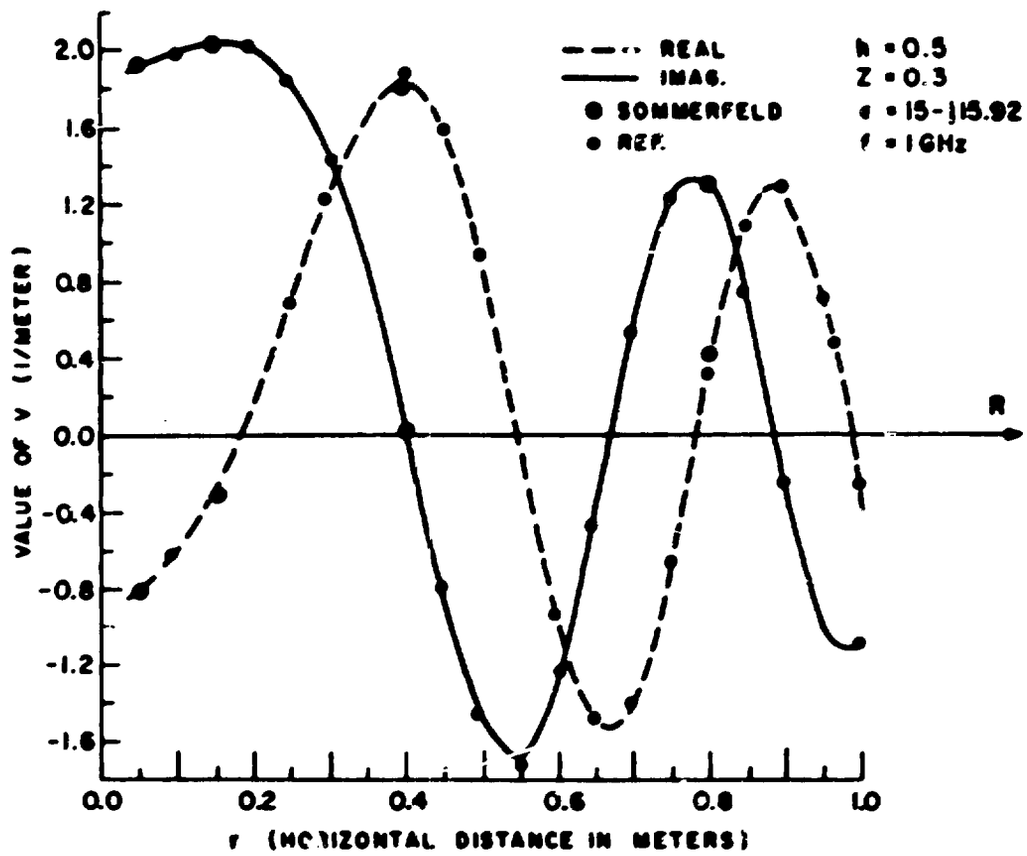

Fig. 2-6. Value of the V integral vs. horizontal distance, h > 0, z > 0. (REF is defined in Fig. 2-3.)

It is noticed that $\nu_E = jk\sqrt{\epsilon_1}$ is just the first term of the expansion. The expansion of (2-24) is valid for $|\nu \sin\psi| \cdot 1$, which is violated when $|\lambda| >> |k|$. However, when that happens, the exponential term $e^{-\nu(z+h)}$ will be sufficiently small to suppress the integrand. That is to say the value $(h+z)$ has to be sufficiently large to make the suppression possible. For frequency at 1 GHz, we find that the value of $(z+h)$ can be as small as 0.05 meter.

B. $(h > 0, z < 0)$[10]

The Sommerfeld's formulas are given by eqs. (2-2) and (2-4). There is ν_E appearing in the exponential term, which changes the behavior of the above integrands drastically. Now the exponential term starts to decay for much larger value of λ than that in case A. Therefore a much better approximation technique is required.

The discussion of Taylor's expansion of ν_E in previous section leads us to believe that more terms in the expansion should be adopted for a better approximation of $e^{-\nu_E h}$. Therefore the following expansion is considered,

$$e^{\nu_E z} = e^{-j\left(\sqrt{k_E^2-k^2}\right)z}\left[1 + \frac{z}{j\sqrt{k_E^2-k^2}}\frac{\nu^2}{2!}\right] . \qquad (2\text{-}25)$$

The above formula is valid only when ν is small. When λ increases toward $\mathrm{Re}(k_E)$, the right hand side of (2-25) grows quadratically, while the left hand side is actually a decaying function. Furthermore, the quadratic growth is rather rapidly before the $e^{-\nu h}$ is able to suppress the integrand, contributing a substantial amount of error to the integration.

Aiming at eliminating the quadratic growth of the expansion, we then

come up with the following approximation:

$$e^{\nu_E z} \approx e^{-j\left(\sqrt{k_E^2-k^2}\right)}\left(1 + \frac{z}{j\sqrt{k_E^2-k^2}} - \frac{\nu^2}{2}\right) + e^{z_o\nu} - \left(1 + z_o\nu + \frac{(z_o\nu)^2}{2}\right) \quad (2\text{-}26)$$

Where in (2-26) we have purposely added to equation (2-25) a term $e^{z_o\nu}$ and subtracted its second order Taylor's expansion. In order to eliminate the second order term, z_o is so chosen such that

$$\frac{(z_o\nu)^2}{2} = \exp(-j\sqrt{k_E^2-k^2}\, z)/[z\nu^2/2j\sqrt{k_E^2-k^2})] \quad . \quad (2\text{-}27)$$

The expansion of (2-26) is now only of linear growth. From Table (2-1) we can see that considerable improvement has been achieved by using this technique.

One of the limitations makes the approximation so difficult is that functions that are used to approximate it must be functions of the form $e^{x\nu}$. This limited forms of functions ensure the further reduction to a fast convergent integral possible. From the plotting of $e^{\nu_E z}$ with respect to λ, we find that the behavior of $e^{\nu_E z}$ is rather smooth when λ is small. This is because when λ is small the effect of λ^2 is neglegible compared with k_E^2. As λ is getting larger, $e^{\nu_E z}$ becomes oscillatory; but then $e^{-\nu h}$ is small enough to suppress the contribution of this portion to the whole integral. Hence a better approximation may be obtained if we have some way to approximate the function $e^{\nu_E z}$ while λ is not too large. This brings the idea of curve-fitting method.

With the experience of previous approximation methods which led to eq. (2-26) we conclude that a reasonable formula for the curve-fitting is

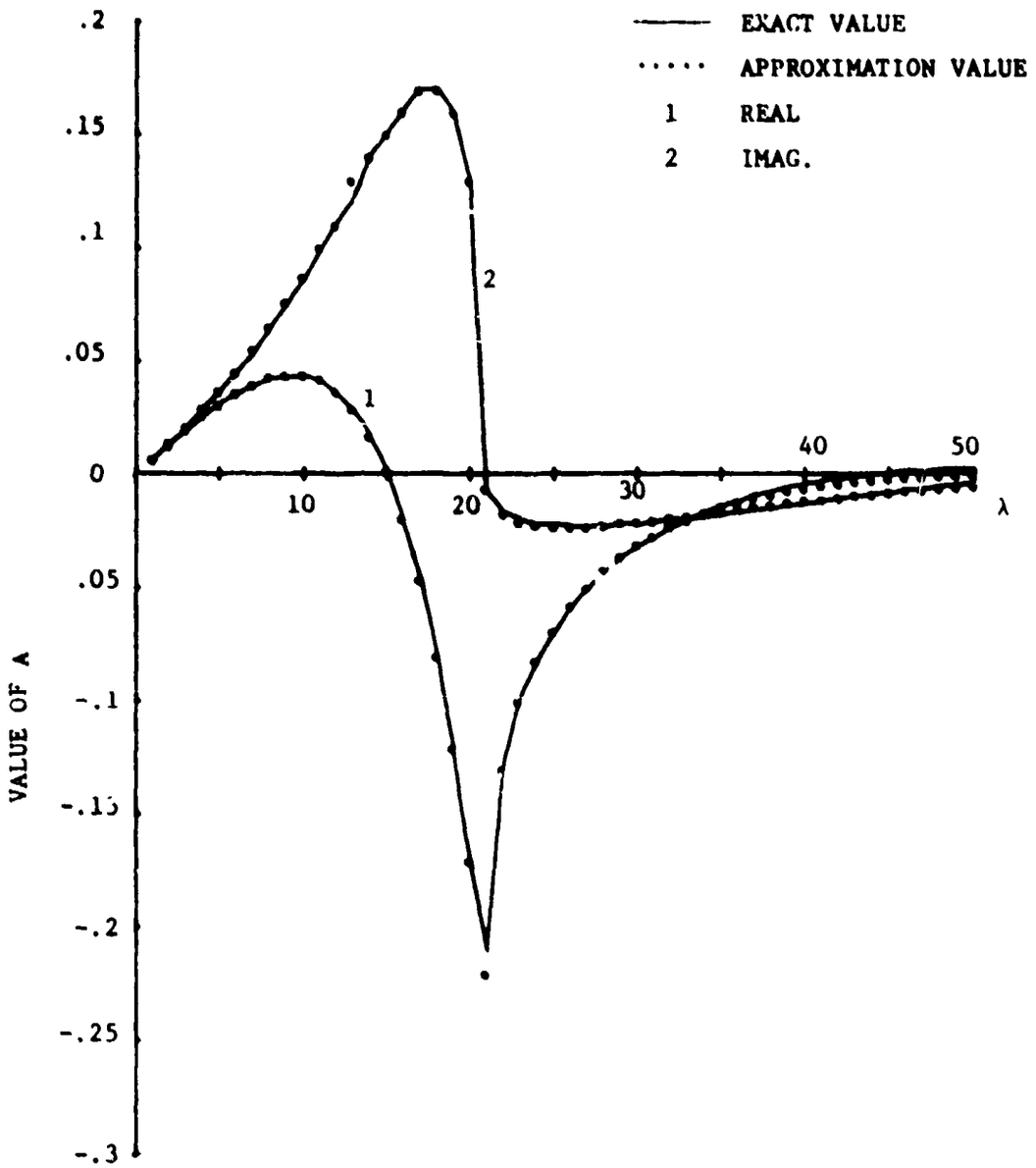

Fig. 2-7. Comparison of curve-fitting approximation and exact formula, $f = 10^9 H_z$, $\epsilon = 15 - j.1592$, $z = -.1m$.
$A = J_0(\lambda\nu)\ \exp(\nu_E z - \nu h)\ \lambda/(\nu+\nu_E)$.

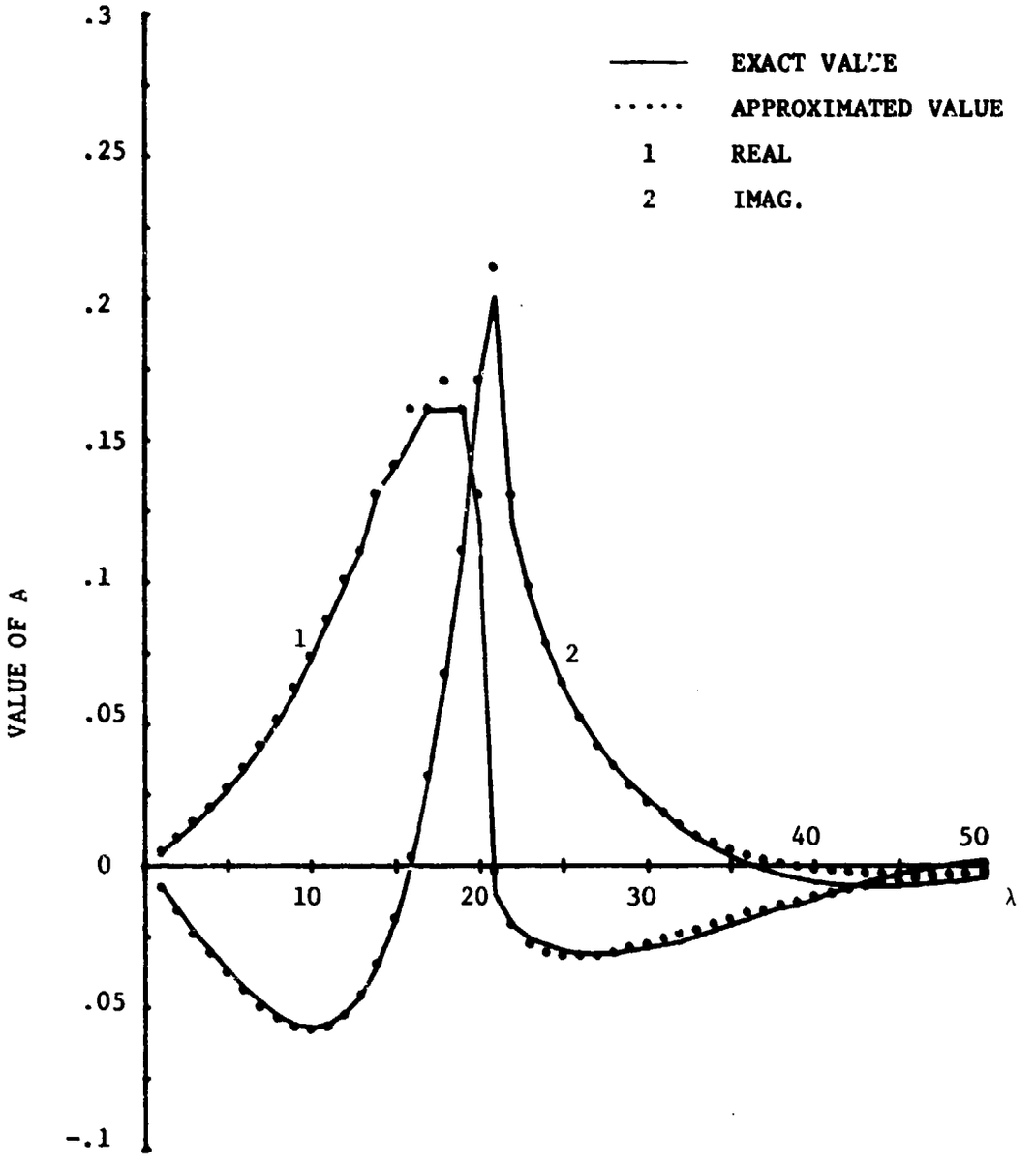

Fig. 2-8. Comparison of curve-fitting approximation and exact formula, $f = 10^9$ Hz. $\epsilon = 15-j.15\Omega$, $z = -.2$m.

A is defined in Fig. 2-7.

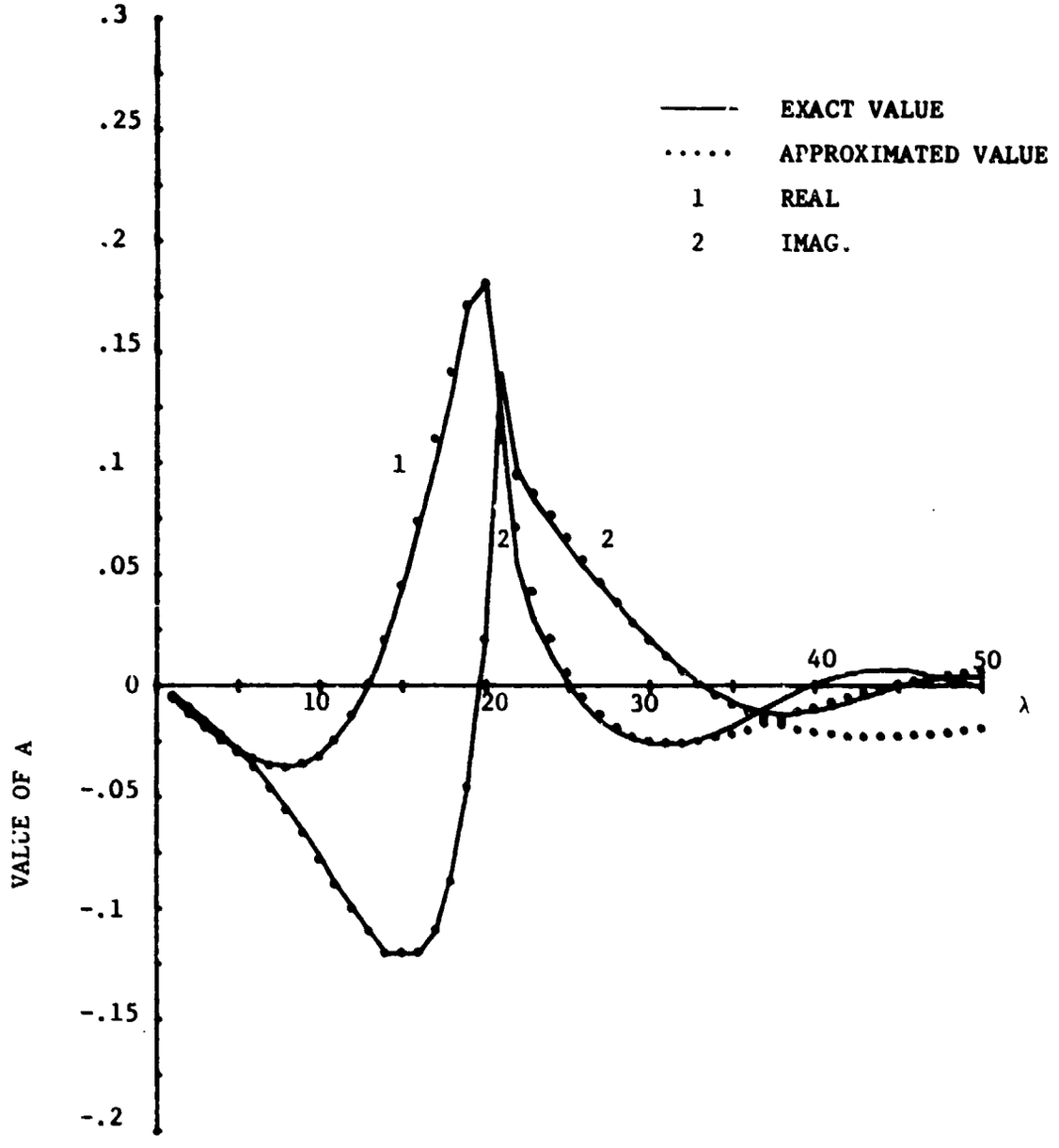

Fig. 2-9. Comparison of curve-fitting approximation and exact formula, $f = 10^9$Hz, $\varepsilon_r = 15\text{-}j.1592$, $z = -.45$m.

A is defined in Fig. 2-7.

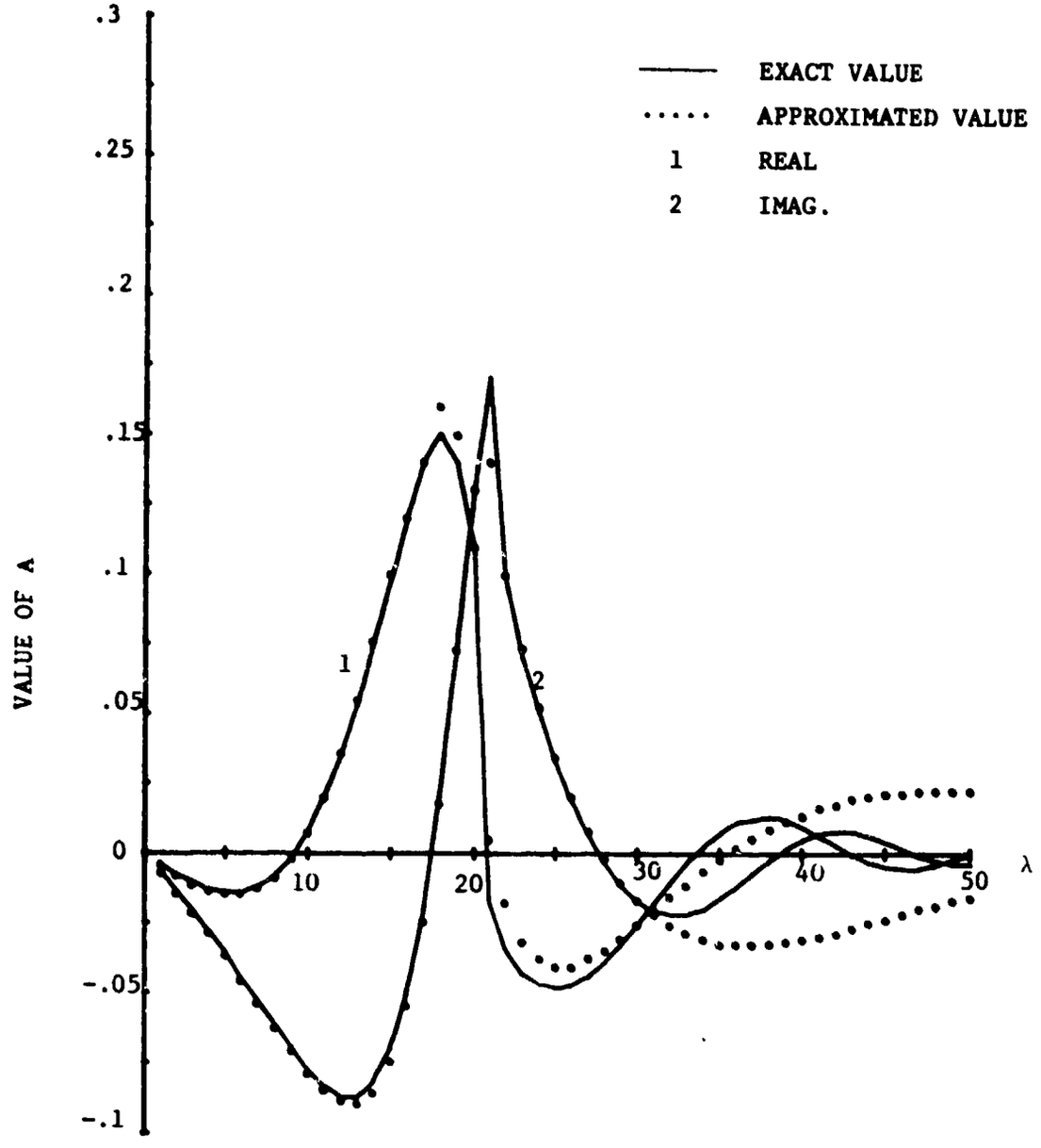

Fig. 2-10. Comparison of curve-fitting approximation and exact formula, $f = 10^9$ Hz, $\epsilon = 15\text{-}j.1592$, $z = -.6$m.

A is defined in Fig. 2-7.

as follows,

$$F(\lambda) = e^{\nu_E z} \approx F_n = a_o e^{z_o \nu} + a_1 + a_2\nu + a_3\nu^2 \ . \qquad (2\text{-}28)$$

In (2-28), z_o is determined the same way as that in (2-27), and the coefficients are found by enforcing $F_n = F(\lambda)$ at four points, namely, $\lambda = \lambda_o$, λ_1, λ_2, λ_3. The choice of λ_i's depends upon k, k_E and z. Usually, two λ_i's are chosen in $\lambda < k$, one at $\lambda = k$ and the other at around $(1/2)k_E$. Note that eq. (2-28) differs from eq. (2-26) by having more freedom on the weight of each term. The zeroth order term of Taylor's expansion in eq. (2-26) is included in a_1 of eq. (2-28).

For the comparison of F_n and $F(\lambda)$, values of the integrand of eq. (2-2) are computed for $\varepsilon = 15 - j\cdot 1592$, f = 1GHz, and are shown in figs. (2-7) to (2-10). It is seen that F_n stays to be a good approximation up to $|z| > .45$ meter. From Fig. (2-10), with z = .6 meter, or equivalently, two free space wave lengths, the approximate curve fails to respond to the oscillatory behavior of $F(\lambda)$ when $\lambda > 30$. This failure when z is so deep under the ground plane is not a serious matter, because, the value of potnetial is so small then, that any approximation, including plane wave approximation, tends to converge to the correct value.

With the approximation of eq. (2-28), we are able to transform eq. (2-2) into

$$\pi_{xE} = \frac{2}{\varepsilon}\left[a_o I_z + a_1 I_o + a_2 I_1 + a_3 I_2\right] \ , \qquad (2\text{-}29)$$

where

$$I_z = \int_0^\infty J_o(\lambda r) e^{-\nu(h-z_o)} \frac{\lambda d\lambda}{jk\sqrt{\varepsilon_1^o} + \nu} \ , \qquad (2\text{-}30)$$

$$I_o = \int_0^\infty J_o(\lambda r) e^{-\lambda h} \frac{\lambda d\lambda}{jk\sqrt{\varepsilon_1^o} + \nu} , \tag{2-31}$$

$$I_1 = -\frac{\partial I_o}{\partial h} , \tag{2-32}$$

$$I_2 = \frac{\partial^2 I_o}{\partial h^2} . \tag{2-33}$$

Wherein the denominators of the above integrals we have replaced ν_E by $jk\sqrt{\varepsilon_1^o}$ as we have done in previous sections. By a similar procedure as that in section A where $z > 0$, I_o is reduced to:

$$I_o = \frac{e^{-jkR''}}{R''} + jk\sqrt{\varepsilon_1^o} \int_{-j\infty}^{h} \frac{e^{-jk[R''_\xi + (\xi-h)\sqrt{\varepsilon_1^o}]}}{R''_\xi} d\xi . \tag{2-34}$$

where $R'' = \sqrt{r^2 + h^2}$ and $R''_\xi = \sqrt{r^2 + \xi^2}$. From eqs. (2-32) and (2-33), I_1, I_2 are easily obtained; their final forms still contain the integral in (2-34). I_z in eq. (2-30) is obtained by replacing h in eq. (2-34) by $(h-z_o)$.

As a comparison of accuracy by using (2-25), (2-26) and (2-28) for the approximation, values of π_{xE} are tabulated in Table (2-1). Figs. (2-11) and (2-12) show the value of π_{xE} in eq. (2-29) as a function of

---

Table 2-1 Comparison of Different Approximation by Using Eqs. (2-25), (2-26), (2-27) and Exact Function.

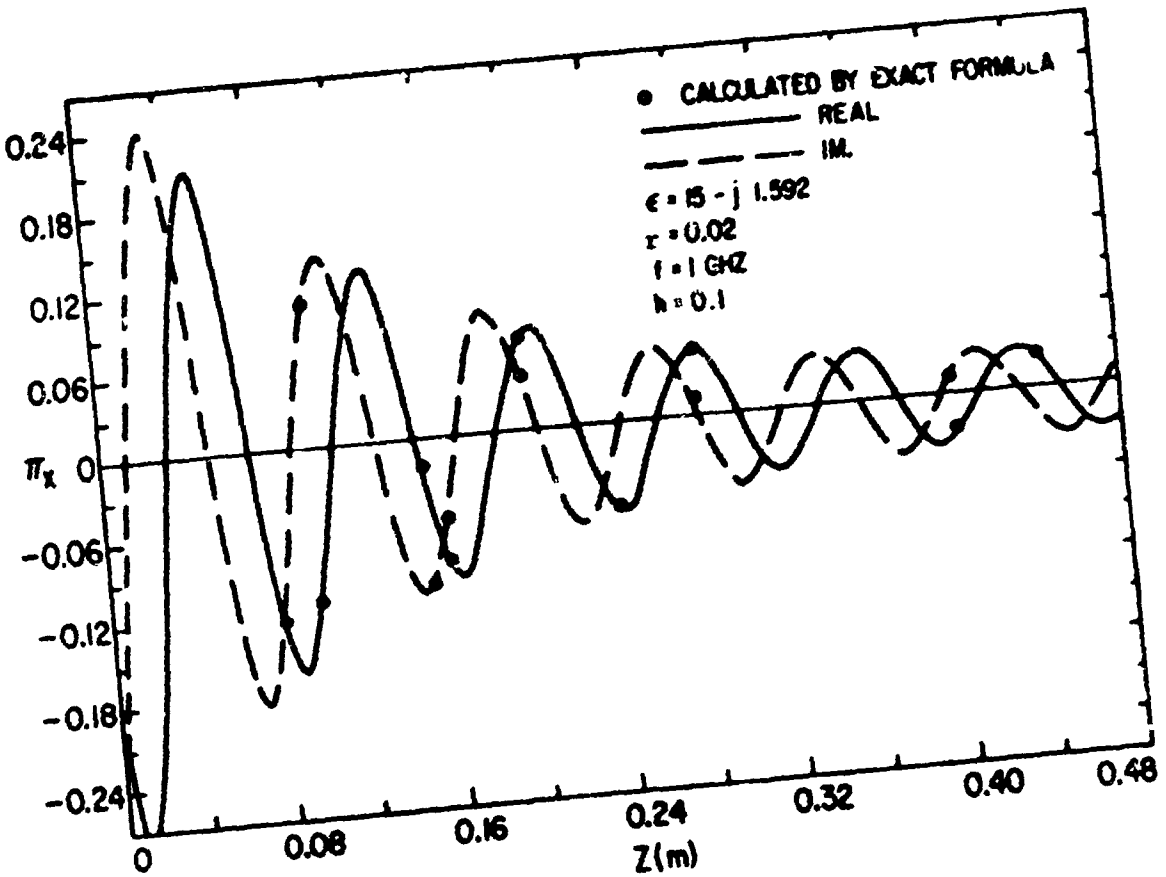

Fig. 2-11. Value of π_x(1/meter) obtained from eq. (2-35) vs. vertical distance with fixed horizontal range, h > 0, z < 0.

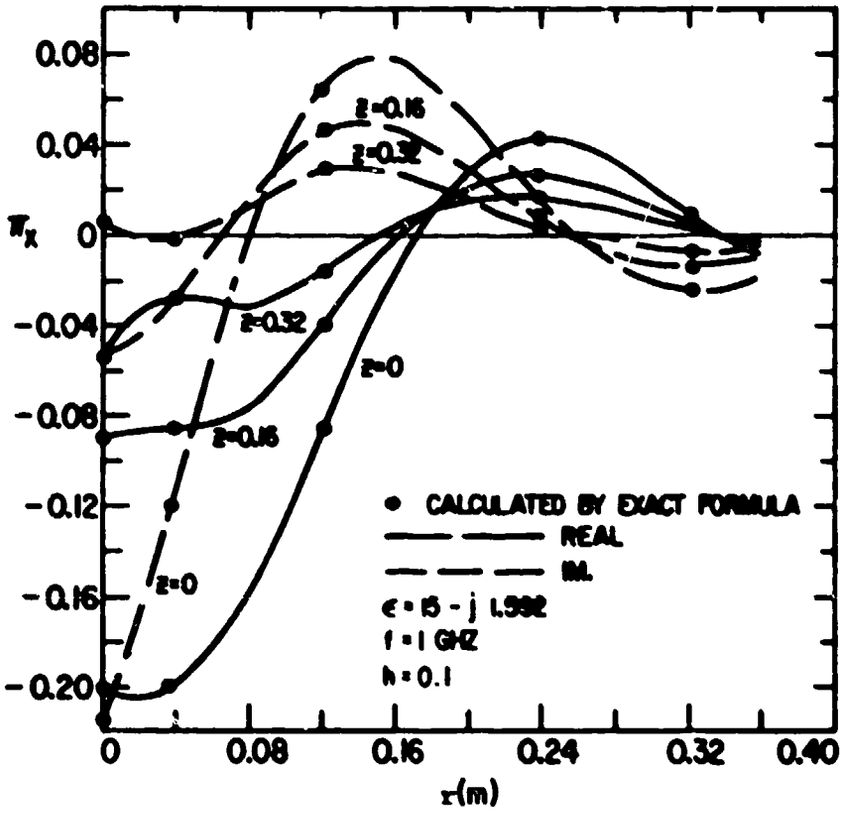

Fig. 2-12. Value of π_x (1/meter) obtained from eq. (2-35) vs. horizontal range, $h > 0$, $z < 0$.

π_{xE} / $z_{(m)}$	exact	curve fitting	eq. (2-24)	eq. (2-23)
-.1	-.0977 + j.1130	-.0998 + j.1142	-.1061 + j.1110	-.1239 + j.130
-.2	.0694 + j.0376	.06912 + j.0363	.0639 + j.0433	.0895 + j.082

z(fixed r) and function of r(fixed z) at 1GHz and $\epsilon_1^o = 15 - j\,1.592$. Exact formula of eq. (2-2) is also evaluated. It is seen from these figures that the curve-fitting method yields a very good result. It is well known that the wave propagating inside a lossy ground from a source in the air behaves like a plane wave. Hence we also compare our curve-fitting method with plane wave approximation and show the result in fig. (2-13). Only the magnitudes are shown, because the phases agree very well everywhere. It is observed that while the phase behaves well the plane wave approximation may result an error up to 40% in magnitude. Earlier, we have observed from fig. (2-10) that when z gets deeper in the ground the accuracy will deteriorate. The degree of inaccuracy, however, is not significant judging from fig. (2-13). Besides, the value of $|\pi_x|$ is sufficiently small when inaccuracy is observed. In that case the information of phase is more important than that of magnitude.

The approximation of eq. (2-26) can also be applied to eq. (2-4) to obtain an approximation to π_{zE}. Then eq. (2-4) becomes

$$\pi_{zE} = \frac{2}{k_E^2} \frac{\partial}{\partial x} \left[a_o I_z + a_1 I_o + a_2 I_1 + a_3 I_2 \right] . \tag{2-35}$$

Where

$$I_z = \int_0^\infty J_o(\lambda r) e^{-\nu(h-z_o)} \frac{\nu - jk\sqrt{\epsilon_1^o}}{\nu + jk\sqrt{\epsilon_1^o}} \lambda d\lambda , \tag{2-36}$$

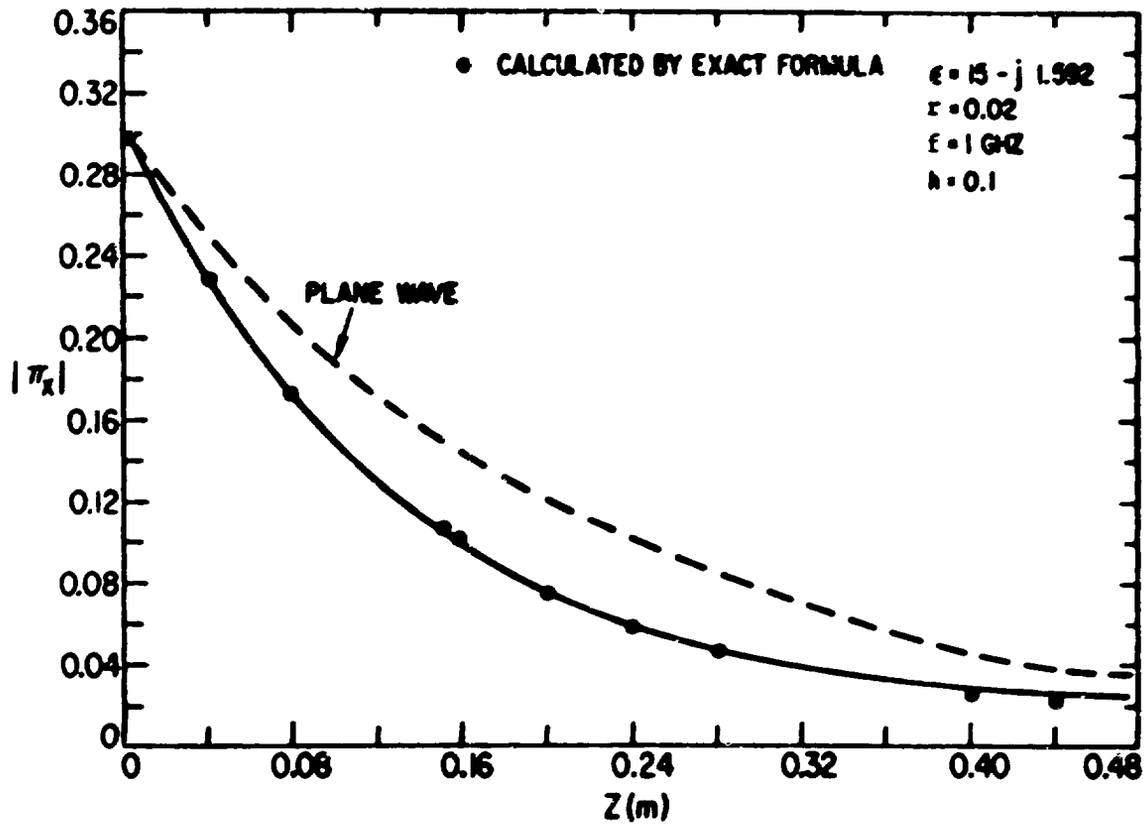

Fig. 2-13. Magnitude of π_x vs. vertical distance with fixed r, h > 0, z < 0.

$$I_o = \int_0^\infty J_o(\lambda r) e^{-\nu h} \frac{\nu - jk\sqrt{\epsilon_1^o}}{\epsilon\nu + jk\sqrt{\epsilon_1^o}} \lambda d\lambda \quad , \tag{2-37}$$

$$I_1 = -\frac{\partial I_o}{\partial h} \quad . \tag{2-38}$$

$$I_2 = \frac{\partial^2 I_o}{\partial^2 h} \quad . \tag{2-39}$$

Comparing (2-37) with (2-14) we find that an expression of the form (2-16) for I_o in (2-37) is immediately obvious.

C. $(h < 0, z < 0)$

The Sommerfeld's formulas are now given by

$$\pi_x = \frac{e^{-jk_E R}}{R} - \frac{e^{-jk_E R'}}{R'} + 2\int_0^\infty J_o(\lambda r) e^{-\nu_E(z+h)} \frac{\lambda}{\nu_E + \nu} \, d\lambda \tag{2-40}$$

$$\pi_z = \frac{-2}{k_E^2} \cos\phi \int_0^\infty J_1(\lambda r) e^{-\nu_E(z+h)} \frac{\nu_E - \nu}{\epsilon\nu + \nu_E} \lambda^2 d\lambda \quad . \tag{2-41}$$

The integrals in (2-40) and (2-41) are similar to those in eq. (A-11) and (A-15) for the case A except now we have ν_E instead of ν. Because of this change we have to approximate ν in the denominators of the above integrands. Approximating ν by a constant is obviously not satisfactory, since the value of ν varies substantially in the range $0 < \lambda < \mathrm{Re}(k_E)$. It is obvious we have to look for an approximation of ν by some function of λ. In search for this suitable function of λ we also have to bear in mind that the approximate function is eventually to be coupled with ν_E and

made the transformation of integral into a fast convergent form possible.

The experience of previous sections leads us to try the approximation of $\frac{1}{\nu + \nu_E}$ by $\sum_i^n \frac{c_i}{\nu_E + d_i}$. Therefore we look into the possible approximation of ν by a polynomial of ν_E. The term $1/(\nu + \nu_E)$ then can be reduced to a sum of terms of the form $1/(\nu_E + \text{constant})$ by partial fraction. Theoretically, polynomial approximation of a function is feasible in an analytical region. But we are restricted by the requirement of computing efficiency such that only a few terms (hopefully less than three) of $1/(\nu_E + \text{constant})$ can be to approximate $1/(\nu + \nu_E)$. Our experience concludes, however, polynomial approximation of ν by ν_E is not satisfactory.

The behavior of rational function composed of two polynomials is more versatile than that of a single polynomial. While keeping the order of each polynomial down, rational function has more degree of freedom. In order to appreciate this, let us consider the following approximation:

$$\nu \simeq \frac{\nu_E^3 + a_1\nu_E^2 + a_2\nu_E + a_3}{a_4\nu_E^2 + a_5\nu_E + a_6} \quad . \tag{2-42}$$

Therefore,

$$\frac{1}{\nu + \nu_E} \simeq \frac{a_4\nu_E^2 + a_5\nu_E + a_6}{(1 + a_4)\nu_E^3 + (a_1 + a_5)\nu_E^2 + (a_2 + a_6)\nu_E + a_3} \quad . \tag{2-43}$$

It is clear now that we can then separate the right hand side of (2-43) into three partial fractions. There are six adjustable constants to be determined by enforcing the equality of both sides of eq. (2-42). This should compare to the single polynomial approximation, where only three adjustable constants are possible to obtain a sum of three partial fractions.

Equation (2-42) is only valid for the region where $\lambda \geq k$, since ν has a branch point at $\lambda = k$. To ensure the continuity of ν at $\nu_E = 0$ and correct functional behavior when λ extends to infinite, we need to fix two constants. Note that $\nu_E = 0$, when $\lambda = k_E$, and eq. (2-42) becomes

$$\nu = \sqrt{k_E^2 - k^2} = a_3/a_6 \ .$$

$$\therefore \ a_6 = a_3/\sqrt{k_E^2 - k^2} = A \ . \tag{2-44}$$

When $\lambda \to \infty$, $\nu = \nu_E$, from eq. (2-42)

$$\nu\Big|_{\lambda \to \infty} = \frac{\nu_E}{a_4}\Big|_{\lambda \to \infty} = \frac{\nu}{a_4}\Big|_{\lambda \to \infty} \ .$$

So that a_4 should be equal to 1, and eq. (2-42) becomes

$$\nu = \frac{\nu_E^3 + a_1\nu_E^2 + a_2\nu_E + a_3}{\nu_E^2 + a_5\nu_E + a_6} \ . \tag{2-45}$$

In order to furnish the approximation for eq. (2-40) let

$$\frac{\nu_E}{\nu + \nu_E} = \frac{a_4\nu_E^3 + a_5\nu_E^2 + a_6\nu_E}{2\nu_E^3 + (a_1 + a_5)\nu_E^2 + (a_2 + a_6)\nu_E + a_3} \tag{2-46}$$

The right hand side and left hand side of eq. (2-46) as a function of λ are compared and shown in fig. (2-14). It is seen that a very good approximation beyond $\lambda > k$ is achieved. For that particular case, $\nu_E = 15\text{-}j1.59$ and $k = 20.958$, equality of eq. (2-46) is enforced at $\lambda = 25$, 50, 100 and $a_5 = 0$. Eq. (2-46) can be decomposed into the

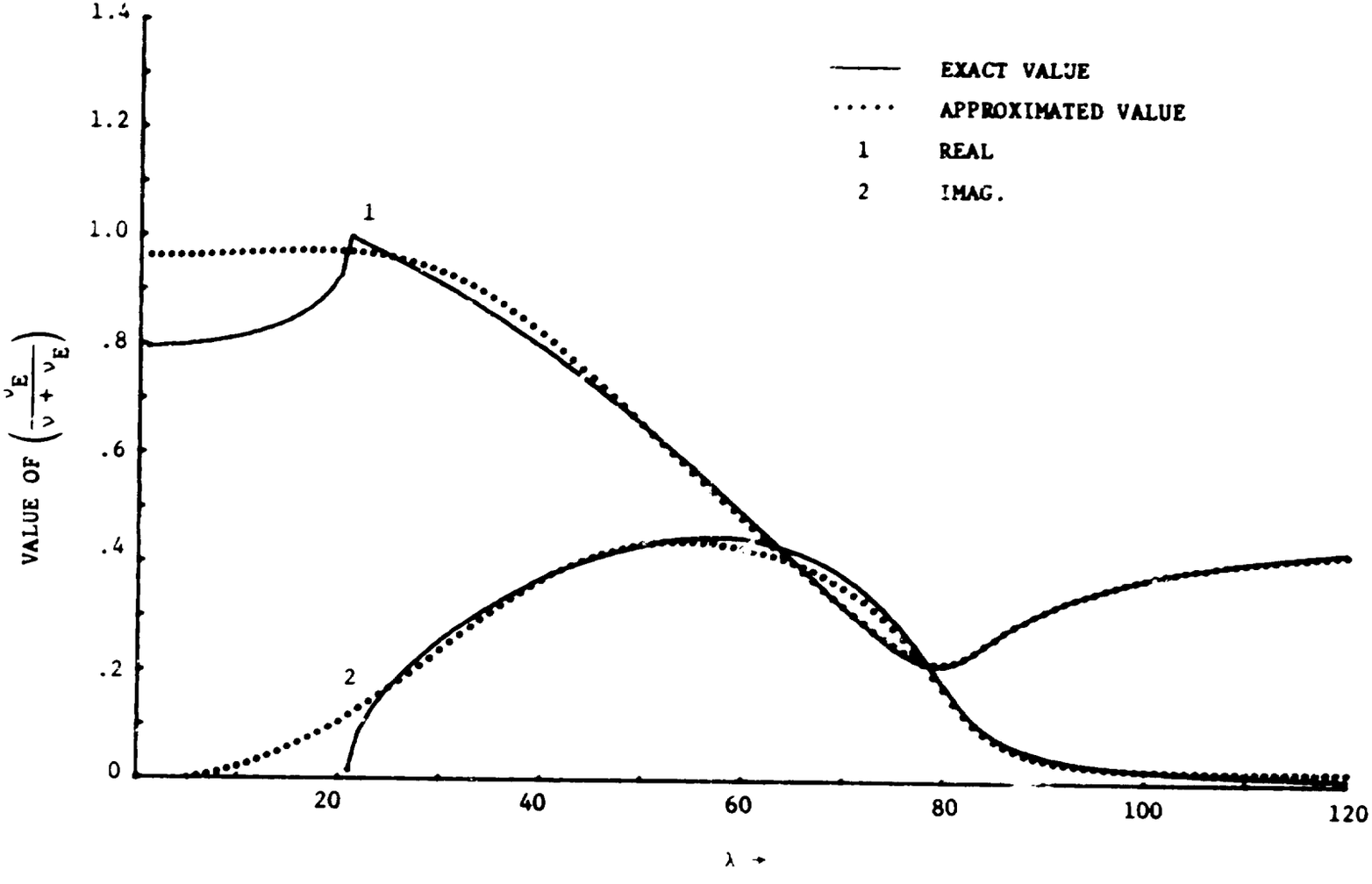

Fig. 2-14. Comparison of rational-function approximation and exact formula, $f = 10^9$ Hz, $\varepsilon = 15\text{-}j1.592$, $\lambda_{i's} = 25, 50, 100$ and $a_5 = 0$ in eq. (2-46).

following form by partial fractions:

$$f(\nu_E) = \frac{\nu_E}{\nu + \nu_E} \simeq \frac{1}{2}\left(1 + \frac{B_1}{\nu_E + b_1} + \frac{B_2}{\nu_E + b_2} + \frac{B_3}{\nu_E + b_3}\right). \tag{2-47}$$

For the convenience of later discussion, the integral term in eq. (2-40) will be singled out and be denoted by U_E. Since eq. (2-47) is good only for $\lambda \geq k$, a correction term should be added for the region $0 \leq \lambda \leq k$. Eq. (2-45) then is substituted into U_E to obtain:

$$U_E \simeq \frac{e^{-jk_E R'}}{2R'} + \sum_{i=1}^{3} U_i + S. \tag{2-48}$$

The first term in (2-48), which is the contribution from the first term on the right side of (2-47), is obtained the same way as that in previous sections. U_i's are given by

$$U_i = \frac{B_i}{2} \int_0^\infty J_o(\lambda r) e^{-\nu_E(z+h)} \frac{\lambda d\lambda}{(\nu_E + b_i)\nu_E}, \tag{2-49}$$

which is the similar integral to the integral term of (2-13). Hence U_i can be easily reduced to the following form:

$$U_i = \frac{B_i}{2} \int_{-j\infty}^{z} e^{-jk_E R'_\xi} e^{-b_i(\xi - |z|)} \frac{d\xi}{R'_\xi}. \tag{2-50}$$

Again, R'_ξ is defined the same as that in section A. S in eq. (2-48) has to be computed by brute force method,

$$S = \int_0^{\lambda_o} J_o(\lambda r) e^{-\nu_E(z+h)} \left[\frac{\nu_E}{\nu_E + \nu} - f(\nu_E)\right] \frac{\lambda}{\nu_E} d\lambda, \tag{2-51}$$

$f(\nu_E)$ is given by eq. (2-47) and the integral limit is $\lambda_o \simeq k$.

Values of U_E are computed according to (2-48), and are shown in figs. (2-15), (2-16). Comparisons are made between results of eq. (2-48) and (2-40) and the agreement is almost perfect. Computing time took for each point of calculation is less than .5 sec. for (2-48) comparing to 30 secs. for (2-40) at a CDC 6400 computer.

For the approximation of eq. (2-41), it is enough to approximate $\frac{\nu_E - \nu}{\varepsilon\nu + \nu_E}$ in terms of a rational function of ν_E. This is done much in the same fashion as that we have just presented. With eq. (2-45),

$$\frac{\nu_E - \nu}{\varepsilon\nu + \nu_E} \simeq \frac{1}{(\varepsilon + 1)} \frac{(a_5 - a_1)\nu_E^2 + (a_6 - a_2)\nu_E - a_3}{\nu_E^3 + \frac{(a_1\varepsilon + a_5)}{\varepsilon + 1}\nu_E^2 + \frac{(a_2\varepsilon + a_6)}{\varepsilon + 1}\nu_E + \frac{a_3\varepsilon}{\varepsilon + 1}} , \quad (2\text{-}52)$$

the right hand side of (2-52) can be decomposed into partial fractions:

$$\frac{\nu_E - \nu}{\varepsilon\nu + \nu_E} \simeq \frac{1}{\varepsilon + 1}\left(\frac{B_1}{\nu_E + b_1} + \frac{B_2}{\nu_E + b_2} + \frac{B_3}{\nu_E + b_3}\right) . \quad (2\text{-}53)$$

The comparison of both sides of eq. (2-53) as functions of λ is shown in Fig. (2-17). All what follows will be similar to the procedures we have just presented.

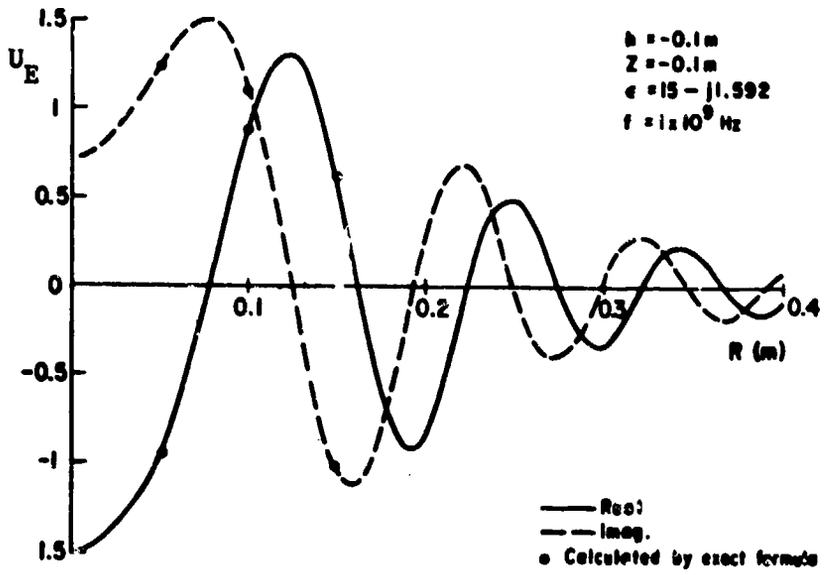

Fig. 2-15. Value of U_E (1/meter) obtained from eq. (2-48) vs. horizontal range $h < 0$, $z < 0$.

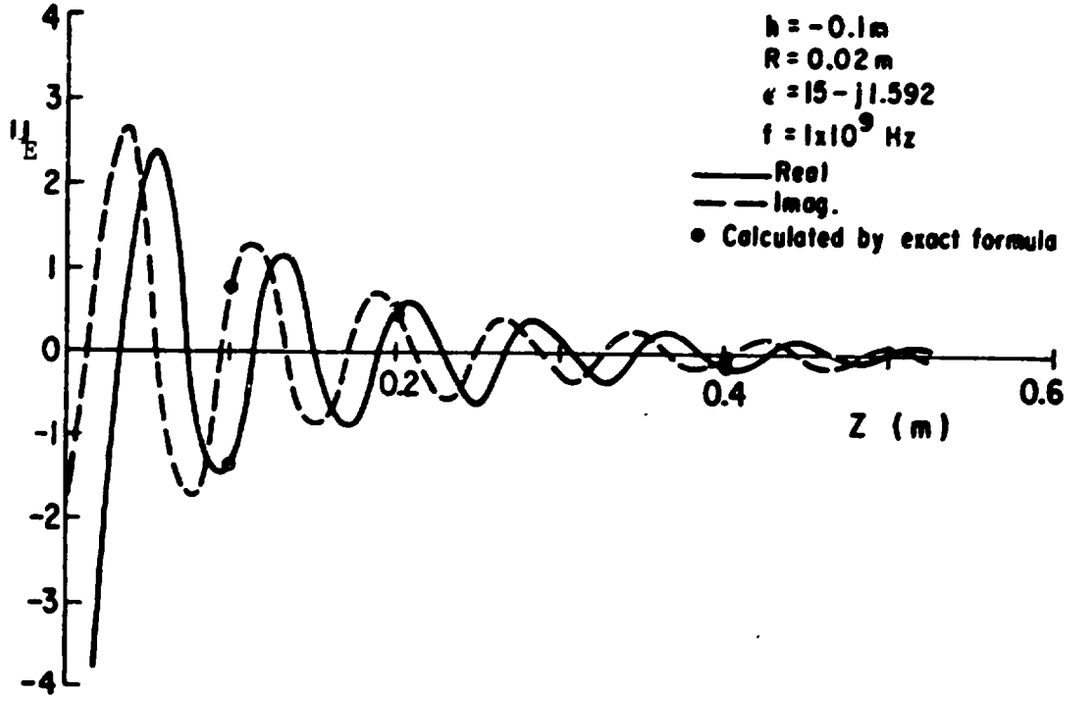

Fig. 2-16. Value of U_E (1/meter) obtained from eq. (2-48) vs. vertical distance, $h < 0$, $z < 0$.

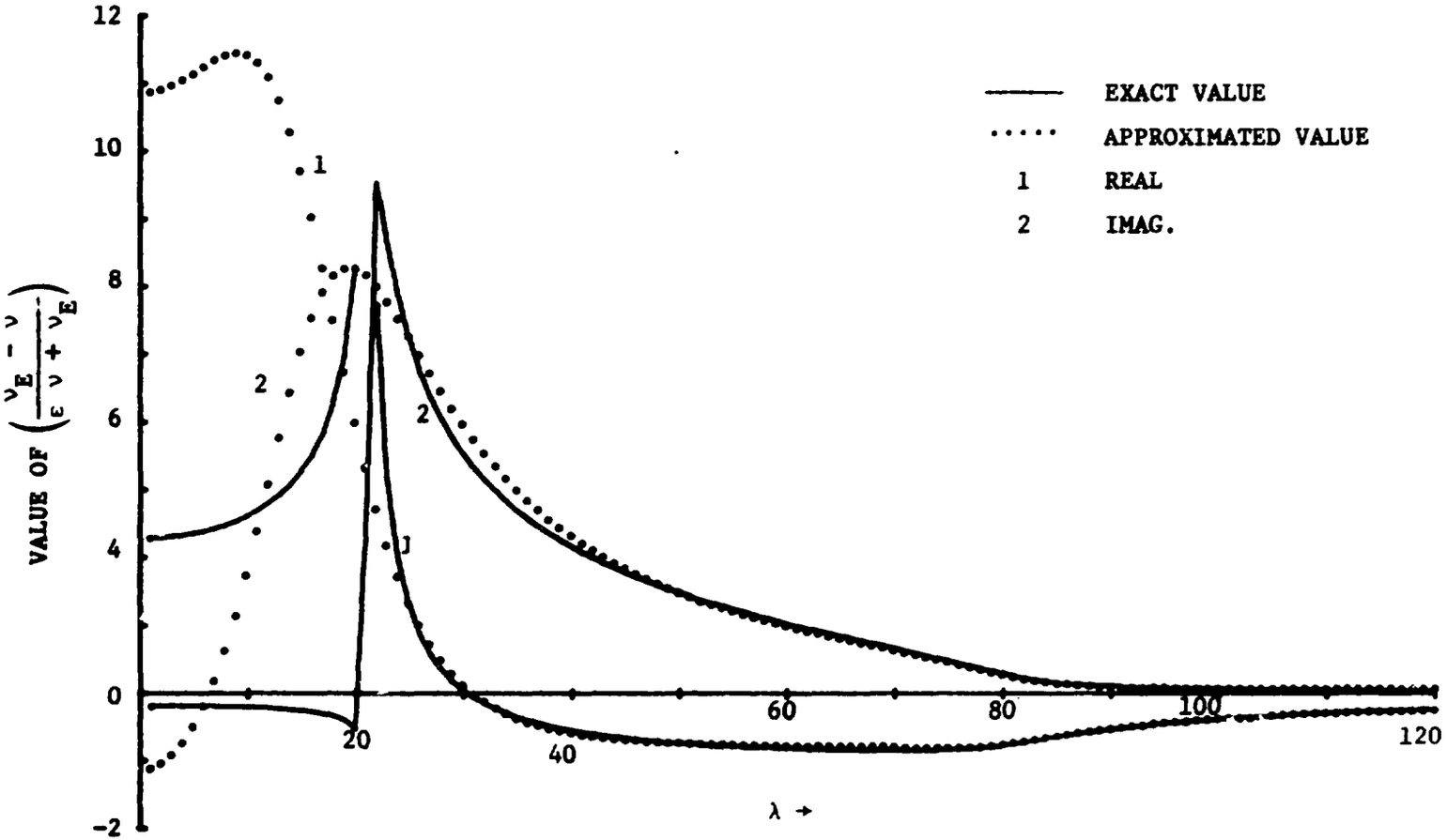

Fig. 2-17. Comparison of rational-function approximation and exact formula, f = 10^9Hz, ϵ = 15-j1.592, λ_i's = 25, 50, 100, and a_5 = 0 in eq. (2-52).

III. Horizontal Dipole Antennas Over Lossy Half-Space

Integral Equation Formulation

As mentioned in Chapter I that the antenna problem involving lossy half-space is similar to that in free space with the free space Green's function replaced by the Sommerfeld's integral. In this chapter we shall discuss the antenna equation in greater detail and the integral equation formulation will be described. It is noticed that the formulation given in Chapter I is an integro-differential equation which is less stable than an integral equation.

The electric fields of an infinitesimal current can be expressed in terms of the vector Hertz potential

$$\bar{E} = (k^2 + \nabla\nabla\cdot)\bar{\psi} \quad , \tag{3-1}$$

where $\bar{\psi}$ satisfies the following equation:

$$(\nabla^2 + k^2)\bar{\psi} = -\frac{1}{j\omega\epsilon}\,\delta(x-x')\hat{x} \quad . \tag{3-2}$$

Applying the boundary conditions of a lossy half-space, for the fields above the ground ($z > 0$), $\bar{\psi}$ happens to be,

$$\bar{\psi} = \frac{1}{4\pi}(\pi_x\hat{x} + \pi_z\hat{z}), \text{ for a x-oriented dipole,} \tag{3-3}$$

where π_x and π_z are the Sommerfeld's integrals given by (2-1) and (2-3) respectively.

For a horizontal linear antenna oriented in the x-direction, we have

$$\bar{\psi} = \frac{1}{4\pi j\omega\epsilon}\int_V J_x(x')\cdot(\pi_x\hat{x} + \pi_z\hat{z})dv', \tag{3-4}$$

where the integration is over the space occupied by the antenna. Substituting (3-4) into (3-1) we get

$$\bar{E}(\bar{r}) = \frac{1}{4\pi j\omega\epsilon} \int_v J_x(x') \cdot (k^2 + \nabla\nabla\cdot)(\pi_x\hat{x} + \pi_z\hat{z})dv', \tag{3-5}$$

where $\bar{E}$ is now the electric field radiated by the current on the antenna. Let $\bar{r}$, the field point, approach the surface of the antenna, the total tangential component of the electric field must vanish, thus

$$E_x(\bar{r}_s) + E_{ox}(\bar{r}_s) = 0, \tag{3-6}$$

where $E_x(\bar{r}_s)$ is the x-component of $\bar{E}(\bar{r}_s)$, and $E_{ox}(\bar{r}_s)$ is the x-component of the electric field produced by a generator. $\bar{r}_s$ is a point on the antenna surface.

Since the x-component of $\nabla\nabla\cdot\bar{\pi}$ is

$$(\nabla\nabla\cdot\bar{\pi})\cdot\hat{x} = \left(\frac{\partial^2\pi_x}{\partial x^2} + \frac{\partial^2\pi_z}{\partial x\partial z}\right), \tag{3-7}$$

we have, after substituting (3-7) and (3-6) in (3-5),

$$j\omega\epsilon E_{ox}(x) = \frac{1}{4\pi}\int_L I_x(x')\left[\left(\frac{\partial}{\partial x^2} + k^2\right)\pi_x(x|x') + \frac{\partial^2}{\partial x\partial z}\pi_z(x|x')\right]dx' \tag{3-8}$$

where a thin linear x-oriented antenna is assumed, and $I_x(x) = 2\pi a J_x(x)$ is now the current, and a is the radius of the thin wire. x and x' are points on the antenna and L is the length of the antenna. Eq. (3-8) is the integro-differential equation similar to Eq. (1-4) in free space. In the following we shall convert (3-8) into an integral equation, which is more stable for numerical computation.

It is well known that the differential equation,

$$\left(\frac{d^2}{dx^2} + k^2\right)\phi(x) = g(x) \tag{3-9}$$

has the most general solution,

$$\phi(x) = A \sin kx + B \cos kx + \frac{1}{k}\int_0^x g(\xi) \sin k(x-\xi)d\xi \ . \tag{3-10}$$

It is obvious from (3-9) and (3-10) that

$$\left(\frac{d^2}{dx^2} + k^2\right)\left[\frac{1}{k}\int_0^x g(\xi) \sin k(x-\xi)d\xi\right] = g(x). \tag{3-11}$$

Now, let's multiply both sides of (3-8) by sin k(x-ξ) and integrate, we get,

$$\int_0^x -j\omega\epsilon E_{ox}(\xi) \sin k(x-\xi)d\xi = \frac{1}{4\pi}\int_L I_x(x')\left\{\frac{1}{k}\int_0^x \left(\frac{\partial^2}{\partial\xi^2} + k^2\right)\pi_x(\xi|x')\sin k(x-\xi)d\xi\right\}dx'$$

$$+ \frac{1}{4\pi}\int_L I_x(x')\left\{\frac{1}{k}\int_0^x \frac{\partial}{\partial\xi}\left[\frac{\partial}{\partial z}\pi_z(\xi|x')\right]\sin k(x-\xi)d\xi\right\}dx'. \tag{3-12}$$

Using (3-11), we find the first term of the right hand side of (3-12) is simply

$$\frac{1}{4\pi}\int_L I_x(x')\left[\frac{1}{k}\int_0^x \left(\frac{\partial^2}{\partial\xi^2} + k^2\right)\pi_x(\xi|x')\sin k(x-\xi)d\xi\right]dx'$$

$$= \frac{1}{4\pi}\int_L I_x(x')\pi_x(x|x')dx' - (A \sin kx + B \cos kx). \tag{3-13}$$

Eq. (3-12) now becomes

$$\frac{1}{4\pi}\int_L I_x(x')\pi_x(x|x')dx' + \frac{1}{4\pi}\int_L I_x(x')\left\{\frac{1}{k}\int_0^x \frac{\partial}{\partial\xi}\left[\frac{\partial}{\partial z}\pi_z(\xi|x')\right]\sin k(x-\xi\ d\xi)dx'\right.$$

$$= A\sin kx + B\cos kx - \frac{j\omega\epsilon}{k}\int_0^x E_{ox}(\xi)\sin k(x-\xi)d\xi \qquad (3\text{-}14)$$

The second term on the left hand side of (3-14) contains no singularity, so in computation we may differentiate before perform the integration.

In actual computation of (3-14) we shall use the fast converging form for π_x and π_z as given in (2-11), (2-12) and (2-13). It should also be noticed that, although (3-14) involves a double integral of the form,

$$P = \frac{1}{4\pi}\int_L I_x(x')\left\{\frac{1}{k}\int_0^x\left[\frac{\partial}{\partial\xi}\ \frac{\partial}{\partial z}\pi_z(\xi|x')\right]\sin k(x-\xi)d\xi\right\}dx' \qquad (3\text{-}15)$$

we can decompose (3-15) in the following terms,

$$P = \frac{1}{4\pi}\int_L I_x(x')\left\{\frac{1}{k}\left[\sin kx\int_0^x \frac{\partial}{\partial\xi}\left(\frac{\partial}{\partial z}\pi_x(\xi|x')\right)\cos k\xi\ d\xi\right.\right.$$

$$\left.\left. - \cos kx\int_0^x \frac{\partial}{\partial\xi}\left(\frac{\partial}{\partial z}\pi_x(\xi|x')\right)\sin k\xi\ d\xi\right]dx'\right\} \qquad (3\text{-}16)$$

In (3-16) the integrands are no longer functions of x, and the integration with respect to ξ to different values of x may be made cummulatively and avoid redundant computations.

Numerical Results

Once the formulation of an antenna equation is properly done, the numerical method of solution is rather straight forward. Numerous references

are available on numerical techniques [3], [11]. In here we present some typical results of computation. In Fig (3-1) the input admittances of a Horizontal dipole antenna as a function of distance above the lossy ground are shown. The antenna parameters are shown in the figure. It is noticed that the proximity of the lossy ground does have a visible effect on the input properties of the antenna and thus its performance.

The program we have written is also capable of computing the horizontal antenna arrays connected by transmission lines such as shown in Figs. (3-2) and (3-3). The computed results we have presented here are original. While there is no comparable theoretical or experimental results available to check our computation, the computations of a few extreme cases, do indicate that the program is free of bugs and gives accurate results. These results will be used to compute the incident fields for the analysis of scattering by buried obstacles in the next chapter.

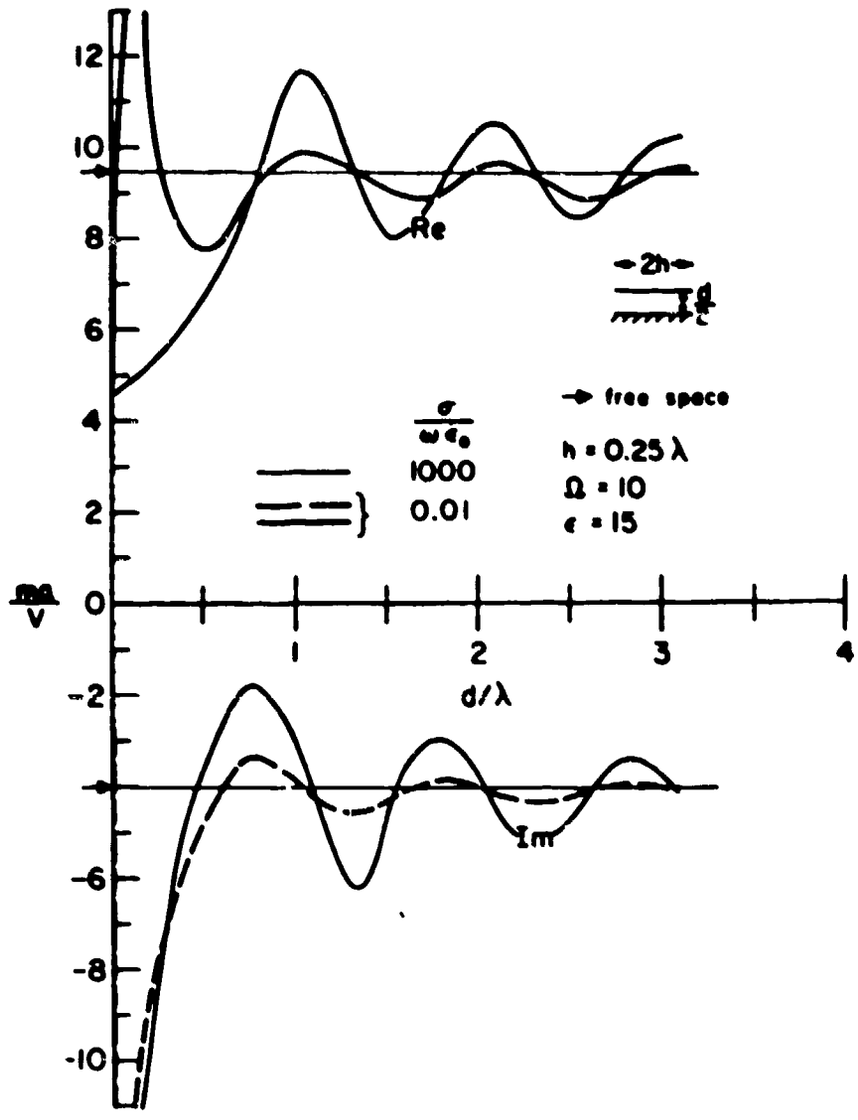

Fig. 3-1. Input admittance of a horizontal antenna over a conducting ground.

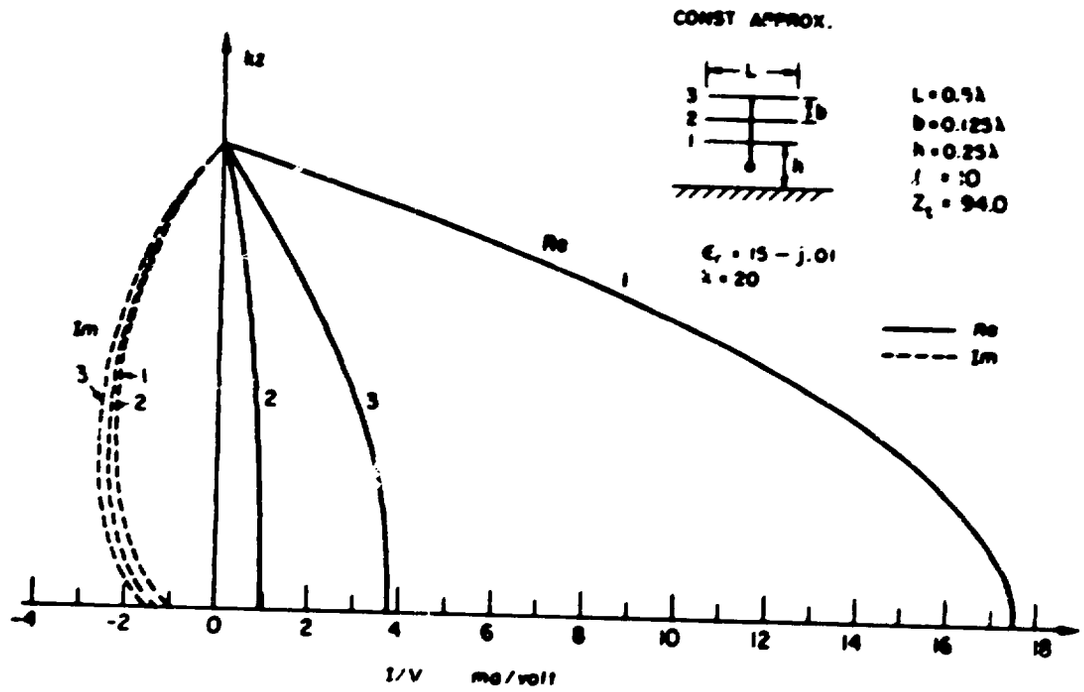

Fig. 3-2. Current distribution on each antenna element normalized by the driving voltage of that element.

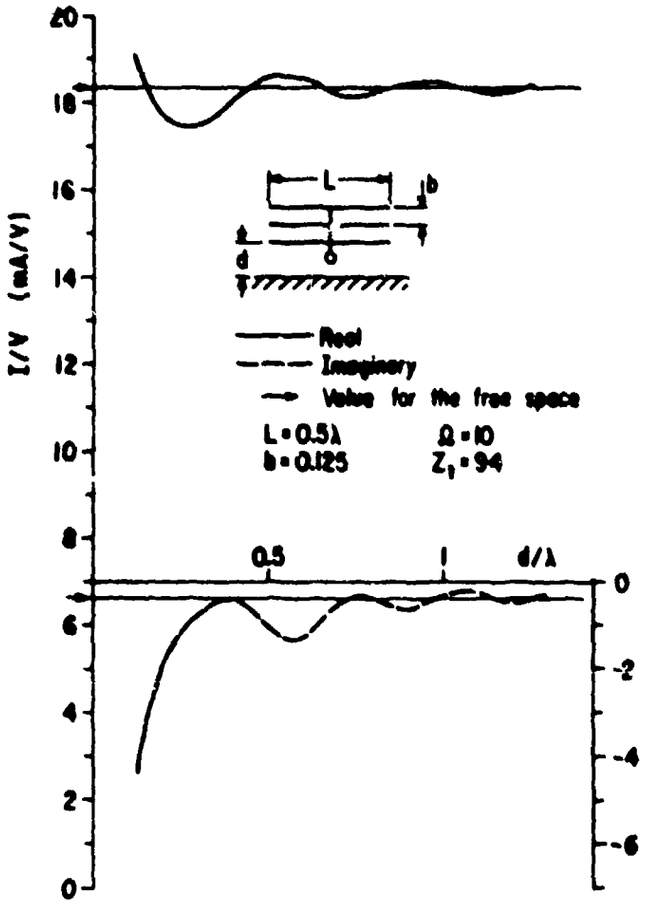

Fig. 3-3. Normalized input current of the most effective element for a 3-element array over a lossy ground.

IV. Incident and Scattering Fields for the Problem of Buried Wire

In the previous chapter, we have discussed the method of solving an antenna problem. The current distribution thus calculated will be applied here to find the electric field everywhere. The field equation (1-2) will be restated in the following manner for an x-oriented current source:

$$\bar{E}^{ij}(\bar{r}) = \frac{1}{j\omega \epsilon_i} \int_L \frac{I_x(x')}{4\pi} (k_j^2 + \nabla \nabla \cdot)(\pi_x^{ij}\hat{x} + \pi_z^{ij}\hat{z})d\ell'$$

$$i = 1, 2; \; j = 1, 2 \; . \qquad (4\text{-}1)$$

Where double indeces are adopted; i and j represent the locations of source and field point respectively. When index is 1 the point is in the air and 2 in the ground. Thus $k_1 = \omega \sqrt{\epsilon_o \mu_o}$, $k_2 = \sqrt{\epsilon}\, k_1$, and $\epsilon_1 = \epsilon$, $\epsilon_2 = 1/\epsilon$. The operator $\nabla \nabla \cdot$ in eq. (4-1) is given by

$$\nabla[\nabla \cdot (\pi_x \hat{x} + \pi_z \hat{z})]$$

$$= \frac{\partial^2}{\partial x^2} [\pi_x + \phi_z]\hat{x} + [\frac{\partial^2}{\partial x \partial y}][\pi_x + \phi_z]\hat{y} + [\frac{\partial^2}{\partial x \partial z}][\pi_x + \phi_z]\hat{z} \; , \qquad (4\text{-}2)$$

where ϕ_z is defined as follows:

$$\phi_z(x|x') = \frac{2}{k_i^2} \frac{\partial}{\partial z} (I_A + I_B), \qquad (4\text{-}3)$$

where I_A and I_B are given by (2-13) and (2-14). The electric field can then be calculated by using proper Hertz potential in Chapter 2.

For a buried horizontal wire, (Fig. 4-1), the incident fields have to be found from eq. (4-1) as a function of horizontal distance. The operator

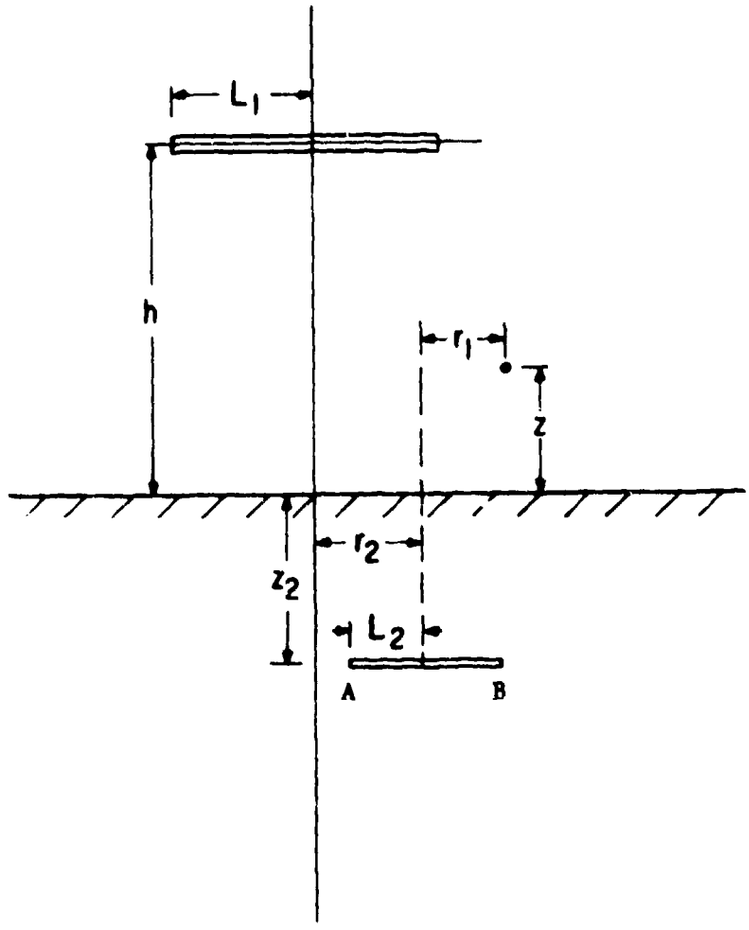

Fig. 4-1. Geometry of the thin wire antenna and scattering problem. All distances are in meter, where L_1 = (antenna length)/2, L_2 = (wire length)/2.

(4-2) has to be evaluated by finite difference methods. In order to avoid the unnecessary repetition of calculation of $\pi_x(x-x')$ and $\pi_z(x-x')$ for different x's, we shall use the numerical method as follows. Instead of computing π_x and π_z at every pair of specific points, we shall compute in a subroutine the value of $\pi_x(m\cdot\Delta x)$ and $\pi_z(m\cdot\Delta x)$, where m = 1, ... M; Δx is a unit distance such as (antenna length/number of divisions); M is an integer such that $(M\cdot\Delta x)$ will cover the maximum distance of (x-x'). When the values $\pi_z(x-x')$ at points other than $m\Delta x$ are required interpolation methods can be applied easily if Δx is sufficiently small.

Fig. (4-2) shows the x-component electric fields as a function of kz for fixed kr = 0.0833π. It is seen from the phase plot that the electric field behaves like a plane wave in the vertical direction as we would expect. From figs. (4-3) to (4-7), |Ex| and accompanied phases are plotted as a function of kr for various fixed values of kz. These magnitudes are reproduced in a three dimensional plot in fig. (4-8).

With the incident fields so determined by (4-1), we are ready to find the current distribution induced on the buried wire (fig. (4-1)). That is, instead of using $Vo\cdot\delta(x)$ for $E_{ox}(\bar{\xi})$ in equation (3-14), the electric field found in (4-1) is used. In eq. (3-14) the Hertz potentials in section C of Chapter 2 are to be used and k_E, $1/\varepsilon$ are to replace k, ε. The current distributions on the wire for different locations and lengths are shown in fig. (4-9), (4-10) and (4-11).

Once the current are determined, eq. (4-1) is applied again to find the scattering fields. For a field point in the air, i = 2, j = 1. Results are shown in fig. (4-12) through (4-16).

As a primary check of the algorithm, we check the results with riciprocity theorem. That theorem states:

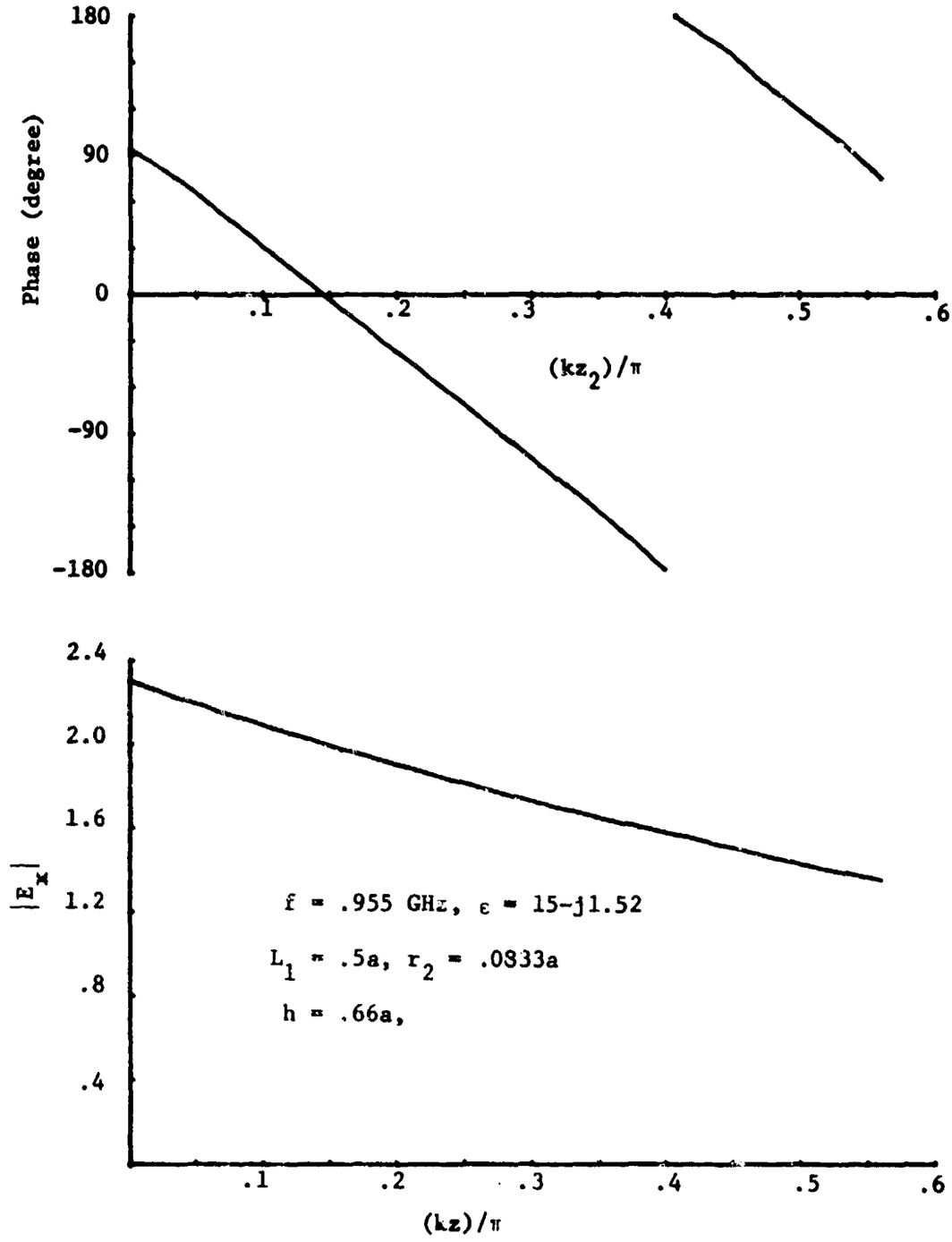

Fig. 4-2. x-component of electric field penetrating into the ground from a horizontal wire antenna. a = (π/k), notation is defined in fig. (4-1).

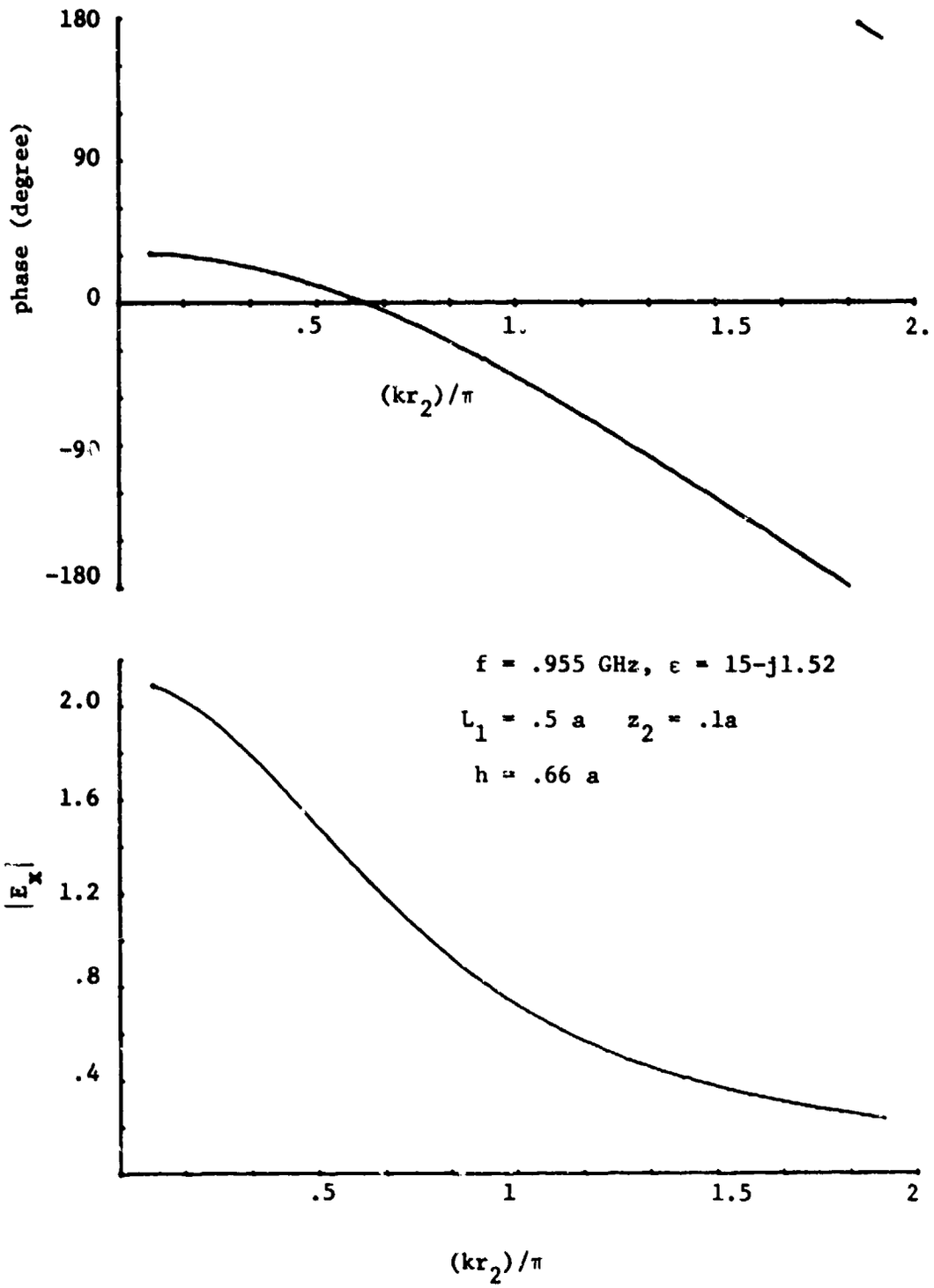

Fig. 4-3. x-component of electric field penetrating into the ground from a horizontal antenna. a = (π/k), notation is defined in fig. (4-1).

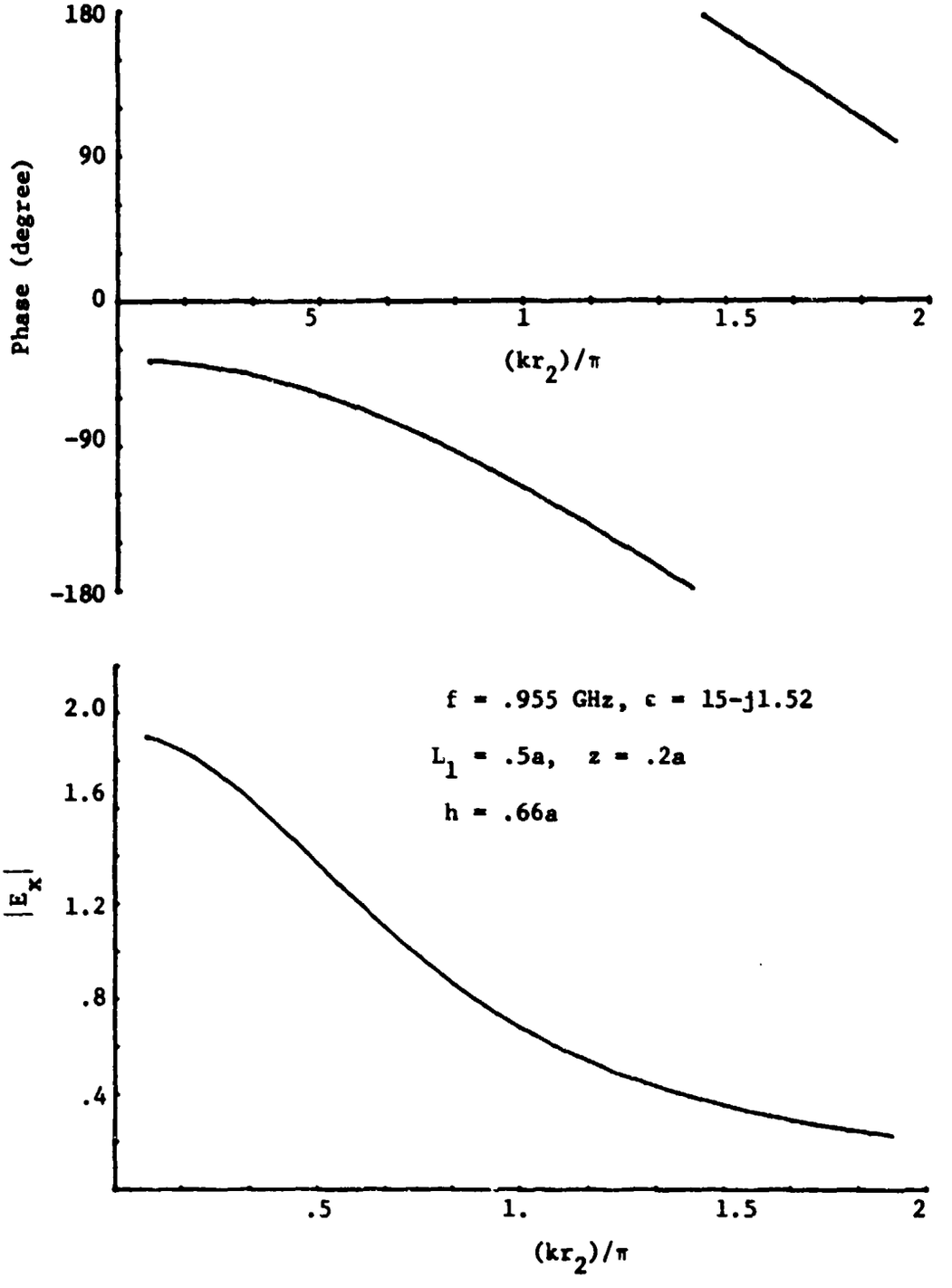

Fig. 4-4. x-component of electric field penetrating into the ground from a horizontal antenna. a = (π/k), notation is defined in fig. (4-1)

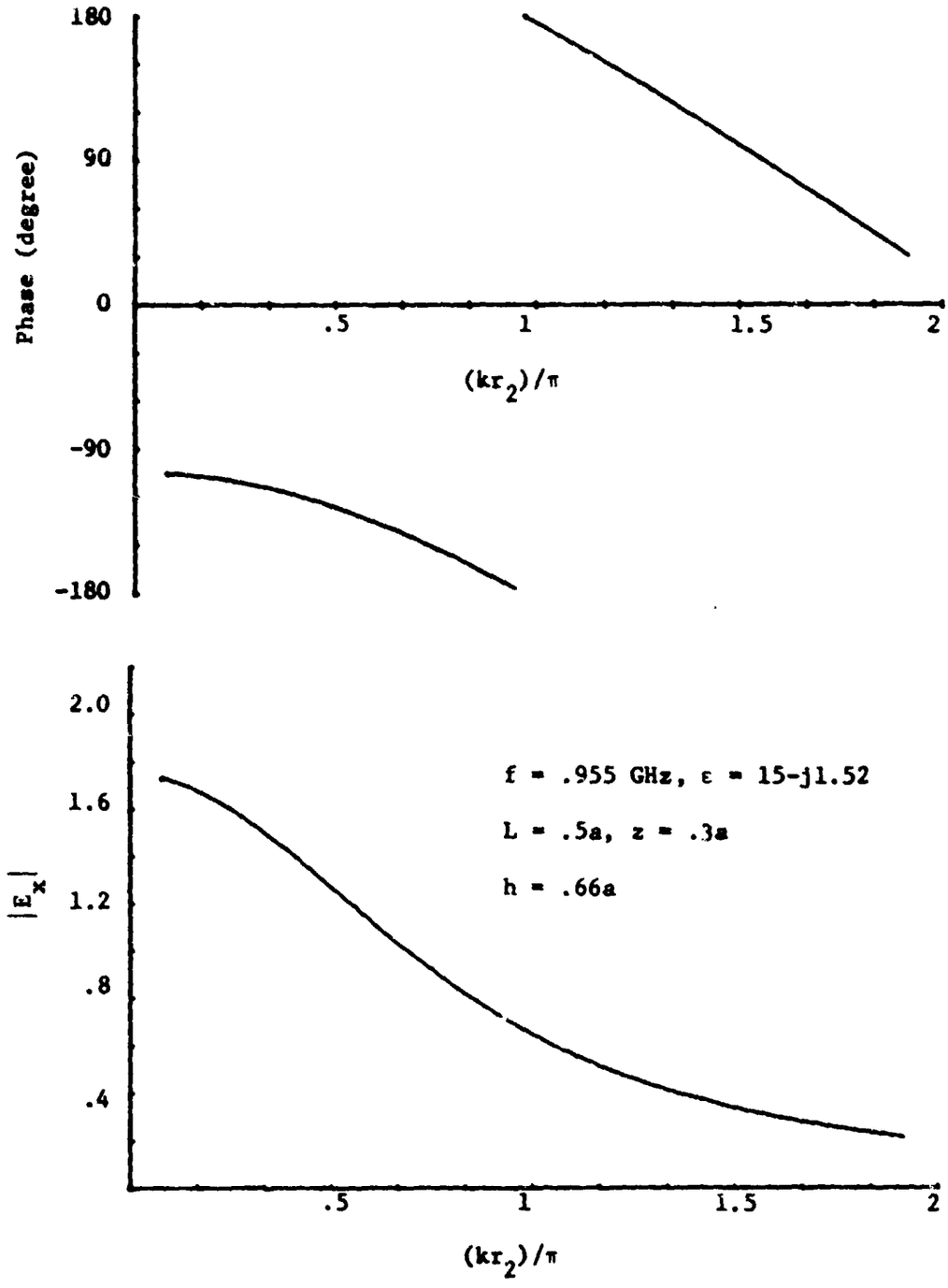

Fig. 4-5. x-component of electric field penetrating into the ground from a horizontal antenna. a = (π/k), notation is defined in fig. (4-1).

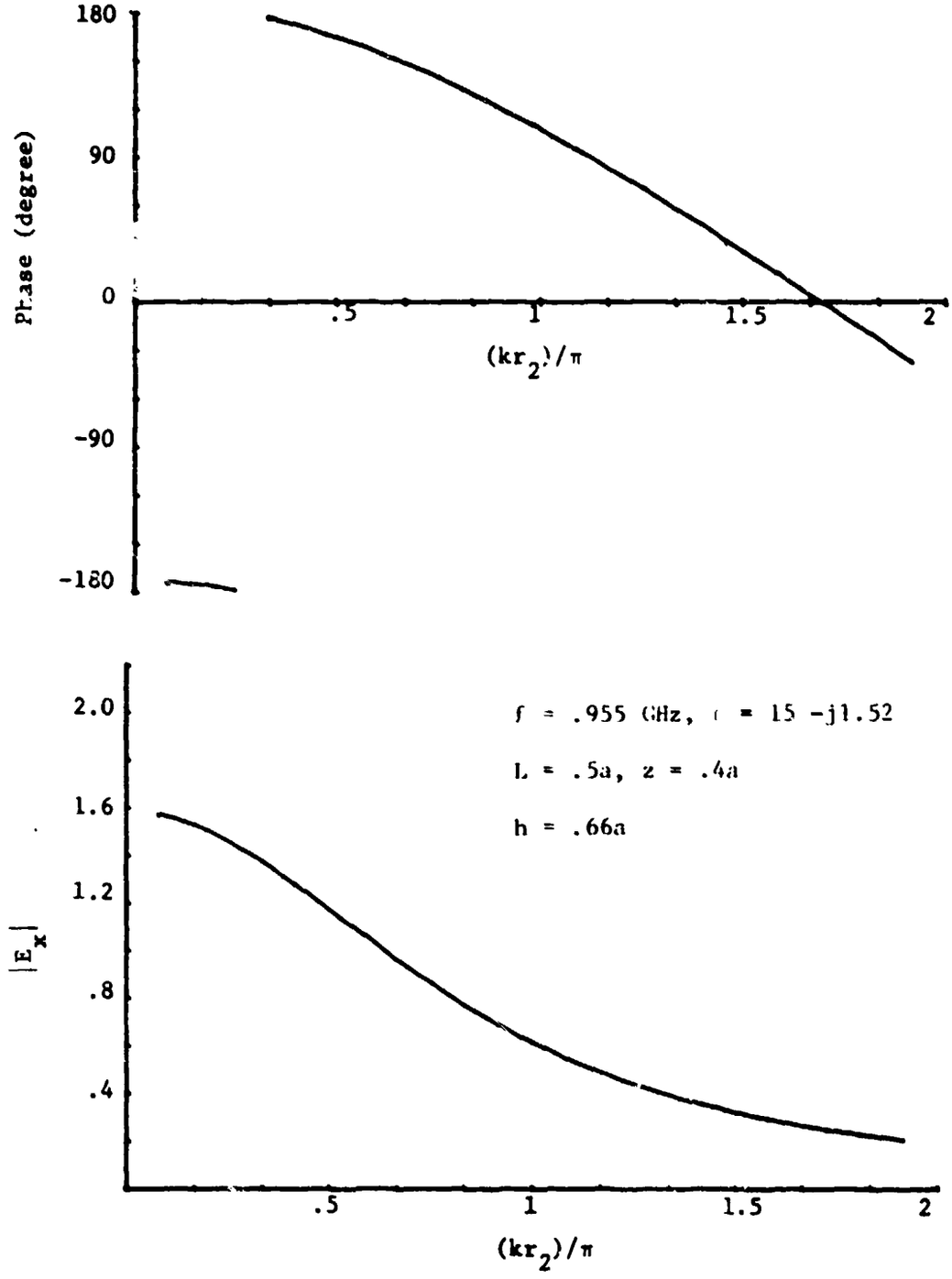

Fig. 4-6. x-component of electric field penetrating into the ground from a horizontal antenna. a = (π/k), notation is defined in fig. (4-1).

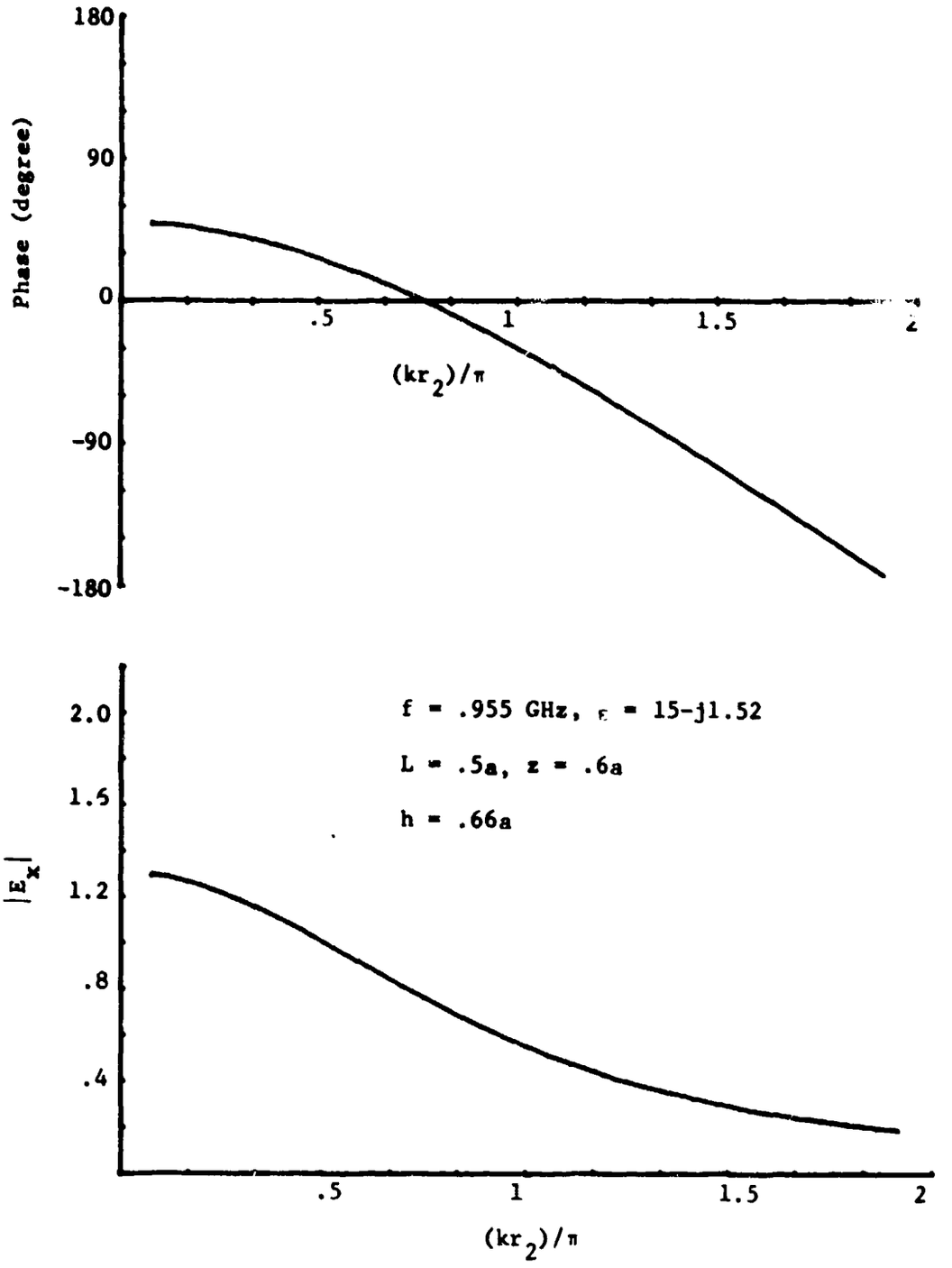

Fig. 4-7. x-component of electric field penetrating into the ground from a horizontal antenna. a = (π/k), notation is defined in fig. (4-1).

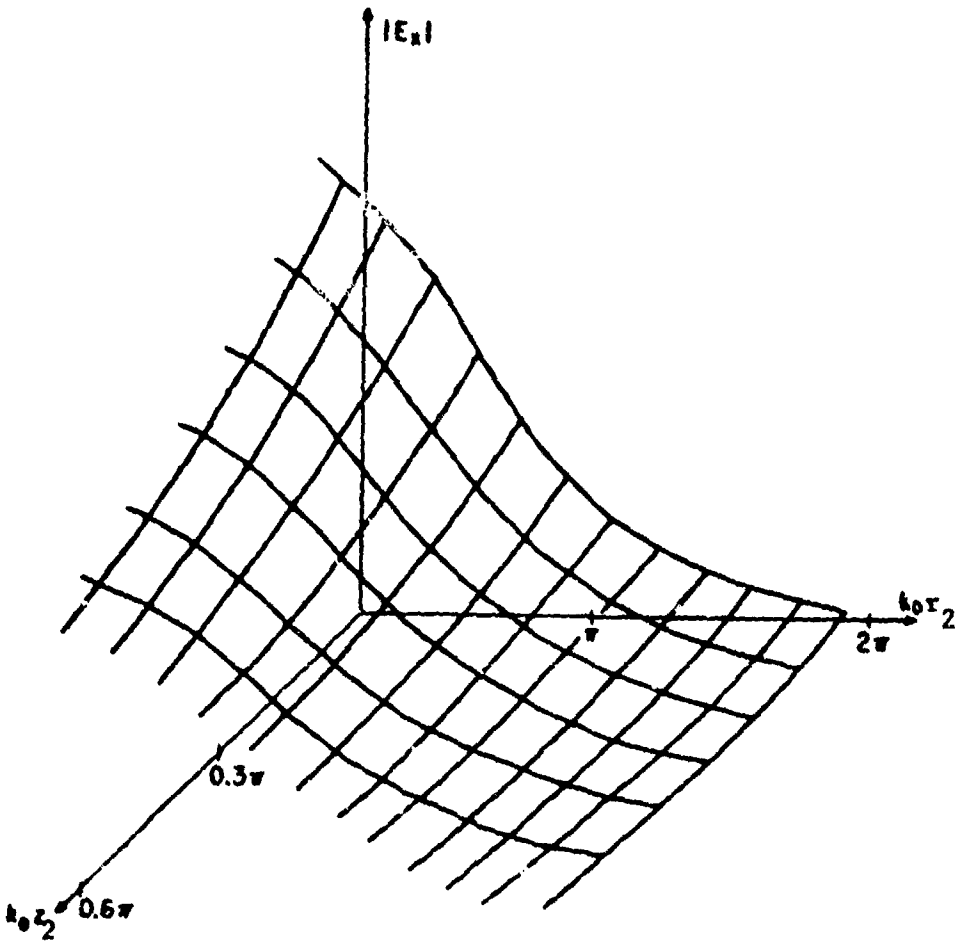

Fig. 4-8. Three-dimensional magnitude plot, which summarizes the results shown in Fig. 4-2 through Fig. 4-7.

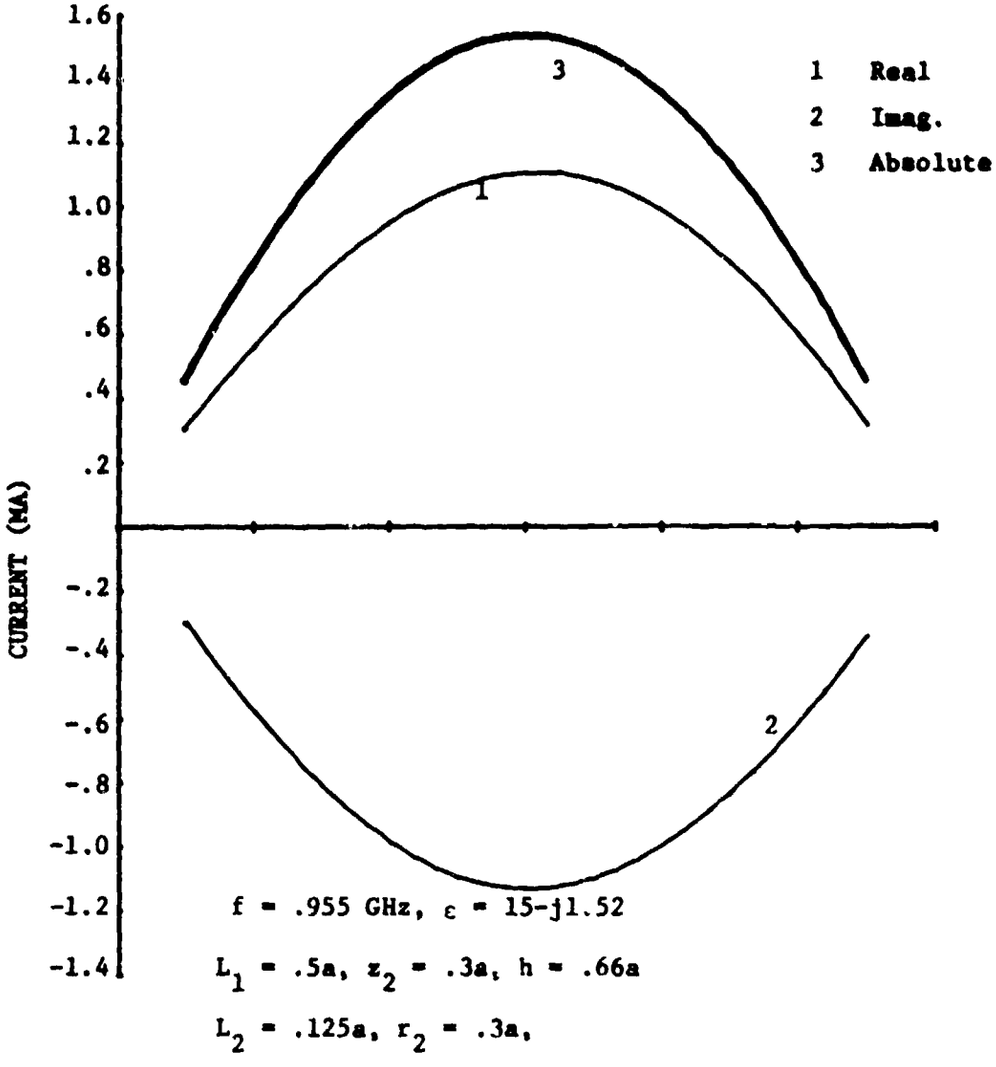

Fig. 4-9. Current induced on a horizontal wire buried in the ground. a = (π/k), notation is defined in fig. (4-1).

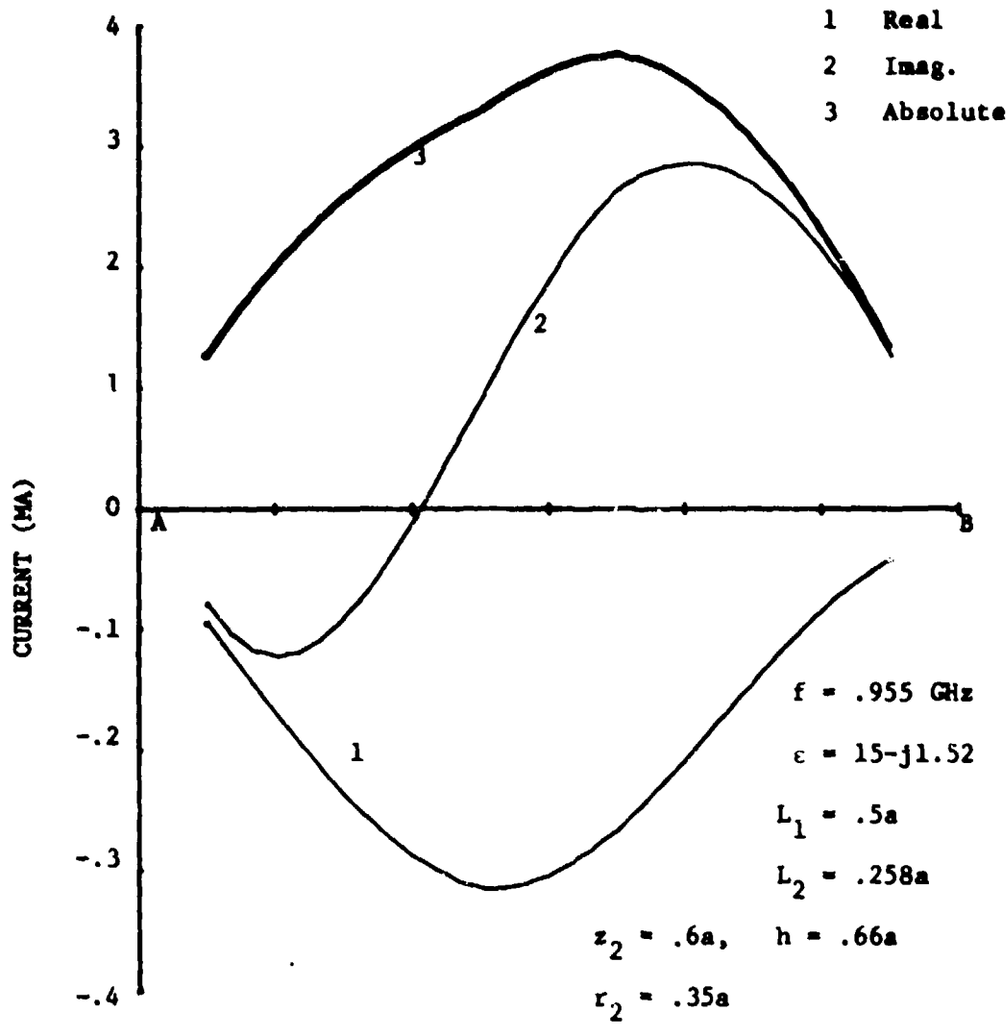

Fig. 4-10. Current induced on a horizontal wire buried in the ground. a = (π/k), notation is defined in fig. (4-1).

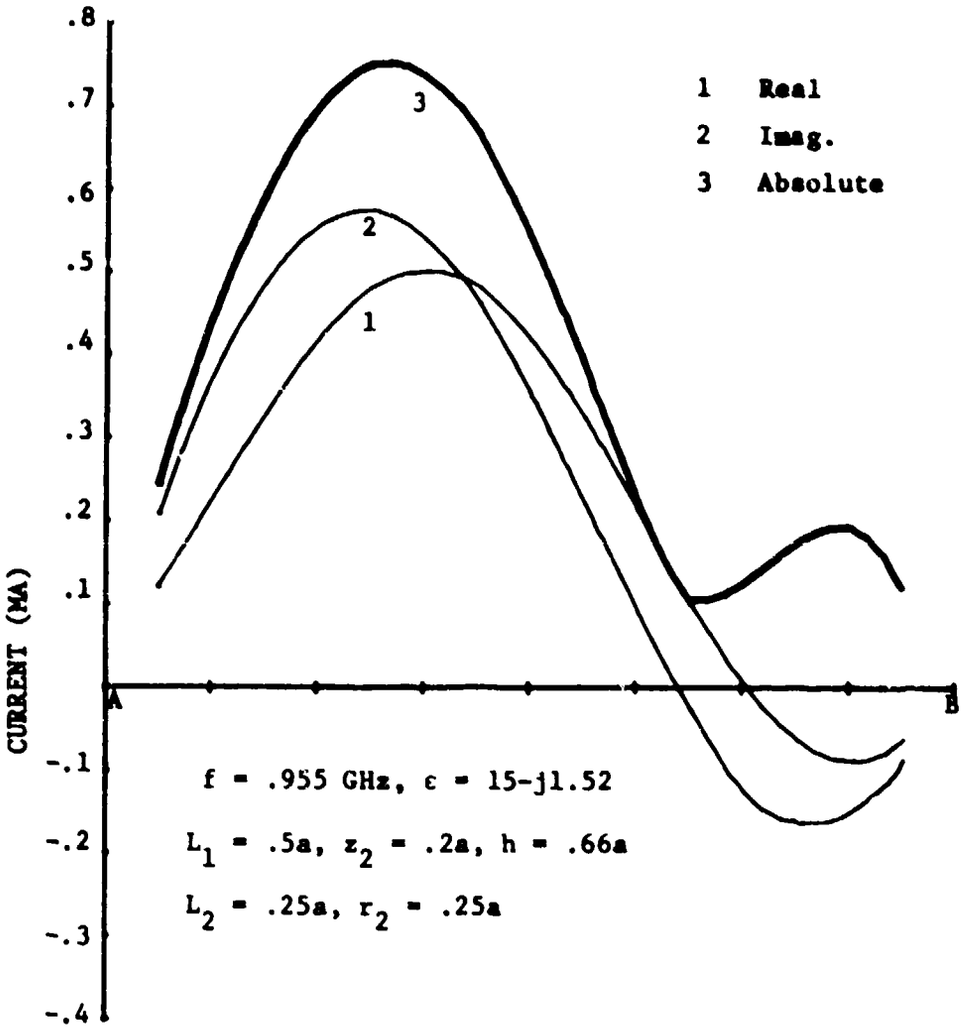

Fig. 4-11. Current induced on a horizontal wire buried in the ground. a = (π/k), notation is defined in fig. (4-1).

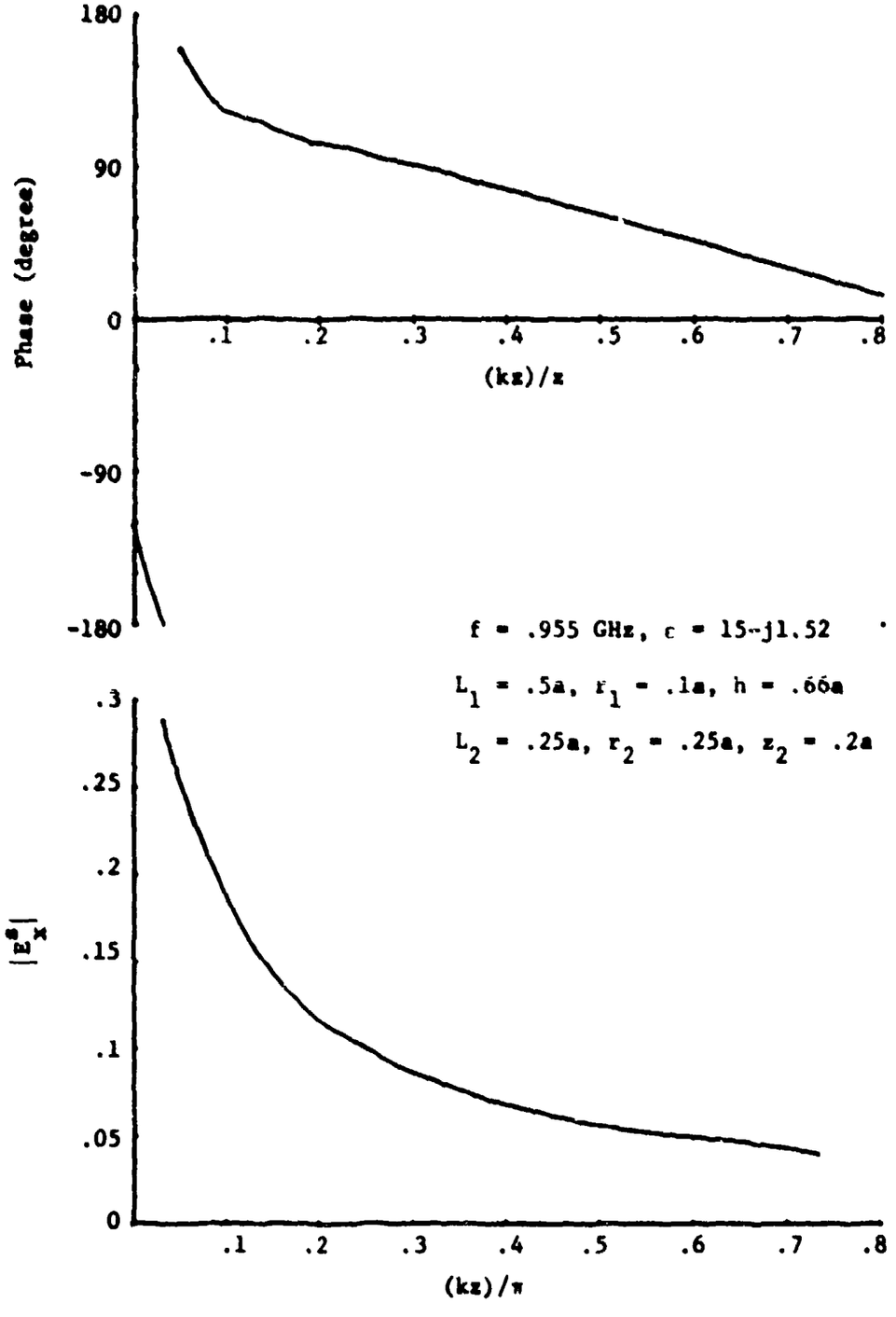

Fig. 4-12. x-component of scattering electric field by a buried wire; a = (π/k), notation is defined in fig. (4-1).

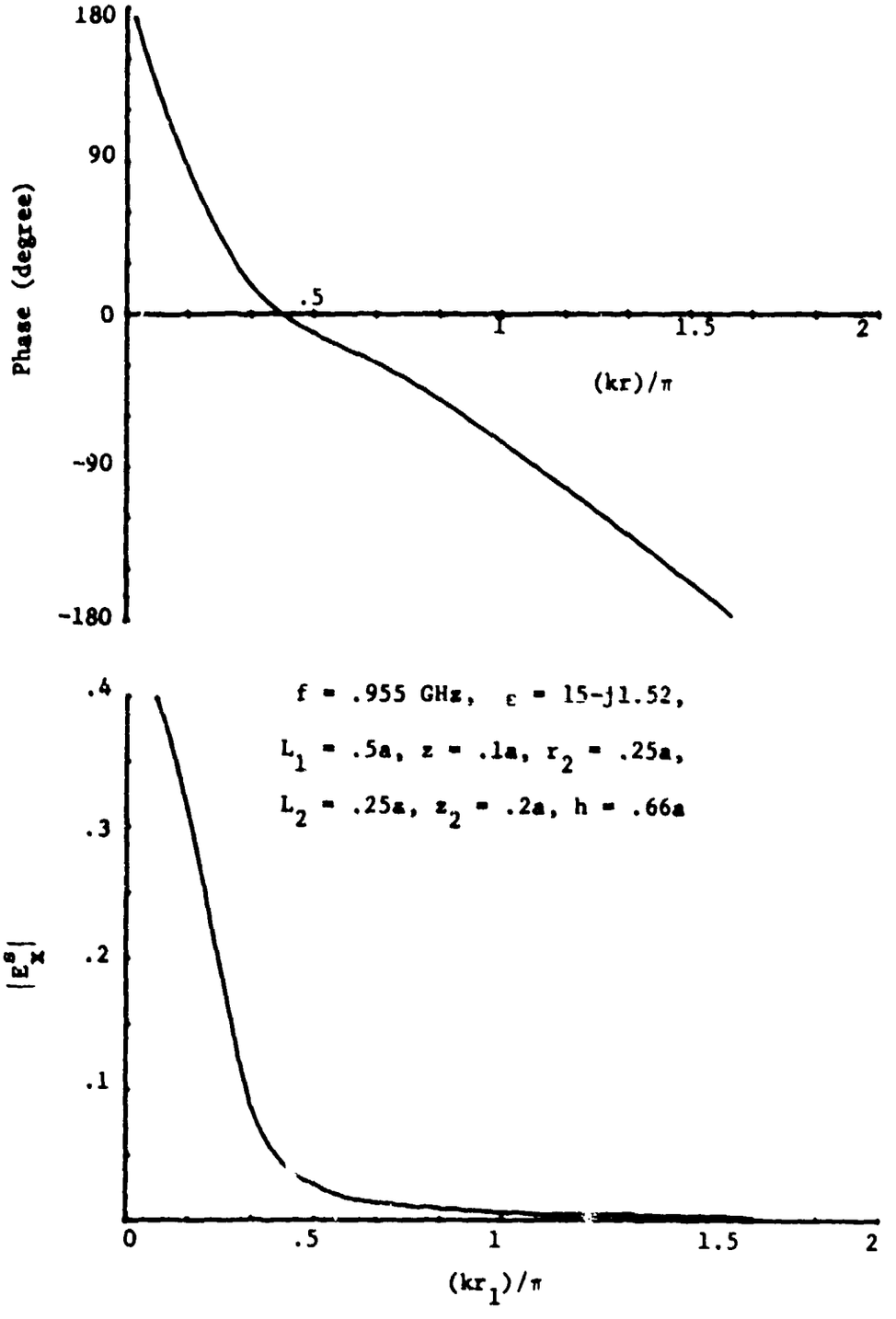

Fig. 4-13. x-component of scattering electric field by a buried wire, a = (π/k), notation is define in fig. (4-1).

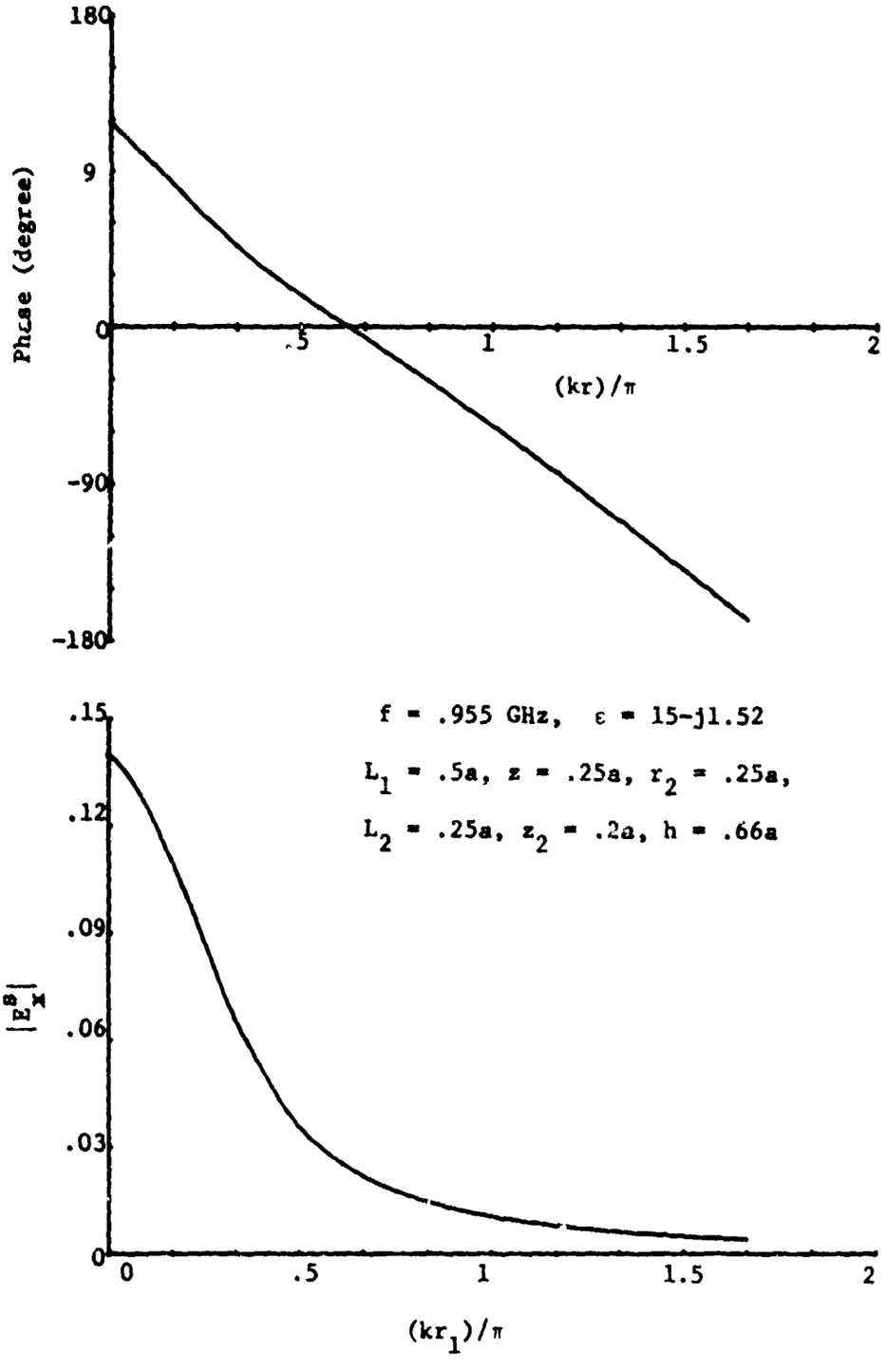

Fig. 4-14. x-component of scattering electric field by a buried wire. $a = (\pi/k)$, notation is defined in fig. (4-1).

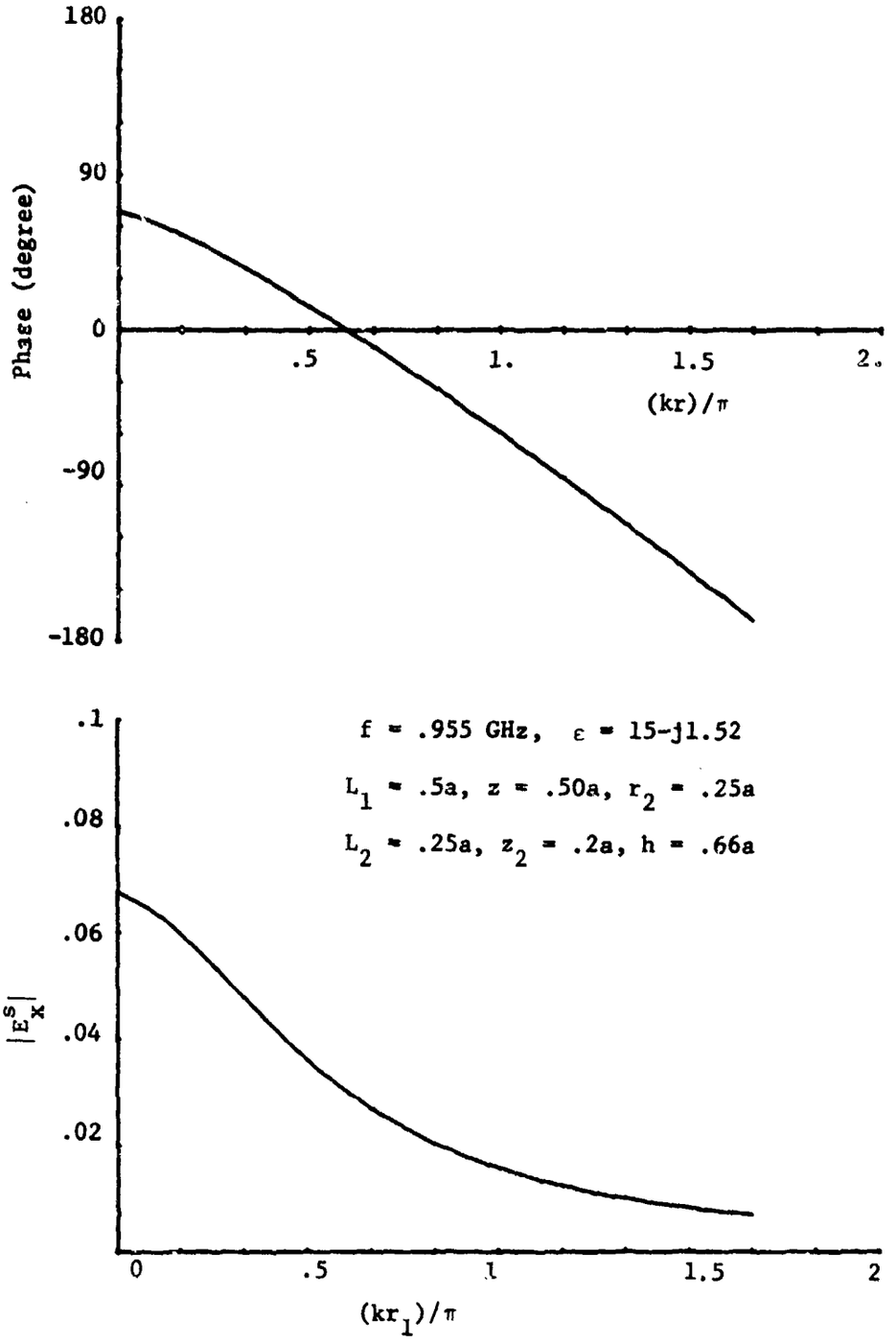

Fig. 4-15. x-component of scattering electric field by a buried wire. a = (π/k), notation is defined in fig. (4-1).

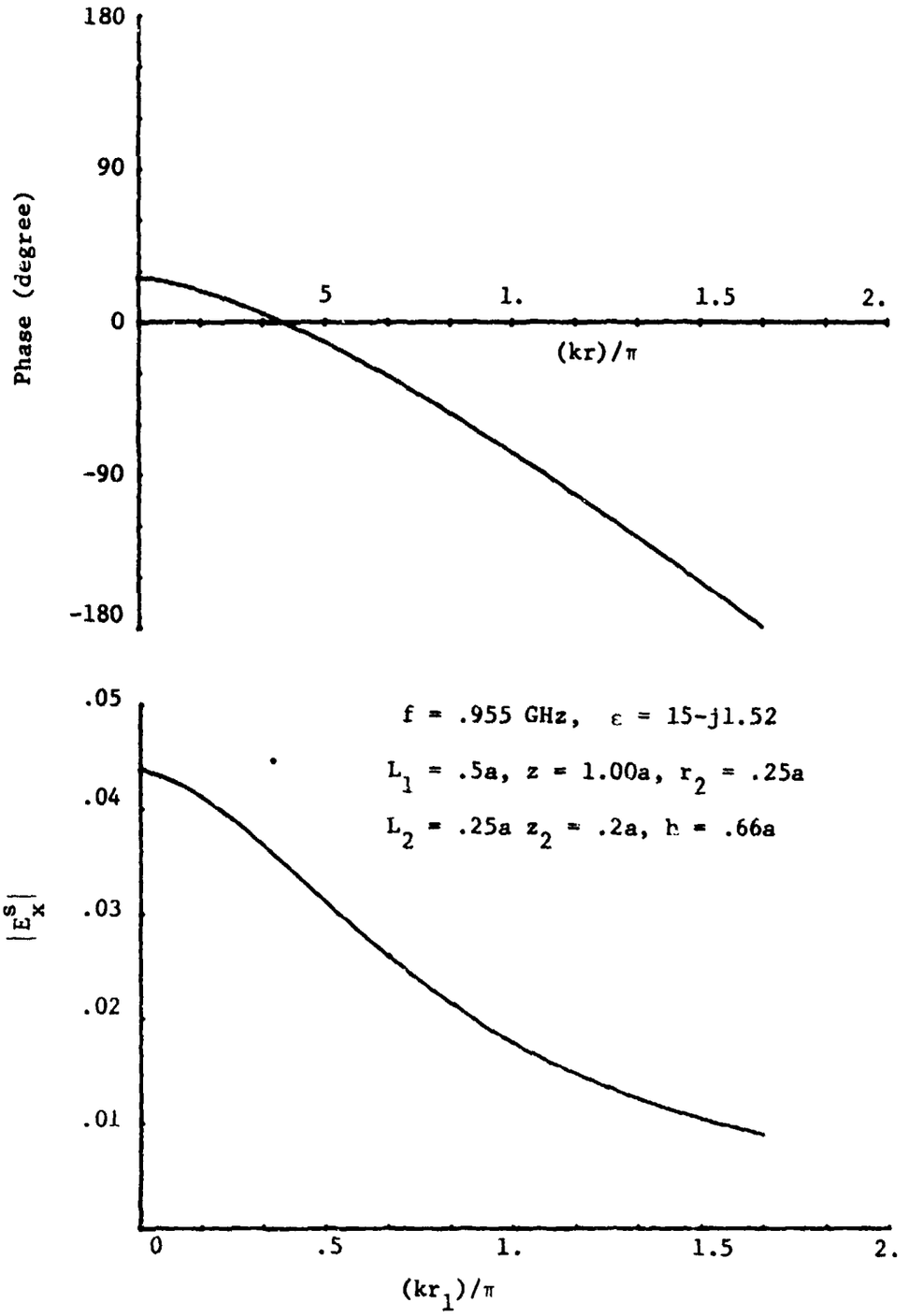

Fig. 4-16. x-component of scattering electric field by a buried wire. a = (π/k), notation is defined in fig. (4-1).

$$\int_V \bar{\bar{E}}^{12} \cdot J^2 dv' = \int_V \bar{\bar{E}}^{21} \cdot J^1 dv'; \qquad (4\text{-}4)$$

where indeces are used the same manner as those in eq. (4-2). For a particular case: $f = .955$ GHz, $\epsilon = 15 - j1.52$, $L_1 = .25\lambda_o$, $L_2 = .129\lambda_o$, $r = .175\lambda_o$, $z_2 = -.3\lambda_o$, and $h = .33\lambda_o$, (all the quantities are to be refered to Fig. (4-1) and λ_o is the free space wavelength). The integral on the right hand side yields a value of $(-1.67353\times10^{-6}-j3.7149\times10^{-7})$, in MKS system, and that of the left hand side $(-1.6727\times10^{-6}-j3.7056\times10^{-7})$.

References

1. Mei, K.K.: "Uni-moment Method of Solving Antenna and Scattering Problems", to be published.
2. Stratton, J.A.: "Electromagnetic Theory", McGraw-Hill, N.Y., (1941).
3. Harrington, R.F.: "Field Computation by Moment Methods", The Macmillan Company, N.Y., (1968).
4. Sommerfeld, A: "Partial Differential Equation in Physics", Academic Press, N.Y., (1964).
5. This part has been presented at 1972 USNC-URSI Spring Meeting, Washington, D.C. April 13-15, 1972.
6. Sommerfeld, A: "Uber die Ausbreitung der Wellen in der Drahtlosen Telegraphie", Ann. Physik, 81, S.1138, (1926).
7. Van der Pol, B.: "Theory of the Reflection of the Light from a Point Source by a finitely Conducting Flat Mirror, with an Application to Radiotelegraphy," Physica, 2 843 (1935).
8. Feynberg, Y.L.: "The Propagation of Radio Waves along the Surface of the Earth", English Trans. by Wright-Patterson Air Force Base, Ohio, (1967).
9. Kuo, W.C. and K.K. Mei: "Horizontal Dipole Arrays over Lossy Ground", U.S. AMERDC, Fort Belvoir, Virginia, Prepared by Electronics Research Lab., U. of Calif., Berkeley, Dec. 1971.
10. This part has been presented at International IEEE 1G-AP Symposium and USNC/URSI Meeting, Boulder, Colo., 21-24 Aug. 1973.
11. Mei, K.K.: "On the Integral Equation of Thin Wire Antennas", IEEE Trans. AP-13, 373, (1965).

Appendix A. Sommerfeld's Integrals for an Horizontal Dipole

For a unit infinitesimal dipole in free space the Hertz potential is given by

$$\pi = \frac{1}{R} e^{-jkR} \tag{A-1}$$

The spherical wave representation of (A-1) can be transformed to cylindrical wave representation by Bessel's transformation to obtain

$$\pi = \frac{e^{-jkR}}{R} = \int_0^\infty J_o(\lambda r) e^{-\nu|z-h|} \frac{\lambda}{\nu} d\lambda. \tag{A-2}$$

Where all distances are in meter and shown in fig. A-1; $J_o(\lambda r)$ is the Bessel's function of the zeroth order, and ν is given by

$$\nu = \sqrt{\lambda^2 - k^2} \tag{A-3}$$

with positive real part to insure the convergence of the integral and its vanishing at $|z| \to \infty$.

Now instead of considering the homogeneous infinite space, the half-space of $z \leq 0$ is the earth with refractive index

$$\varepsilon_r = \varepsilon' - j\,\varepsilon''/\varepsilon^o , \tag{A-4}$$

where ε' and ε'' are the real and imaginary part of the complex permitivity; ε'' is the loss factor for the ground, which is dominated by conduction loss in high frequencies. Since our major concern is application in high frequencies hence ε_r from now on will be understood by

$$\varepsilon_r = \varepsilon = (\varepsilon' - j\sigma/\omega)/\varepsilon_o$$

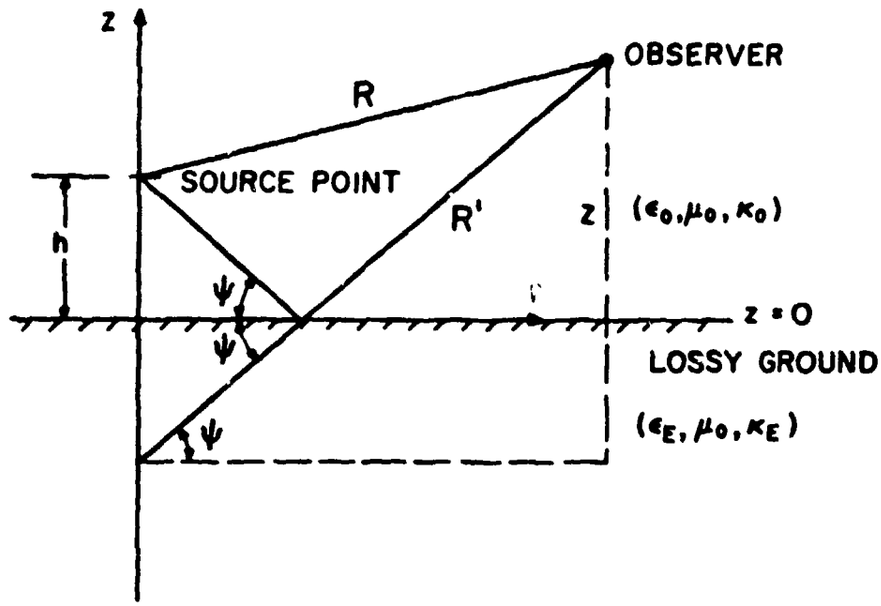

Fig. A-1. Geometry of a dipole over a lossy ground.

where σ is the conductivity. The magnetic permeability in the ground is taken as the same as that of free space and is noted as μ_o. Without loss of generality, the orientation of dipole axis is chosen along the x-direction in rectangular coordinate. The Hertz potential $\bar{\pi}$ is related to electric and magnetic field by the following relations:

$$\bar{E} = \nabla(\nabla\cdot\bar{\pi}) + k^2\bar{\pi} \ , \tag{A-5}$$

$$\bar{H} = j\omega \epsilon_o(\nabla x\bar{\pi}) \text{ for } z > 0, \tag{A-6}$$

where

$$\bar{\pi} = \hat{x}\, \pi_x + \hat{z}\, \pi_z,$$

$$\bar{E}_E = \nabla(\nabla\cdot\bar{\pi}_E) + k^2\bar{\pi}_E \ , \tag{A-5'}$$

$$\bar{H}_E = j\omega \epsilon (\nabla x\bar{\pi}_E) \quad \text{for } z < 0. \tag{A-6'}$$

Continuity of tangential electric and magnetic field at the plane z=0 requires

$$\pi_x = \epsilon\ \pi_{xE}; \frac{\partial \pi_x}{\partial z} = \frac{\epsilon\, \partial \pi_{xE}}{\partial z} \tag{A-7}$$

$$\pi_z = \epsilon\, \pi_{zE}; \frac{\partial \pi_z}{\partial z} - \frac{\partial \pi_{zE}}{\partial z} = \frac{\partial \pi_{xE}}{\partial x} - \frac{\partial \pi_x}{\partial x} \ . \tag{A-8}$$

Now for a point source above the ground, we may imagine that there is an image source in the ground, which produces a similar Hertz potential as in (A-2). The solution of the problem for $z > 0$ is then the composition of contribution from the primary source in the absence of the ground and secondary source induced by the ground. For $z < 0$, the Hertz potential will be represented in a similar manner, only then there is no primary

source. We shall consider the x-component first.

$$\pi_x = \pi_x^{prim} + \pi_x^{sec.} \tag{A-9}$$

$$= \int_0^\infty J_o(\lambda r) e^{-\nu|z-h|} \frac{\lambda}{\nu} d\lambda + \int_0^\infty F_1(\lambda) J_o(\lambda r) e^{-\nu(z+h)} d\lambda ,$$

$$\pi_{xE} = \int_0^\infty F_2(\lambda) J_o(\lambda r) e^{\nu_E z - rh} d\lambda , \tag{A-10}$$

where $\nu_E = \sqrt{\lambda^2 - k_E^2}$ with positive real part and $F_1(\lambda)$, $F_2(\lambda)$ are weighting factors yet to be determined. Using (A-9) and (A-10) in (A-12) we find that

$$F_1(\lambda) = \frac{\lambda}{\nu} \left(-1 + \frac{2\nu}{\nu + \nu_E}\right), \quad F_2(\lambda) = \frac{1}{\varepsilon} \frac{2\lambda}{\nu + \nu_E} .$$

And the solutions are then,

$$\pi_x = \frac{e^{-jkR}}{R} - \frac{e^{-jkR'}}{R'} + 2 \int_0^\infty J_o(\lambda r) e^{-\nu(z+h)} \frac{\lambda d\lambda}{\nu + \nu_E} , \tag{A-11}$$

$$\pi_{xE} = \frac{2}{\varepsilon} \int_0^\infty J_o(\lambda r) e^{\nu_E z - \nu h} \frac{\lambda d\lambda}{\nu + \nu_E} , \tag{A-12}$$

where $R^2 = r^2 + (z-h)^2$, $R'^2 = r^2 + (z+h)^2$.

To find π_z and π_{zE}, note first that there is no primary component for π_z, since the dipole is x-oriented. Note also that there is $(\partial \pi_x / \partial x)$ in boundary condition (A-8), and

$$\frac{\partial \pi_x}{\partial x} = \frac{\partial \pi_x}{\partial r} \frac{\partial r}{\partial x} = \cos \phi \frac{\partial \pi_x}{\partial r} ,$$

where ϕ is the angle between x-axis and $\bar{r}$, hence π_z must contain the factor cos ϕ and will be constructed by $J_1(\lambda r)$ instead of $J_o(\lambda r)$. Thus

$$\pi_z = \cos\phi \int_0^\infty J_1(\lambda r) e^{-\nu(z+h)} \Phi_1(\lambda) d\lambda \tag{A-13}$$

$$\pi_{zE} = \cos\phi \int_0^\infty J_1(\lambda r) e^{\nu_E z - \nu h} \Phi_2(\lambda) d\lambda \tag{A-14}$$

where $\Phi_1(\lambda)$ and $\Phi_2(\lambda)$ like $F_1(\lambda)$ and $F_2(\lambda)$ are factors to be determined. Solving (A-8), (A-13) and (A-14), we find that

$$\Phi_1 = -\frac{2\lambda^2}{k^2} \frac{\nu - \nu_E}{\varepsilon\nu - \nu_E} \text{ and } \Phi_2 = \Phi_1/\varepsilon$$

Therefore

$$\pi_z = -\frac{2}{k} \cos\phi \int_0^\infty J_1(\lambda r) e^{-\nu(z+h)} \frac{\nu - \nu_E}{\varepsilon\nu + \nu_E} \lambda^2 d\lambda \tag{A-15}$$

$$\pi_{zE} = -\frac{2}{k_E^2} \cos\phi \int_0^\infty J_1(\lambda r) e^{\nu_E z - \nu h} \frac{\nu - \nu_E}{\varepsilon\nu + \nu_E} \lambda^2 d\lambda \tag{A-16}$$

Equation (A-11), (A-12), (A-15), (A-16) form the complete set of Hertz potential for a horizontal dipole above the ground. The dependence of both source and observation point appears only on the exponential terms of all integrals in these equations. These exponential terms, however, are crucial to the convergence of integrals.

Since we are solving boundary value problem without using the knowledge of specific property of parameters. Hence if the dipole is located in the ground we expect to obtain a set of solutions similar to those of equation (A-11), (A-12), (A-15) and (A-16). Only now k_E, k,

ν_E, ν, $1/\varepsilon$ have to replace k, k_E, ν, ν_E, ε respectively.

Appendix B. Transformation of Sommerfeld's Integral

We wish to transform eq. (2-13) to the form of eq. (2-15).

$$I = \int_0^\infty J_o(\lambda r) e^{-\nu(z+h)} \frac{\lambda}{\nu + jk\sqrt{\varepsilon_1^o}} \frac{d\lambda}{\nu} \quad . \tag{B-1}$$

Multiplying both sides by $e^{-jk\sqrt{\varepsilon_1^o}\, z}$ we get

$$e^{-jk\sqrt{\varepsilon_1^o}\, z} I = \int_0^\infty J_o(\lambda r) e^{-(\nu+jk\sqrt{\varepsilon_1^o})z} e^{-\nu h} \frac{\lambda d\lambda}{(\nu + jk\sqrt{\varepsilon_1^o})\nu} \quad .$$

Differentiating both sides with respect to z

$$\frac{\partial}{\partial z}\left(e^{-jk\sqrt{\varepsilon_1^o}\, z} I\right) = - \int_0^\infty J_o(\lambda r) e^{-(z+h)} \frac{\nu}{\lambda} e^{-jk\sqrt{\varepsilon_1^o}\, z} d\lambda$$

$$= - e^{-jkR'} e^{-jk\sqrt{\varepsilon_1^o}\, z} \quad .$$

$$\therefore \quad I = - e^{-jk\sqrt{\varepsilon_1^o}\, z} \int_c^z \frac{e^{-jkR'_\xi}}{R'_\xi} e^{-jk\sqrt{\varepsilon_1^o}\, \xi} d\xi$$

$$= - \int_c^z e^{-jk[R'_\xi + \sqrt{\varepsilon_1^o}\,(\xi - z)]} \frac{d\xi}{R'_\xi} \quad . \tag{B-2}$$

where R' and R'_ξ are defined the same as those in Chapter 2. c is the integral limit such that the integral converges. It is proved that c may be chosen as $-j\infty$, since at this limit the integrand vanishes.

PART THREE

TWO-DIMENSIONAL SCATTERING BY DIELECTRIC BODIES

[The formula and figure number referred to in this part all belong to this part.]

I. Introduction

Consider the electromagnetic scattering properties of dielectric cylinders with finite cross-section. If the dimension of the scatterer is of several wavelengths or larger, the problem can be solved by geometrical optics approximation. On the other hand, the well-known low-frequency Rayleigh approximation is suitable to solve the small problems with dimension less than fractions of a wavelength. For the problems around the size of a wavelength, integral equations played an important role in computing the scattering fields [2], [3], [5], [6]. Another way to calculate the fields is the analytic continuation method [4]. Recently the blooming techniques of the Finite Element Methods in solving boundary value problems enable us to develop a numerical technique to tackle the problem with great versatility. In this report, the Uni-moment Method [1] is applied to calculate the scattering fields of dielectric cylinders of arbitrary cross-section or of inhomogeneously loaded material. The basic technique of the method is the use of the Finite Element Methods inside a mathematical circle, which encloses the inhomogeneous body. The fields outside are expanded in the usual cylindrical expansion. The interior and exterior problems are first solved separately and later coupled by the continuity condition of the E and H fields. The versatility is increased greatly by introducing the method of "Inhomogeneous Element". The advantage of the proposed method is the simplicity and efficiency in programming. Various problems can be solved by the same program. And the input control for the shape and material can be made very simple.

The following discussions will include both E-wave ($E_z \neq 0$, $H_z = 0$) and H-wave ($E_z = 0$, $H_z \neq 0$) scattering of dielectric cylinders of arbitrary crossection, or of inhomogeneous material such as Luneberg lens. With-

out any further effort, scattering of multiple cylinders is also computable by the same program. The incident wave is remained unrestricted in the method; it may be a plane wave, waves generated by line sources, or waves generated by other kind of sources. All the fields computed are assumed to have the conventional exp(jwt) harmonic time dependence.

II. The Uni-moment Method

Consider the incident waves propagate in the direction normal to the z-axis--the axis of the dielectric cylinder. The whole system is uniform in the axial direction. From the differential form of Maxwell's equations, we know that E-wave and H-wave are separable. Thus, we may investigate these two kinds of fields separately. A circle with radius r = a is drawn to enclose the entire scatterer. (Fig. 1).

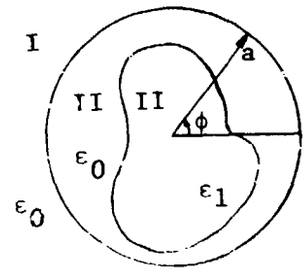

Fig. 1. Construction of the Mathematical Circle

Let the incident wave be represented by E_z^{inc} for E-wave and H_z^{inc} for H-wave. Let E_z^I (or H_z^I) be the scattered field in region I ($r > a$); E_z^{II} (or H_z^{II}) be the field in region II ($r < a$). At the artificial circular boundary ($r = a$), the tangential components of E and H fields are continuous, i.e., for E-wave:

$$E_z^{II}(a,\phi) = E_z^{inc}(a,\phi) + E_z^{I}(a,\phi); \quad 0 \leq \phi \leq 2\pi \tag{1}$$

and

$$\frac{\partial E_z^{II}}{\partial r}(r,\phi)\bigg|_{r=a} = \frac{\partial E_z^{inc}}{\partial r}(r,\phi)\bigg|_{r=a} + \frac{\partial E_z^{I}}{\partial r}(r,\phi)\bigg|_{r=a}; \quad 0 \leq \phi \leq 2\pi \tag{2}$$

Or for H-wave:

$$H_z^{II}(a,\phi) = H_z^{inc}(a,\phi) + H_z^{I}(a.\phi);\ 0 \leq \phi \leq 2\pi \tag{1'}$$

and

$$\frac{\partial H_z^{II}}{\partial r}(r,\phi)\bigg|_{r=a} = \frac{\partial H_z^{inc}}{\partial r}(r,\phi)\bigg|_{r=a} + \frac{\partial H_z^{I}}{\partial r}(r,\phi\ \bigg|_{r=a};\ 0 \leq \phi \leq 2\pi \tag{2'}$$

Since the normal derivative value of H_z at a dielectric boundary is discontinuous, it is convenient to have the artificial circle a little larger to make sure that both eqs. (1') and (2') hold.

$E_z^I(r,\phi)$ [or $H_z^I(r,\phi)$] is an outgoing wave in free space. The general solution is expressed by

$$E_z^I(r,\phi)\ [or\ H_z^I(r,\phi)] = \sum_{n=0}^{\infty} H_n^{(2)}(k_o r)\ (A_n \cos n\phi + B_n \sin n\phi) \tag{3}$$

where $H_n^{(2)}$ is the Hankel's function of second kind of order n,

$$k_o = w\sqrt{\mu_o \varepsilon_o}$$

A_n, B_n are arbitrary constants to be determined.

There are two different kinds of the Uni-moment Methods which work equally well: the Dirichlet type and the Neumann type. We shall discuss these two methods in detail separately.

(A) The Dirichlet type:

The main idea of the method is to replace $E_z^{II}(a,\phi)$ [or $H_z^{II}(a,\phi)$] by a linear combination of a set of basis functions $e_n(\phi)$, n = 1, 2, 3, ... of the continuous functional space $C[0,2\pi]$. That is, assume

$$E_z^{II}(a,\phi) \text{ [or } H_z^{II}(a,\phi)] = \sum_{n=1}^{\infty} c_n e_n(\phi) \tag{4}$$

where $e_n(\phi)$ are assigned known functions (e.g., polynomials, or sin $n\phi$ and cos $n\phi$); c_n are called moments, which are unknown. Then, by the linearity of the material (i.e., ε, μ are independent of the field strength,) $E_z^{II}(r,\phi)$ [or $H_z^{II}(r,\phi)$] can be expressed by

$$E_z^{II}(r,\phi) \text{ [or } H_z^{II}(r,\phi)] = \sum_{n=1}^{\infty} c_n \psi_n(r,\phi) \ . \tag{5}$$

In eq. (5), $\psi_n(r,\phi)$ is the solution of the following system:

E-wave:

$$\nabla^2 \psi_n(r,\phi) + k_o^2 \varepsilon_r(r,\phi) \psi_n(r,\phi) = 0 \tag{6}$$

H-wave:

$$\nabla \cdot \left[\frac{1}{\varepsilon_r(r,\phi)} \nabla \psi_n(r,\phi) \right] + k_o^2 \psi_n(r,\phi) = 0 \tag{7}$$

subject to the boundary condition

$$\psi_n(a,\phi) = e_n(\phi); \quad 0 \le \phi \le 2\pi \tag{8}$$

where

$$\varepsilon_r(r,\phi) = \varepsilon(r,\phi)/\varepsilon_o \ .$$

The numerical solution of $\psi_n(r,\phi)$ are generated by the Finite Element Methods which will be described in the next section. From the values of $\psi_n(r,\phi)$ obtained, it is possible to calculate $\frac{\partial \psi_n}{\partial r}(r,\phi)\Big|_{r=a}$. Hence

$$\frac{\partial E_z^{II}}{\partial r}(r,\phi)\bigg|_{r=a} \left[\text{or } \frac{\partial H_z^{II}}{\partial r}\bigg|_{r=a}\right] = \sum_{n=1}^{\infty} c_n \frac{\partial \psi_n}{\partial r}(r,\phi)\bigg|_{r=a} . \tag{9}$$

From eqs. (3), (4), and (9), plugg into eqs. (1) and (2) [or eqs. (1'), and (2')] we get

$$\sum_{n=1}^{\infty} c_n e_n(\phi) = E_z^{inc}(a,\phi) \ [\text{or } H_z^{inc}(a,\phi)] + \sum_{n=0}^{\infty} H_n^{(2)}(k_o a)(A_n \cos n\phi + B_n \sin n\phi) \tag{10}$$

and

$$\sum_{n=1}^{\infty} c_n \frac{\partial \psi_n}{\partial r}(r,\phi)\bigg|_{r=a} = \frac{\partial E_z^{inc}}{\partial r}(r,\phi)\bigg|_{r=a} \left[\text{or } \frac{\partial H_z^{inc}}{\partial r}(r,\phi)\bigg|_{r=a}\right]$$

$$+ \sum_{n=0}^{\infty} k_o H_n^{(2)'}(k_o a)(A_n \cos n\phi + B_n \sin n\phi) . \tag{11}$$

The unknown coefficients A_n's, B_n's, and C_n's can be solved from eq. (10) and eq. (11). Approximate solutions are obtained by either point-matching or weighted least-square method. It is more convenient if we choose $e_n(\phi)$ to be trigonometric functions sin $n\phi$ and cos $n\phi$. If this is the case,

$$E_z^{II}(a,\phi) \ [\text{or } H_z^{II}(a,\phi)] = \sum_{n=0}^{\infty} (C_n \cos n\phi + D_n \sin n\phi) . \tag{12}$$

Let $\psi_n^{c(s)}(r,\phi)$ be the solution of eq. (6) [or eq. (7)] with the boundary condition

$$\psi_n^c(a,\phi) = \cos n\phi \ (13) , \tag{14}$$

$$\psi_n^s(a,\phi) = \sin n\phi .$$

Similar to eq. (10), we have

$$\sum_{n=0}^{\infty}(C_n \cos n\phi + D_n \sin n\phi) = E_z^{inc}(a,\phi)[\text{or } H_z^{inc}(a,\phi)]$$

$$+ \sum_{n=0}^{\infty} H_n^{(2)}(k_o a)(A_n \cos n\phi + B_n \sin n\phi) . \qquad (15)$$

Similar to eq. (11), we have

$$\sum_{n=0}^{\infty} \left(C_n \frac{\partial \psi_n^c}{\partial r}(r,\phi)\Big|_{r=a} + D_n \frac{\partial \psi_n^s}{\partial r}(r,\phi)\Big|_{r=a}\right) = \frac{\partial E_z^{inc}}{\partial r}(r,\phi)\Big|_{r=a} \left[\text{or } \frac{\partial H_z^{inc}}{\partial r}(r,\phi)\Big|_{r=a}\right]$$

$$+ \sum_{n=0}^{\infty} k_o H_n^{(2)'}(k_o a)(A_n \cos n\phi + B_n \sin n\phi) . \qquad (16)$$

So, from eq. (15),

$$C_n = A_n H_n^{(2)}(k_o a) + f_n^c , \qquad (17)$$

$$D_n = B_n H_n^{(2)}(k_o a) + f_n^s , \qquad (18)$$

where

$$f_n^c = \frac{1}{\pi}\int_0^{2\pi} E_z^{inc}(a,\phi) \left[\text{or } H_z^{inc}(a,\phi)\right] \cos n\phi \, d\phi , \qquad (19)$$

$$f_n^s = \frac{1}{\pi}\int_0^{2\pi} E_z^{inc}(a,\phi) \left[\text{or } H_z^{inc}(a,\phi)\right] \sin n\phi \, d\phi . \qquad (20)$$

From eqs. (16), (17), and (18),

$$\sum_{n=0}^{\infty} \left[A_n \left(H_n^{(2)}(k_o a) \frac{\partial \psi_n^c}{\partial r}(r,\phi)\Big|_{r=a} - k_o H_n^{(2)'}(k_o a) \cos n\phi\right) + B_n \left(H_n^{(2)}(k_o a) \frac{\partial \psi_n^s}{\partial r}(r,\phi)\Big|_{r=a}\right.\right.$$

$$\left.\left. - k_o H_n^{(2)'}(k_o a) \sin n\phi\right)\right] = \frac{\partial E_z^{inc}}{\partial r}(r,\phi)\Big|_{r=a} \left[\text{or } \frac{\partial H_z^{inc}}{\partial r}(r,\phi)\Big|_{r=a}\right]$$

$$- \sum_{n=0}^{\infty} \left[f_n^c \frac{\partial \psi_n^c}{\partial r}(r,\phi)\Big|_{r=a} + f_n^s \frac{\partial \psi_n^s}{\partial r}(r,\phi)\Big|_{r=a}\right] \qquad (21)$$

The above summation is truncated to N terms. Following the analysis given by Wilton & Mittra (4) and the numerical data available, N is chosen to be a number slightly larger than $k_o a$. Then, multiplying both sides of eq. (21) by sin $n\phi$, (n = 1, 2, ... N) and cos $n\phi$ (n = 0, 1, 2, ... N) an' integrating from 0 to 2π, we end up with a set of linear equations which can be used to solve for A_n's and B_n's. Note that only the right hand side vector is affected by the incident fields.

(B) The Neumann type:

The idea is quite similar to the Dirichlet type. The only difference is to assume

$$\frac{\partial E_z^{II}}{\partial r}(r,\phi)\bigg|_{r=a} \left[\text{or } \frac{\partial H_z^{II}}{\partial r}(r,\phi)\bigg|_{r=a}\right] = \sum_{n=1}^{\infty} C_n e_n(\phi) \tag{21}$$

where C_n, e_n are defined as before. Following the same argument as that in the Dirichlet type, eq. (5) holds, and $\psi_n(r,\phi)$ is the solution of eq. (6) or eq. (7) subject to the boundary condition

$$\frac{\partial \psi_n}{\partial r}(r,\phi)\bigg|_{r=a} = e_n(\phi); \quad 0 \le \phi \le 2\pi \ . \tag{22}$$

The numerical solution of $\psi_n(r,\phi)$ are generated by the Finite Element methods. Hence,

$$E_z^{II}(a,\phi) \ [\text{or } H_z^{II}(a,\phi)] = \sum_{n=1}^{\infty} C_n \psi_n(a,\phi) \ . \tag{23}$$

From eq. (21) and eq. (23), similar results as eq. (10) and eq. (11) are

$$\sum_{n=1}^{\infty} C_n \psi_n(a,\phi) = E_z^{inc}(a,\phi)[\text{or } H_z^{inc}(a,\phi)] + \sum_{n=0}^{\infty} H_n^{(2)}(k_o a)(A_n \cos n\phi + B_n \sin n\phi) \tag{24}$$

and

$$\sum_{n=1}^{\infty} C_n e_n(\phi) = \frac{\partial E_z^{inc}}{\partial r}(r,\phi)\Big|_{r=a} \left[\text{or } \frac{\partial H_z^{inc}}{\partial r}(r,\phi)\Big|_{r=a}\right]$$

$$+ \sum_{n=0}^{\infty} k_o H_n^{(2)'}(k_o a)(A_n \cos n\phi + B_n \sin n\phi). \qquad (25)$$

The unknown coefficients A_n's, B_n's, and C_n's are then solved from eqs. (24) and (25) in a similar way as that of the Dirichlet type.

Several advantages have been found in the methods discussed above:

(1) The artificial circle enables us to solve the interior and exterior problems separately. Only the interior problem involves inhomogeneous materials of various scatterers.

(2) In case the boundary conditions of the interior problem is expanded into Fourier series, the number of terms in the infinite summation to be truncated can be determined a priori.

(3) Since the interior and exterior problems are coupled at the circle, the Hankel's function and its derivatives are computed only once at r = a, the radius of the artificial circle.

(4) Most of the computations do not involve the incident fields. Calculation for various incident waves add only little effort.

(5) The versatility is developed in the Finite Element Methods which can solve the irregular problems relatively easily. The method of "Inhomogeneous Element" enables us to compute various problems by a single program and to simplify the input control.

III. The Finite Element Methods

It is impossible, for most cases, to solve $\psi_n(r,\phi)$ analytically for differential equation eq. (6) or eq. (7) with boundary conditions eq. (8) or eq. (22). The Finite Element Methods for solving partial differential equations has been investigated by many civil engineers and some authors in Electrical Engineering such as Silvester and Wexler [7], [8]. It can be shown that the solution of eq. (6) subject to the Dirichlet boundary condition eq. (8) is equivalent to solving the function ψ_n which gives the stationary value of the variational formula I,

$$I = \iint_S (|\nabla\psi_n|^2 - k_o^2\varepsilon_r\psi_n^2)ds \ . \tag{26}$$

The integration region is the entire disc enclosed by the artificial circle ($r \leq a$).

With some manipulations, the variational formula for eq. (7) subject to the Dirichlet boundary condition eq. (8) is

$$I = \iint_S (\frac{1}{\varepsilon_r}|\nabla\psi_n|^2 - k_o^2\psi_n^2)ds \ . \tag{27}$$

The region S of the integration is the same as that of eq. (26).

Following the procedures suggested by Wexler [8], the variational formula for the Neumann boundary condition eq. (22) can be derived from eq. (26) and eq. (27). That is, the formula for eq. (6) subject to the boundary condition eq. (22) is

$$I = \iint_S (|\nabla\psi_n|^2 - k_o^2\varepsilon_r\psi_n^2)ds - 2\oint_C \psi_n b(\phi)d\ell \tag{28}$$

where

$$b(\phi) = \frac{\partial \psi_n}{\partial r}(r,\phi)\Big|_{r=a} . \tag{29}$$

The region of integration S is the entire disc enclosed by the artificial circle ($r \leq a$) and C is the contour of the circle. The direction of the contour integral is counter-clockwise.

Similarly, the variational formula for eq. (7) subject to the boundary condition eq. (22) is

$$I = \iint_S \left(\frac{1}{\varepsilon_r} |\nabla \psi_n|^2 - k_o^2 \psi_n^2 \right) ds - 2 \oint_C \psi_n b(\phi) d\ell \tag{30}$$

where $b(\phi)$ is defined in eq. (29). The region and contour of integration are the same as that of eq. (28). The integrand of the contour integral in eq. (30) should be divided by ε_r. But since the artificial circle is larger than the scatterer, ε_r is unity at the contour.

The region S is then divided into many small triangular elements. The way to construct the triangles is very flexible. The only restrictions are convergence and programmability. It is not necessary to consider the inhomogeneity of the material in constructing the elements. The method of "Inhomogeneous Element" will handle the inhomogeneity or irregular boundary of the scatterer. Fig. 2. is an example.

(A) Dirichlet problems:

Assign a number to each node of the triangles in the circle. Let ψ_i be the value of the function ψ at the i-th node. Let i = K+1, K+2, ..., K+K' be the boundary nodes on the artificial circle, and i = 1, 2, 3, ... K be the nodes in the interior of the circle. Approximate the function in each triangular element by a linear function which passes

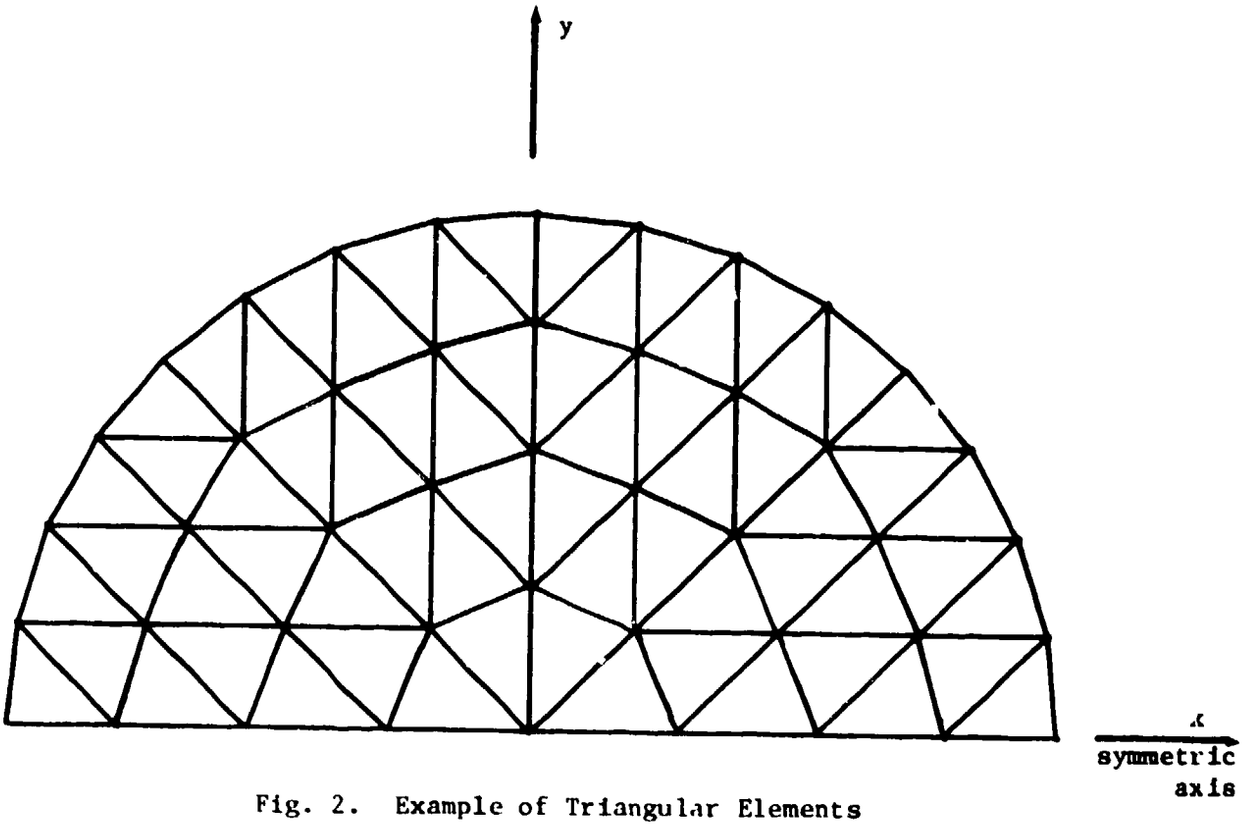

Fig. 2. Example of Triangular Elements

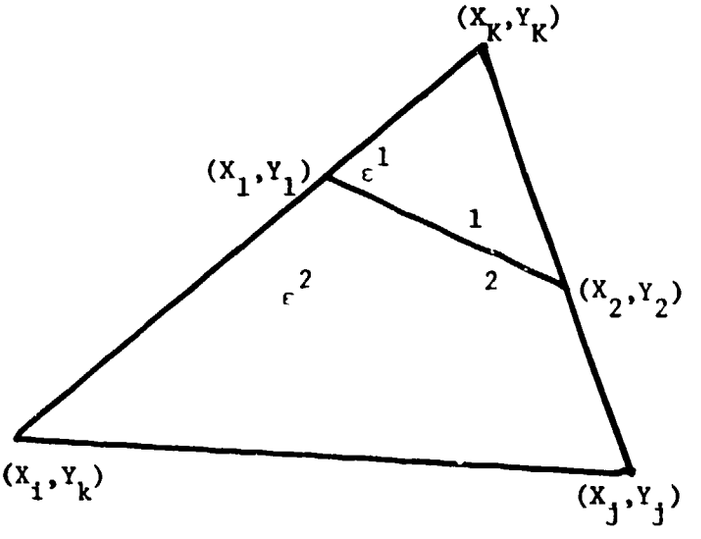

Fig. 3. Inhomogeneous Element

through the functional values at three nodes. Then integrate eq. (26) or eq. (27) through that element. Add the contributions of all elements together to get the global integration of I, which is a quadratic function of ψ_i, i = 1, 2, ... K, K+1, K+2, ..., K+K'. To make the functional I stationary, take derivative of I with respect to ψ_i and let it be zero, i.e., $\frac{\partial I}{\partial \psi_i} = 0$, i = 1, 2, ..., K. Since I is quadratic function of ψ_i's, the above equations become a system of linear equations, which can be written in the matrix form:

$$S \begin{bmatrix} \psi_1 \\ \psi_2 \\ \vdots \\ \psi_K \end{bmatrix} = B \begin{bmatrix} \psi_{K+1} \\ \vdots \\ \psi_{K+K'} \end{bmatrix} . \qquad (31)$$

The matrices S and B are obtained from the integration of all elements. The vector $[\psi_1, \psi_2, \ldots\ldots\ldots, \psi_K]^T$ is to be solved. The vector $[\psi_{K+1}, \psi_{K+2}, \ldots\ldots, \psi_{K+K'}]^T$ is an array of the boundary values which are known. The unknown vector can be solved by Gaussian elimination of eq. (31), or the block by block method, or a sparse matrix algorithm. Once ψ_i, i = 1, 2, 3, ..., K are known, the normal derivative $\frac{\partial \psi}{\partial r}\Big|_{r=a}$, which is required by section II, is readily calculated.

The rest of the problem is to construct the matrix S and B. This requires the integration in every element. If the material is uniform in an element, the formula of the element has been derived by Silvester (7). We shall discuss the case when the dielectric constant in the element is a continuously varying function, and the case when the element contains

two different materials. This technique is called the "Inhomogeneous Element" method.

(1) The triangle contains two materials:

For this case, we approximate the dielectric boundary in the element by a straight line as in Fig. 3. This approximation is valid whenever the scatterer surface is quite smooth or the element is quite small.

(i) E-wave:

Since E_z and its derivatives are continuous across a dielectric boundary, a linear function is used as a trial function.

$$\psi = ax + by + c \quad , \tag{32}$$

$$\therefore \begin{bmatrix} \psi_i \\ \psi_j \\ \psi_k \end{bmatrix} = \begin{bmatrix} x_i & y_i & 1 \\ x_j & y_j & 1 \\ x_k & y_k & 1 \end{bmatrix} \begin{bmatrix} a \\ b \\ c \end{bmatrix} \quad . \tag{33}$$

Let

$$\underset{\sim}{\psi} = \begin{bmatrix} \psi_i \\ \psi_j \\ \psi_k \end{bmatrix} \quad , \tag{34}$$

$$N = \begin{bmatrix} x_i & y_i & 1 \\ x_j & y_j & 1 \\ x_k & y_k & 1 \end{bmatrix} \quad , \tag{35}$$

$$\underset{\sim}{a} = \begin{bmatrix} a \\ b \\ c \end{bmatrix} \quad . \tag{36}$$

Then eq. (33) becomes

$$\underset{\sim}{\psi} = N \underset{\sim}{a} \quad . \tag{37}$$

So,

$$\underset{\sim}{a} = N^{-1} \underset{\sim}{\psi} \quad . \tag{38}$$

From eq. (26),

$$I_{\Delta_{ijk}} = \iint_{\Delta_{ijk}} |\nabla\psi|^2 dxdy - k_o^2 \iint_{\Delta_{ijk}} \varepsilon_{2r}\psi^2 dxdy + k_o^2 \iint_{\Delta_{12k}} (\varepsilon_{2r}-\varepsilon_{1r})\psi^2 dxdy. \tag{39}$$

Plugg ψ in eq. (32) into eq. (39) and integrate to obtain $I_{\Delta_{ijk}}$ as a polynomial of a, b, c. Then replace a, b, c, by $\underset{\sim}{\psi}$ from eq. (38). The integration may be achieved by many ways [9].

(ii) H-wave:

This case is more complicated than E-wave because the normal derivative of H_z is discontinuous accross the dielectric boundary. A linear function can not closely approximate the function ψ. It is convenient to assume two trial functions in the element. That is, let

$$\psi^1 = a_1 x + b_1 y + c_1 \qquad \text{in } \Delta_{12k} \text{ (Fig. 3.)} \tag{40}$$

and

$$\psi^2 = a_2 x + b_2 y + c_2 \qquad \text{in } \Delta_{ijk} - \Delta_{12k} \quad . \tag{41}$$

We enforce the trial functions to satisfy the following conditions:

(a) Pass through the nodal values, i.e.,

$$\left.\begin{aligned} \psi_i &= a_2 x_i + b_2 y_i + c_2 \\ \psi_j &= a_2 x_j + b_2 y_j + c_2 \\ \psi_k &= a_1 x_k + b_1 y_k + c_1 \end{aligned}\right\} . \tag{42}$$

(b) Continuous at both sides of the line segment between point 1 and point 2, i.e.,

$$\left.\begin{aligned} (a_1 x_1 + b_1 y_1 + c_1) - (a_2 x_1 + b_2 y_1 + c_2) &= 0 \\ (a_1 x_2 + b_1 y_2 + c_1) - (a_2 x_2 + b_2 y_2 + c_2) &= 0 \end{aligned}\right\} . \tag{43}$$

(c) The normal derivatives at the line segment between point 1 and point 2 are related by the following equation:

$$\frac{1}{\epsilon_1} \nabla \psi^1 \cdot \hat{n} = \frac{1}{\epsilon_2} \nabla \psi^2 \cdot \hat{n} .$$

[This equation is derived from the continuity of the tangential components of the electric field.] So,

$$\frac{1}{\epsilon_1} [b_1(x_1-x_2) - a_1(y_1-y_2)] = \frac{1}{\epsilon_2} [b_2(x_1-x_2) - a_2(y_1-y_2)] . \tag{45}$$

Combine eqs. (42), (43), and (45) into a matrix form:

$$N \underset{\sim}{a} = M \underset{\sim}{\psi} \tag{46}$$

where

$$N = \begin{bmatrix} x_i & y_i & 1 & 0 & 0 & 0 \\ x_j & y_j & 1 & 0 & 0 & 0 \\ 0 & 0 & 0 & x_k & y_k & 1 \\ x_1 & y_1 & 1 & -x_1 & -y_1 & -1 \\ x_2 & y_2 & 1 & -x_2 & -y_2 & -1 \\ \frac{1}{\varepsilon_2}(y_2-y_1) & -\frac{1}{\varepsilon_2}(x_2-x_1) & 0 & -\frac{1}{\varepsilon_1}(y_2-y_1) & \frac{1}{\varepsilon_1}(x_2-x_1) & 0 \end{bmatrix}, \quad (47)$$

$$M = \begin{bmatrix} I_3 \\ \hline O_3 \end{bmatrix} \quad ; \quad \text{where } I_3 \text{ is a } 3\times3 \text{ identity matrix,} \quad (48)$$

O_3 is a 3×3 null matrix,

$$\underline{a} = \begin{bmatrix} a_2 \\ b_2 \\ c_2 \\ a_1 \\ b_1 \\ c_1 \end{bmatrix}, \quad (49) \qquad \underline{\psi} = \begin{bmatrix} \psi_i \\ \psi_j \\ \psi_k \end{bmatrix}. \quad (50)$$

$$\therefore \underline{a} = N^{-1}M\,\underline{\psi} \quad (51)$$

Let

$$N^{-1}M = \begin{bmatrix} H_1 \\ \hline H_2 \end{bmatrix}. \quad (52)$$

Then

$$\begin{bmatrix} a_2 \\ b_2 \\ c_2 \end{bmatrix} = H_1\,\underline{\psi}, \quad (53)$$

and

$$\begin{bmatrix} a_1 \\ b_1 \\ c_1 \end{bmatrix} = H_2 \, \underset{\sim}{\psi} \, . \tag{54}$$

From eq. (27),

$$\begin{aligned} I_{\Delta_{ijk}} &= \iint_{\Delta_{ijk}} \left[\frac{1}{\varepsilon_r} |\nabla\psi|^2 - k_o^2 \psi^2 \right] dxdy \\ &= \iint_{\Delta_{ijk}} \left[\frac{1}{\varepsilon_2} |\nabla\psi^2|^2 - k_o^2 \psi^{2^2} \right] dxdy \\ &\quad - \iint_{\Delta_{12k}} \left[\frac{1}{\varepsilon_2} |\nabla\psi^2|^2 - k_c^2 \psi^{2^2} \right] dxdy + \iint_{\Delta_{12k}} \left[\frac{1}{\varepsilon_1} |\nabla\psi^1|^2 - k_o^2 \psi^{1^2} \right] dxdy . \end{aligned} \tag{55}$$

From eq. (40) and eq. (53),

$$\frac{1}{\varepsilon_2} |\nabla\psi^2|^2 - k_o^2 \psi^{2^2} = [a,b,c] \begin{bmatrix} \frac{1}{\varepsilon_2} - k_o^2 x^2 & - k_o^2 xy & - k_o^2 x \\ - k_o^2 xy & \frac{1}{\varepsilon_2} - k_o^2 y^2 & - k_o^2 y \\ - k_o^2 x & - k_o^2 y & - k_o^2 \end{bmatrix} \begin{bmatrix} a \\ b \\ c \end{bmatrix}$$

$$= \underset{\sim}{\psi}^T H_1^T \begin{bmatrix} \frac{1}{\varepsilon_2} - k_o^2 x^2 & - k_o^2 xy & - k_o^2 x \\ - k_o^2 xy & \frac{1}{\varepsilon_2} - k_o^2 y^2 & - k_o^2 y \\ - k_o^2 x & - k_o^2 y & - k_o^2 \end{bmatrix} H_1 \, \underset{\sim}{\psi} \, .$$

Similar result can be obtained for $\frac{1}{\varepsilon_1} |\nabla\psi^1|^2 - k_o^2 \psi^{1^2}$,

$$\therefore \quad I_{\Delta_{ijk}} = \underset{\sim}{\psi}^T [H_1^T T_1 H_1 + H_2^T T_2 H_2] \underset{\sim}{\psi} \tag{56}$$

where

$$T_1 = \begin{bmatrix} \frac{1}{\epsilon_2}(p_{oo}-\bar{p}_{oo}) - k_o^2(p_{20}-\bar{p}_{20}) & -k_o^2(p_{11}-\bar{p}_{11}) & -k_o^2(p_{10}-\bar{p}_{10}) \\ -k_o^2(p_{11}-\bar{p}_{11}) & \frac{1}{\epsilon_2}(p_{oo}-\bar{p}_{oo}) - k_o^2(p_{o2}-\bar{p}_{o2}) & -k_o^2(p_{o1}-\bar{p}_{o1}) \\ -k_o^2(p_{10}-\bar{p}_{10}) & -k_o^2(p_{o1}-\bar{p}_{o1}) & -k_o^2(p_{oo}-\bar{p}_{oo}) \end{bmatrix} \tag{57}$$

and

$$T_2 = \begin{bmatrix} \frac{1}{\epsilon_1}\bar{p}_{oo} - k_o^2\bar{p}_{20} & -k_o^2\bar{p}_{11} & -k_o^2\bar{p}_{10} \\ -k_o^2\bar{p}_{11} & \frac{1}{\epsilon_1}\bar{p}_{oo} - k_o^2\bar{p}_{o2} & -k_o^2\bar{p}_{o1} \\ -k_o^2\bar{p}_{10} & -k_o^2\bar{p}_{o1} & -k_o^2\bar{p}_{oo} \end{bmatrix} . \tag{58}$$

The definitions of $p_{\nu\zeta}$ and $\bar{p}_{\nu\zeta}$ in eqs. (57) and (58) are

$$p_{\nu\zeta} = \iint_{\Delta_{ijk}} x^\nu y^\zeta dxdy; \quad \nu = 0, 1, 2, \ldots, \zeta = 0, 1, 2, \ldots. \tag{59}$$

$$\bar{p}_{\nu\zeta} = \iint_{\Delta_{12k}} x^\nu y^\zeta dxdy; \quad \nu = 0, 1, 2, \ldots, \zeta = 0, 1, 2, \ldots. \tag{60}$$

The integration of eq. (59) and eq. (60) can be performed in several ways [9].

(2) The dielectric constant is a continuously varying function:

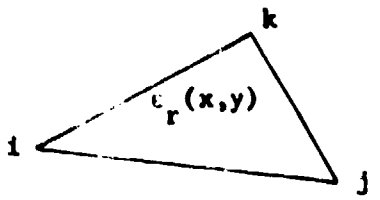

Fig. 4.

Let eqs. (32) through (38) all hold and the same notations are used.

(i) E-wave:

Approximate $\varepsilon_r(x,y)$ in Δ_{ijk} with

$$\varepsilon_r(x,y) = \xi x + \eta y + \zeta \ . \tag{61}$$

Let $\varepsilon_\nu = \varepsilon_r(x_\nu, y_\nu)$ where $\nu = i, j, k$. (62)

Since ε_r is a known function, ξ, η, ζ are solved by eq. (63).

$$\begin{bmatrix} \xi \\ \eta \\ \zeta \end{bmatrix} = N^{-1} \begin{bmatrix} \varepsilon_i \\ \varepsilon_j \\ \varepsilon_k \end{bmatrix} . \tag{63}$$

From eq. (26)

$$I_{\Delta_{ijk}} = \iint_{\Delta_{ijk}} (|\nabla\psi^2| - k_o^2 \varepsilon_r \psi^2) dxdy = \underset{\sim}{\psi}^T (N^{-1})^T \, T_3 \, (N^{-1}) \underset{\sim}{\psi} \tag{64}$$

where

$$T_3 = \begin{bmatrix} p_{oo}-k_o^2(\xi p_{30}+\eta p_{21}+\zeta p_{20}) & -k_o^2(\xi p_{21}+\eta p_{12}+\zeta p_{11}) & -k_o^2(\xi p_{20}+\eta p_{11}+\zeta p_{10}) \\ -k_o^2(\xi p_{21}+\eta p_{12}+\zeta p_{11}) & p_{oo}-k_o^2(\xi p_{12}+\eta p_{o3}+\zeta p_{o2}) & -k_o^2(\xi p_{11}+\eta p_{o2}+\zeta p_{o1}) \\ -k_o^2(\xi p_{20}+\eta p_{11}+\zeta p_{10}) & -k_o^2(\xi p_{11}+\eta p_{o2}+\zeta p_{o1}) & -k_o^2(\xi p_{10}+\eta p_{o1}+\zeta p_{oo}) \end{bmatrix} \tag{65}$$

$p_{\nu\zeta}$, $\nu = 0, 1, 2, 3, \ldots,$ $\zeta = 0, 1, 2, 3,$ are defined in eq. (59).

(ii) H-wave:

Approximate $\frac{1}{\epsilon_r(x,y)}$ in Δ_{ijk} with

$$\frac{1}{\epsilon_r(x,y)} = \xi x + \eta y + \zeta \tag{66}$$

Let the assumption of eq. (62) hold,

$$\begin{bmatrix} \xi \\ \eta \\ \zeta \end{bmatrix} = N^{-1} \begin{bmatrix} 1/\epsilon_i \\ 1/\epsilon_j \\ 1/\epsilon_k \end{bmatrix} \tag{67}$$

Then from eq. (27)

$$I_{\Delta_{ijk}} = \iint_{\Delta_{ijk}} \left(\frac{1}{\epsilon_r} |\nabla\psi|^2 - k_o^2\psi^2 \right) dxdy = \underset{\sim}{\psi}^T (N^{-1})^T \, T_4 (N^{-1}) \underset{\sim}{\psi} \tag{68}$$

where

$$T_4 = \begin{bmatrix} \xi p_{10}+\eta p_{01} + \zeta - k_o^2 p_{20} & - k_o^2 p_{11} & - k_o^2 p_{10} \\ - k_o^2 p_{11} & \xi p_{10}+\eta p_{01}+\zeta - k_o^2 p_{02} & - k_o^2 p_{01} \\ - k_o^2 p_{10} & - k_o^2 p_{01} & - k_o^2 p_{00} \end{bmatrix} \tag{69}$$

$p_{\nu\zeta}$, $\nu = 0, 1, 2, \ldots,$ $\zeta = 0, 1, 3 \ldots$ are defined in eq. (59).

(B) Neumann Problems:

If we assume the boundary condition to be

$$\left.\frac{\partial \psi(r,\phi)}{\partial r}\right|_{r=a} = b(\phi) \quad , \tag{70}$$

the variational formulae eq. (28) or eq. (30) should be used. The first part in either formulae, i.e., the surface integral, is exactly the same as that in eq. (26) or eq. (27). The only two differences are:

(a) At the boundary points $i = K + 1, \ldots\ldots, K + K'$, the function ψ is unknown, but we restrict ψ to have the following property.

$$\frac{\partial I}{\partial \psi_i} = 0 \quad \text{for } i = 1, 2, \ldots., K, K + 1, \ldots., K + K' . \tag{71}$$

In matrix form, eq. (71) can be written by

$$S \begin{bmatrix} \psi_1 \\ \psi_2 \\ \vdots \\ \psi_{K+K'} \end{bmatrix} = \begin{bmatrix} 0 \\ \vdots \\ 0 \\ B \end{bmatrix} \begin{matrix} \\ \\ K \text{ elements} \\ \\ K' \text{ elements} \end{matrix} \tag{72}$$

(b) The vector B in eq. (72) is derived from the line integral of the variational formula. We shall discuss the line integral in detail because it requires some techniques in spline analysis. It is essential to evaluate the line integral

$$I' = \int_0^{2\pi} \psi(a,\phi) b(\phi) d\phi \ . \tag{73}$$

The result of eq. (73) is in terms of a linear function of ψ_i, $i = K+1, \ldots\ldots, K+K'$. Then

$$2 \frac{\partial I'}{\partial \psi_{i+K}} = B_i$$

where B_i is the i-th element of B in eq. (72).

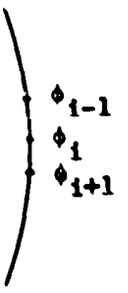

Fig. 5.

Let $$\phi_{i+1} - \phi_i = \phi_i - \phi_{i-1} = \delta \tag{74}$$

Let $$\theta = \phi - \phi_i \tag{75}$$

The idea is to approximate $\psi(a,\phi)$ by a quadratic polynomial of θ for the interval $[-\frac{\delta}{2}, \frac{\delta}{2}]$

$$\psi(a,\phi) = \psi(a,\theta) = a\theta^2 + b\theta + c; \ -\frac{\delta}{2} \leq \theta \leq \frac{\delta}{2} \tag{76}$$

And the polynomial satisfies

$$\left.\begin{aligned} \psi(a,-\delta) &= \psi_{i-1+K} = a\delta^2 - b\delta + c \\ \psi(a,0) &= \psi_{i+K} = a\cdot 0 + b\cdot 0 + c = c \\ \psi(a,\delta) &= \psi_{i+1+K} = a\delta^2 + b\delta + c \end{aligned}\right\} \quad (77)$$

Solve eq. (77), we have

$$\left.\begin{aligned} a &= \frac{\psi_{i-1+K} + \psi_{i+1+K} - 2\psi_{i+K}}{2\delta^2} \\ b &= \frac{\psi_{i+1+K} - \psi_{i-1+K}}{2\delta} \\ c &= \psi_{i+K} \end{aligned}\right\} \quad (78)$$

From eq. (76) and eq. (78), we have

$$\psi(a,\theta) = \psi_{i+K}\left(1 - \frac{\theta^2}{\delta^2}\right) + \psi_{i-1+K}\left(\frac{\theta^2}{2\delta^2} - \frac{\theta}{2\delta}\right) + \psi_{i+1+K}\left(\frac{\theta^2}{2\delta^2} + \frac{\theta}{2\delta}\right) . \quad (79)$$

Let's partition eq. (73) by letting

$$I_i = \int_{\phi_i - \frac{\delta}{2}}^{\phi_i + \frac{\delta}{2}} \psi(a,\phi) b(\phi) d\phi .$$

Changing of variable ϕ to θ, and use eq. (79),

$$I_i = \int_{-\frac{\delta}{2}}^{\frac{\delta}{2}} \left[\psi_{i+K}\left(1 - \frac{\theta^2}{\delta^2}\right) + \psi_{i-1+K}\left(\frac{\theta^2}{2\delta^2} - \frac{\theta}{2\delta}\right) + \psi_{i+1+K}\left(\frac{\theta^2}{2\delta^2} + \frac{\theta}{2\delta}\right)\right] b(\phi_i + \phi) d\phi$$

$$= R_i\psi_{i+K} + S_i\psi_{i-1+K} + T_i\psi_{i+1+K} \quad (80)$$

where

$$R_i = \int_{\frac{\delta}{2}}^{\frac{\delta}{2}} \left(1 - \frac{\theta^2}{\delta^2}\right) b(\phi_i+\theta)d\theta \tag{81}$$

$$S_i = \int_{\frac{\delta}{2}}^{\frac{\delta}{2}} \left(\frac{\theta^2}{2\delta^2} - \frac{\theta}{2\delta}\right) b(\phi_i+\theta)d\theta \tag{82}$$

$$T_i = \int_{\frac{\delta}{2}}^{\frac{\delta}{2}} \left(\frac{\theta^2}{2\delta^2} + \frac{\theta}{2\delta}\right) b(\phi_i+\theta)d\theta \tag{83}$$

The total integration I' becomes

$$I' = \sum_{i=1}^{K'} I_i = \sum_{i=1}^{K'} (R_i\psi_{i+K} + S_i\psi_{i-1+K} + T_i\psi_{i+1+K})$$

$$= \sum_{i=1}^{K'} (R_i + S_{i+1} + T_{i-1})\ \psi_{i+K} \quad . \tag{84}$$

From eq. (84) and eq. (73), we get

$$B_i = 2(R_i + S_{i+1} + T_{i-1}) \quad . \tag{85}$$

It is important to note that the numerical solutions of R_i, S_i, and T_i from eq. (81), eq. (82), and eq. (83) may be very inaccurate when δ is very small. This is due to the fact that the integration comes out with a very small value is divided by a small value. Round off error is very significant. One possible way to overcome this defect is to expand $b(\phi_i+\theta)$ in Taylor series expansion around ϕ_i before integration. That is

$$b(\phi_i+\delta) = b(\phi_i) + \frac{\partial b(\phi_i)}{\partial \phi}\,\delta + \frac{1}{2}\,\frac{\partial^2 b(\phi_i)}{\partial \phi^2}\,\delta^2 + \ldots. \qquad (86)$$

Truncate eq. (86) to finite terms (since δ is small) then insert eq. (86) into eq. (81), eq. (82), and eq. (83) respectively to obtain R_i, S_i, T_i as functions of δ. This will give us polynomials of δ which have no numerical instabilities.

IV. Numerical Results:

Based on the theories discussed in this report, a FORTRAN program has been written to compute the expansion coefficients and far fields of the scattered waves of dielectric cylinders with arbitrary shape or inhomogenuity incidented by a plane wave. A CDC 6400 computer has been used to run the program. The validity of the program is demonstrated by the automatic error checking for dielectric circular cylinders. For this case, the program prints out both the numerical and exact values of the Finite Element solutions and the resulting scattering fields. Also, the results for dielectric elliptical cylinder with ka = 1.2, kb = 1.0198, ϵ_r = 2.0, E-wave, matches perfectly with that given by Wilton & Mittra [4]. Besides, the dielectric ring problem is compared with Richmond's result. As is shown in fig. 6., the solution of the uni-moment method is closer to the true solution than that given by Richmond [3].

Two kinds of error may exist to affect the final result of the scattering fields: the truncation error of the infinite series in the Uni-moment methods, and the error due to the Finite Element Methods. There is not much thing that we can do for the first error since the terms to be truncated are determined a priori according to the size of the scatterer. The contribution of the second error is presented in tables 1 through 3 . It can be seen from these tables that when the normal derivative values at the circle are relatively small for some modes, the relative error of the finite element solution may be very large. But this affects the final result very little because of its small value. As the normal derivative values for some modes being large, the interior system reaches resonance condition. The error for this mode is so large as we could expect. Fortunately enough, the physical systems are mostly irregular,

for which the resonance conditions are usually very complicated. The convergence property of the method is shown in Fig. 7. It is easily seen that the numerical results converge to the true solution as long as the size of the elements becoming smaller and smaller. The computation time as a function of the number of unknowns is plotted in Fig. 8. The number of unknown is inversely proportional to the square of the element size. Some other results are also shown in Fig. 9 through 13, in which several interesting geometries were investigated to show the capability of the method.

V. Conclusion

The analysis and results presented in this part are solid evidence that the "uni-moment method" is a valid, economical, numerical method to compute scattering problems involving inhomogeneous media. We are confident that it will be successfully applied to many interesting problems in field theories.

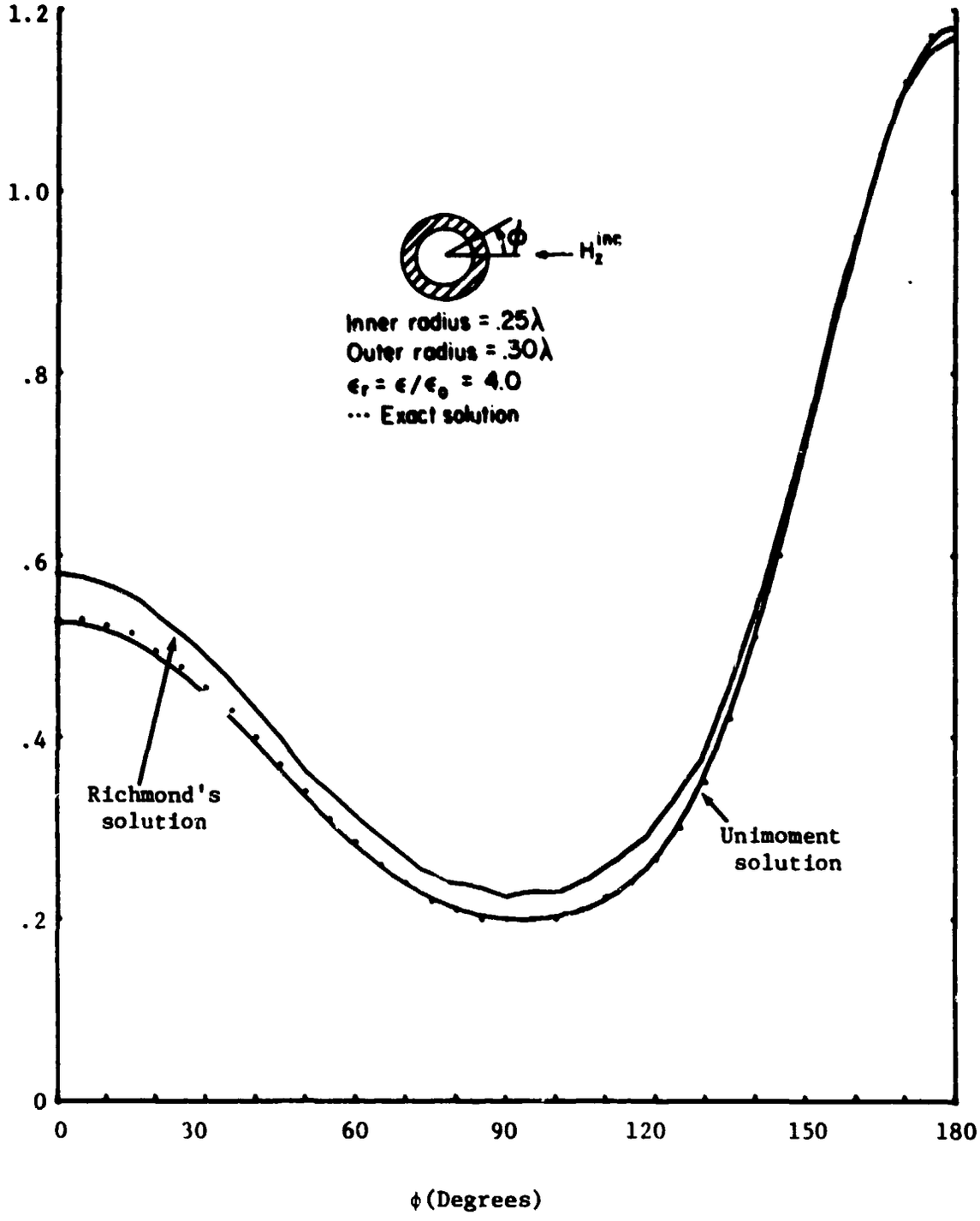

Fig. 6. Comparison with Richmond's Result.

Table 1.(*)

h = 1 unit, $\varepsilon_r = 2$, a = .1λ, A = .1125λ ka = .89 E-wave

a. Error of FEM Solution

e_n	error	$\max[\frac{\partial\psi}{\partial n}]$
Const.	2.8×10^{-3}	2.9×10^{-2}
cos φ	1.3×10^{-3}	4.4×10^{-2}
sin φ	1.9×10^{-3}	4.4×10^{-2}
cos 2φ	2.4×10^{-3}	1.0×10^{-1}
sin 2φ	2.2×10^{-3}	1.0×10^{-1}

b. Expansion coefficient

	Computed	Exact
A_0	$-9.61\times10^{-2}-j.295$	$-9.65\times10^{-2}-j.295$
A_1	$3.09\times10^{-2}-j4.8\times10^{-4}$	$3.10\times10^{-2}-j4.8\times10^{-4}$
A_2	too small	

c. Far Field Pattern

φ		0°	45°	90°	135°	180°
$\lvert E_z \rvert$	Computed	.281	.289	.310	.331	.340
	Exact	.282	.290	.310	.332	.341
$\angle E_z$	Computed	-110°	-109°	-108°	-107°	-107°
	Exact	-110°	-109°	-108°	-107°	-107°

(*) In tables 1 through 3, the notations are defined as the following:

h = relative element size. 1 unit = $\frac{1}{80}\lambda$

a = radius of the dielectric circular cylinder.

A = radius of the artificial circle.

$$\max\left[\frac{\partial\psi}{\partial n}\right] = \max_{0^\circ \le \phi \le 360^\circ}\left[\frac{\partial\psi}{\partial r}(r,\phi)\right]_{r=A}$$

$$\text{error} = \left[\sum_{i=1}^{K'}\left|\frac{\partial\psi'}{\partial r}(A,\phi_i) - \frac{\partial\psi}{\partial r}(A,\phi_i)\right|\right]\Big/\left[\sum_{i=1}^{K'}\left|\frac{\partial\psi}{\partial r}(A,\phi_i)\right|\right]$$

where prime means computed value.

Table 2.

h = 2 units, $\varepsilon_r = 2$, a = .2λ, A = .2250λ, ka = 1.78, E-wave

a. Error of FEM Solution

e_n	error	$\max[\frac{\partial\psi}{\partial n}]$
const.	7.4×10^{-3}	2.7×10^{-1}
cos ϕ	4.7×10^{-1}	6.5×10^{-4}
sin ϕ	5.7×10^{-1}	6.5×10^{-4}
cos 2ϕ	7.3×10^{-3}	8.1×10^{-2}
sin 2ϕ	5.2×10^{-3}	8.1×10^{-2}
cos 3ϕ		
sin 3ϕ		

b. Expansion coefficient

	Computed	Exact
A_0	-.403-j.491	-.406-j.491
A_1	.494-j.130	.496-j.132
A_2	$2.19\times10^{-4}+j2.89\times10^{-2}$	$4.58\times10^{-4}+j3.03\times10^{-2}$
A_3	too small	

c. Far Field Pattern

ϕ		0°	45°	90°	135°	180°
$\lvert E_z \rvert$	Computed	.274	.342	.613	.974	1.15
	Exact	.275	.342	.614	.978	1.15
$\angle E_z$	Computed	-174.71°	-155.5°	-131.11°	-120.55°	-117.76°
	Exact	-175.03°	-155.76°	-131.32°	-120.66°	-117.84°

Table 3.

$h = \frac{8}{3}$ units, $\epsilon_r = 2$, $a = .4\lambda$, $A = .433\lambda$ $ka = 3.55$, E-wave

a. Error of FEM Solution

e_n	error	$\max[\frac{\partial \psi}{\partial n}]$
const.	4.7×10^{-2}	1.8×10^{-2}
$\cos\phi$	3.39	9.72
$\sin\phi$	3.35	9.72
$\cos 2\phi$	2.2×10^{-2}	5.6×10^{-2}
$\sin 2\phi$	1.88×10^{-2}	5.6×10^{-2}
$\cos 3\phi$	1.7×10^{-2}	4.4×10^{-2}
$\sin 3\phi$	1.7×10^{-2}	4.4×10^{-2}

b. Expansion coefficient

	Computed	Exact
A_0	-.625-j.484	-.632-j.482
A_1	.836-j1.55	.828-j1.56
A_2	1.13+j.992	1.15+j.989
A_3	-.213+j.023	-.217+j.024

c. Far Field Pattern

ϕ		0°	45°	90°	135°	180°
$\lvert E_z \rvert$	Computed	.476	.453	.706	1.93	4.18
	Exact	.482	.457	.713	1.94	4.21
$\angle E_z$	Computed	-112°	-3.8°	44.4°	-152°	-143°
	Exact	-114°	-4.5°	43.5°	-152°	-143°

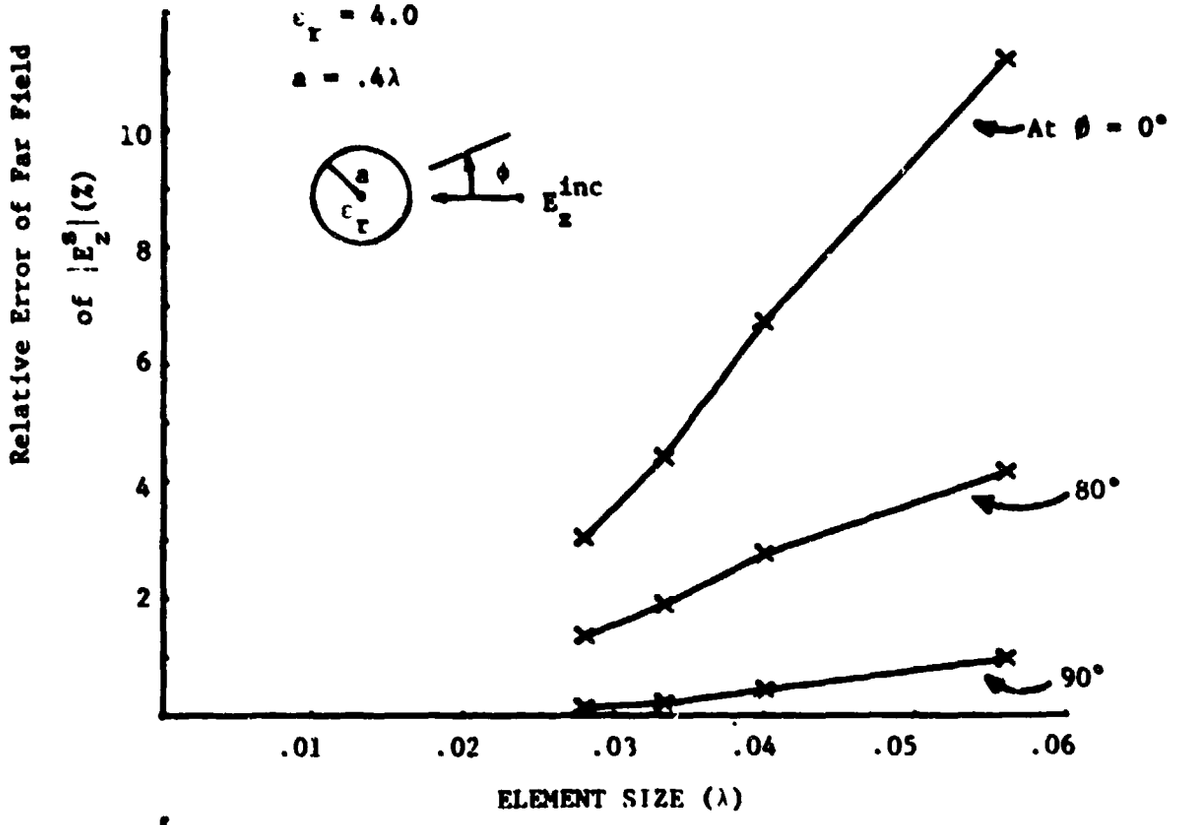

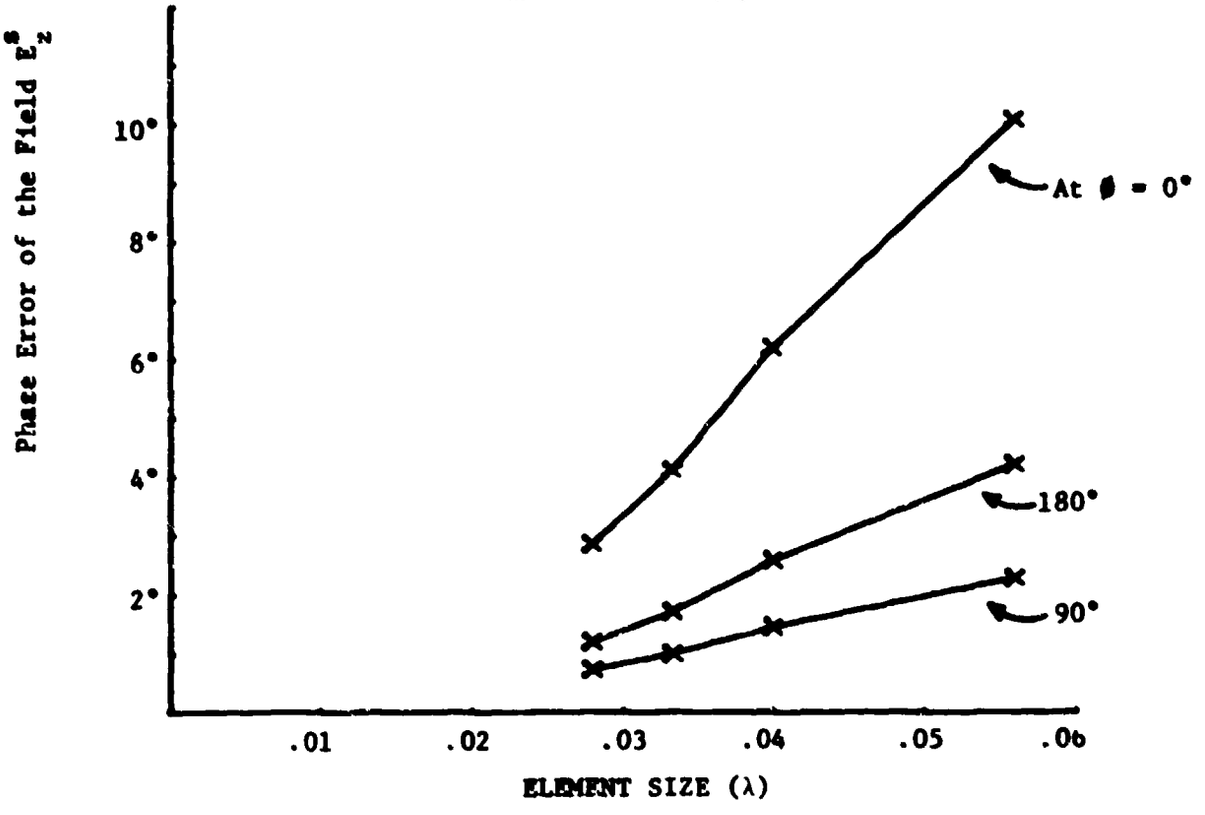

Fig. 7. Convergence Test

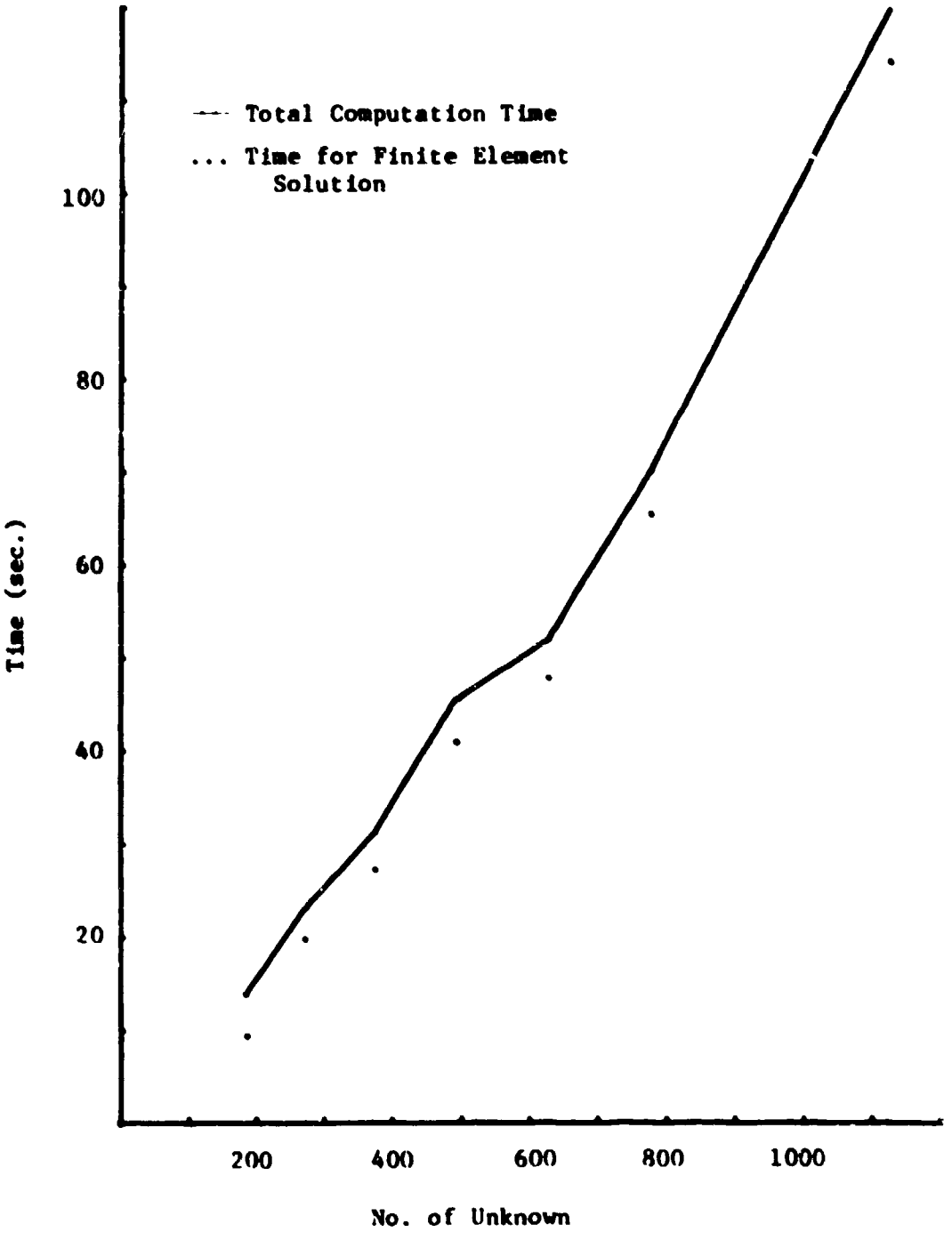

Fig. 8. Computation Time.

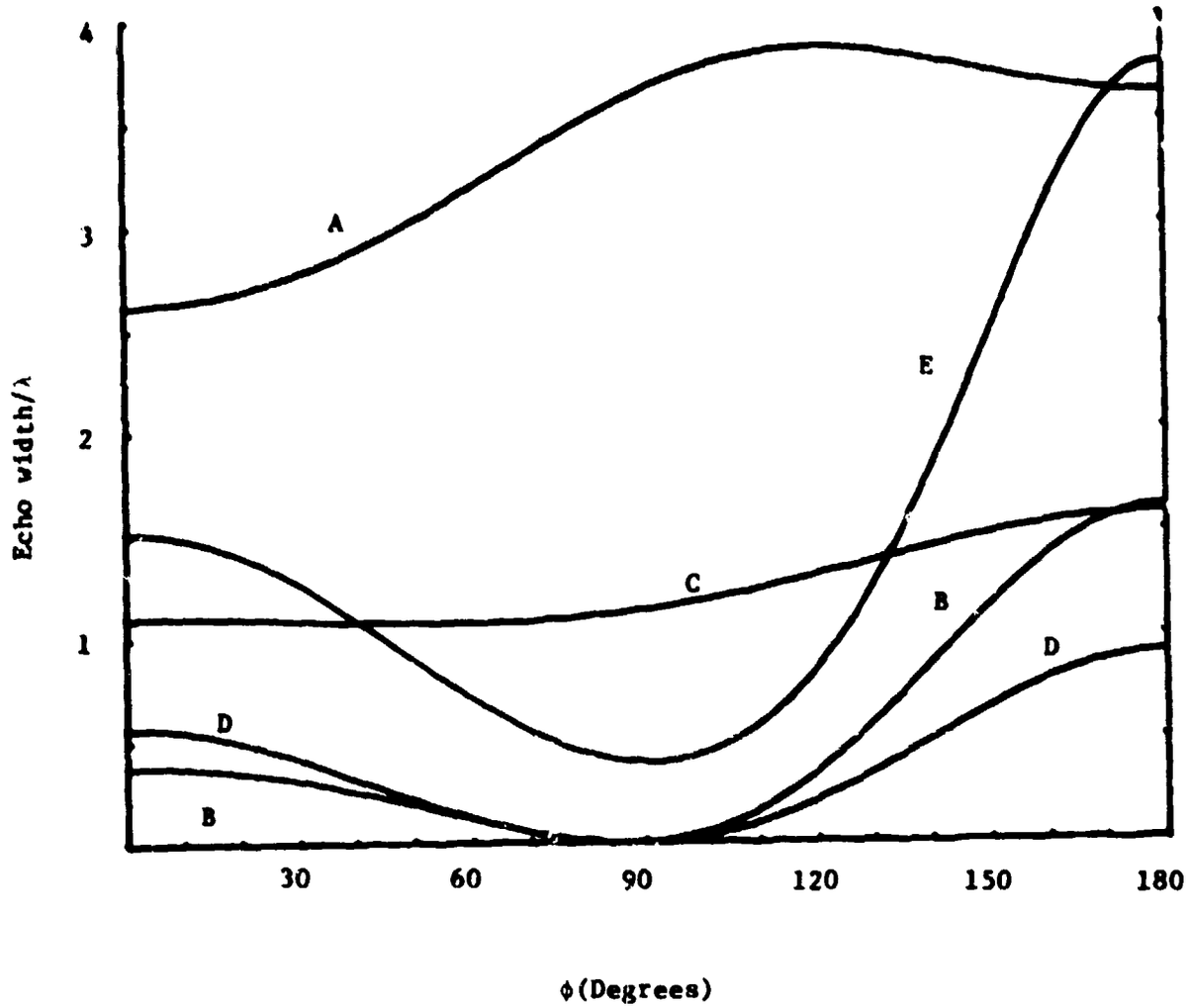

Fig. 9. Scattering by Various Scatterers.

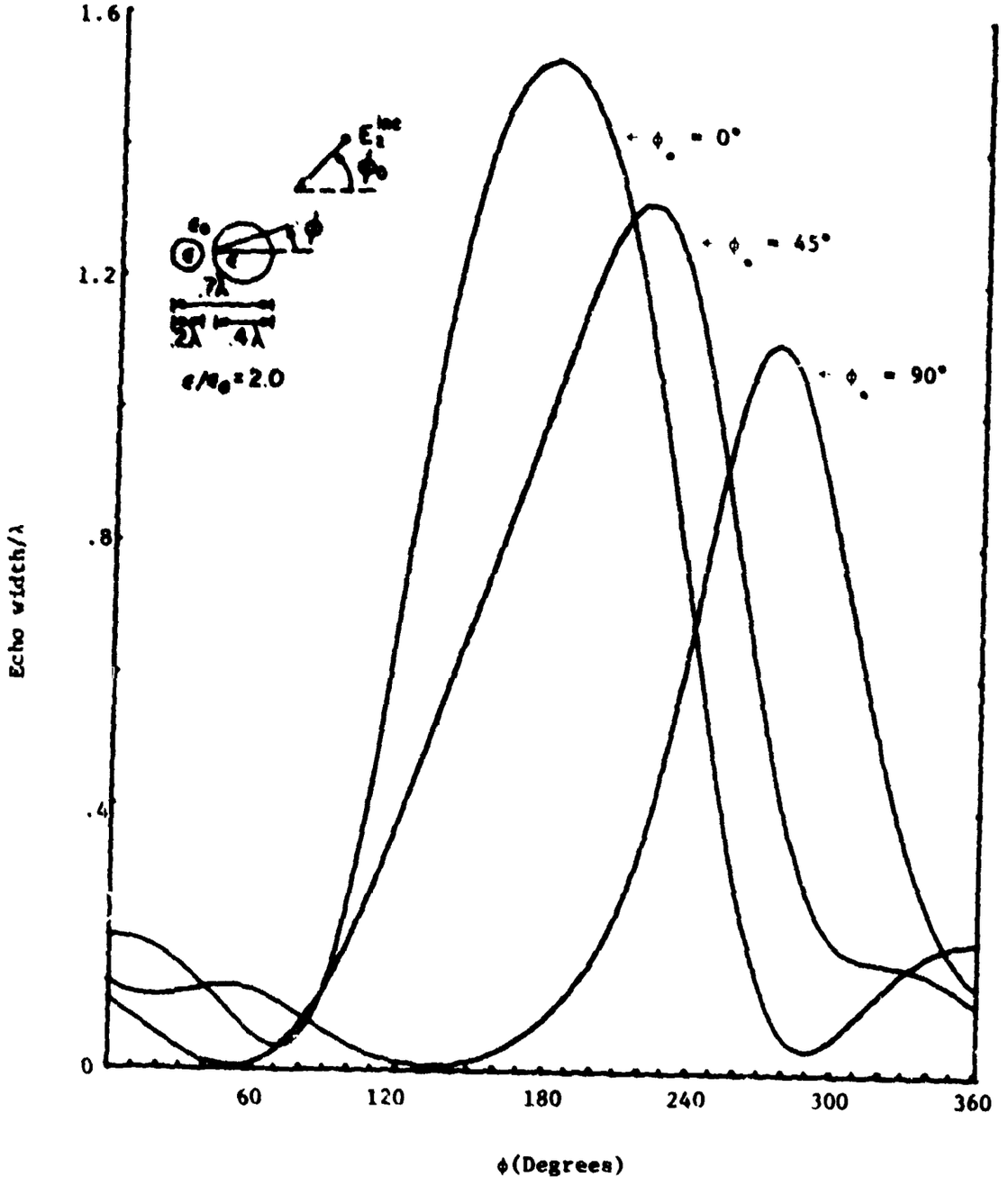

Fig. 10. Scattering by two Circular Cylinders.

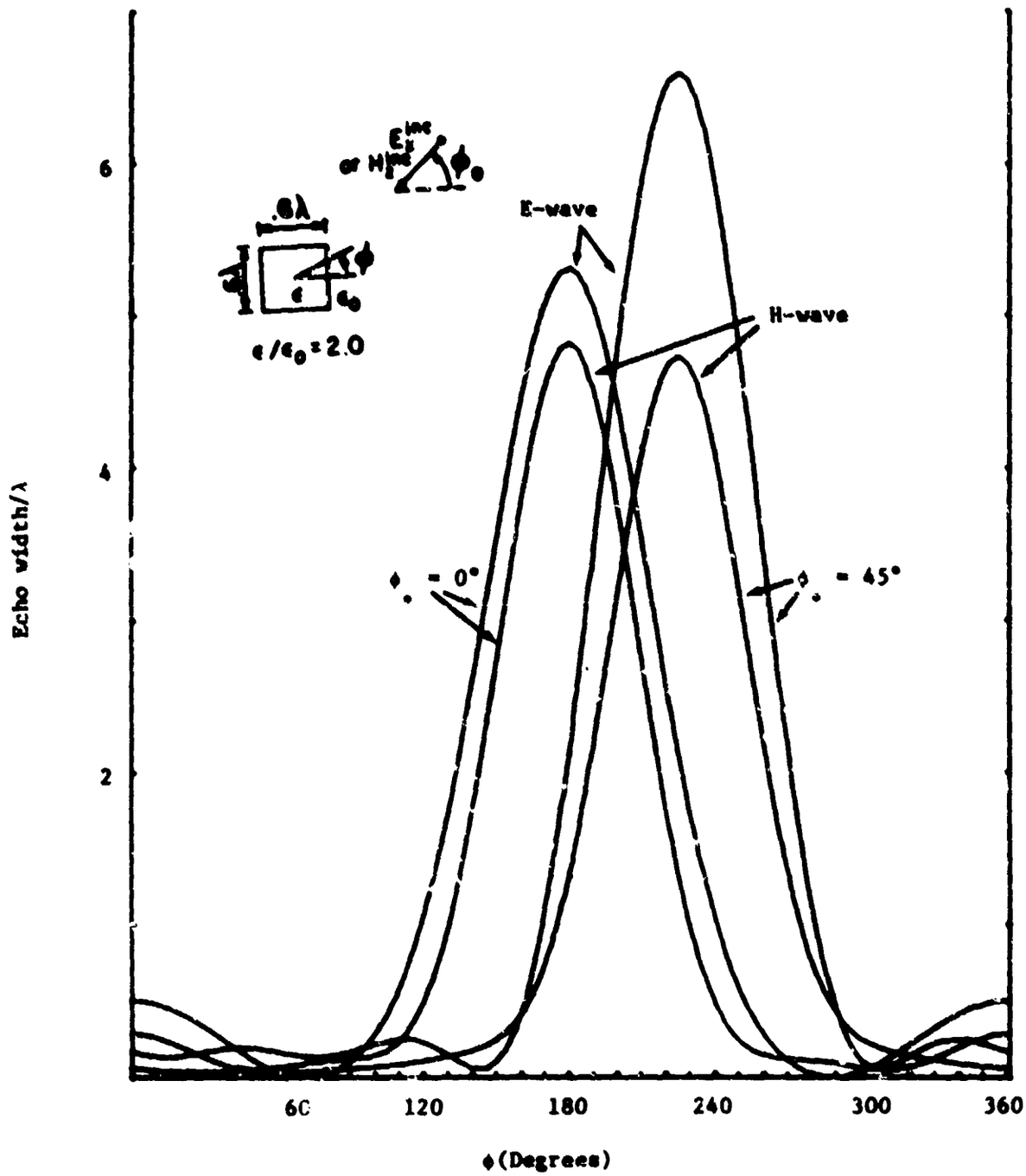

Fig. 11. Scattering by Square Cylinder.

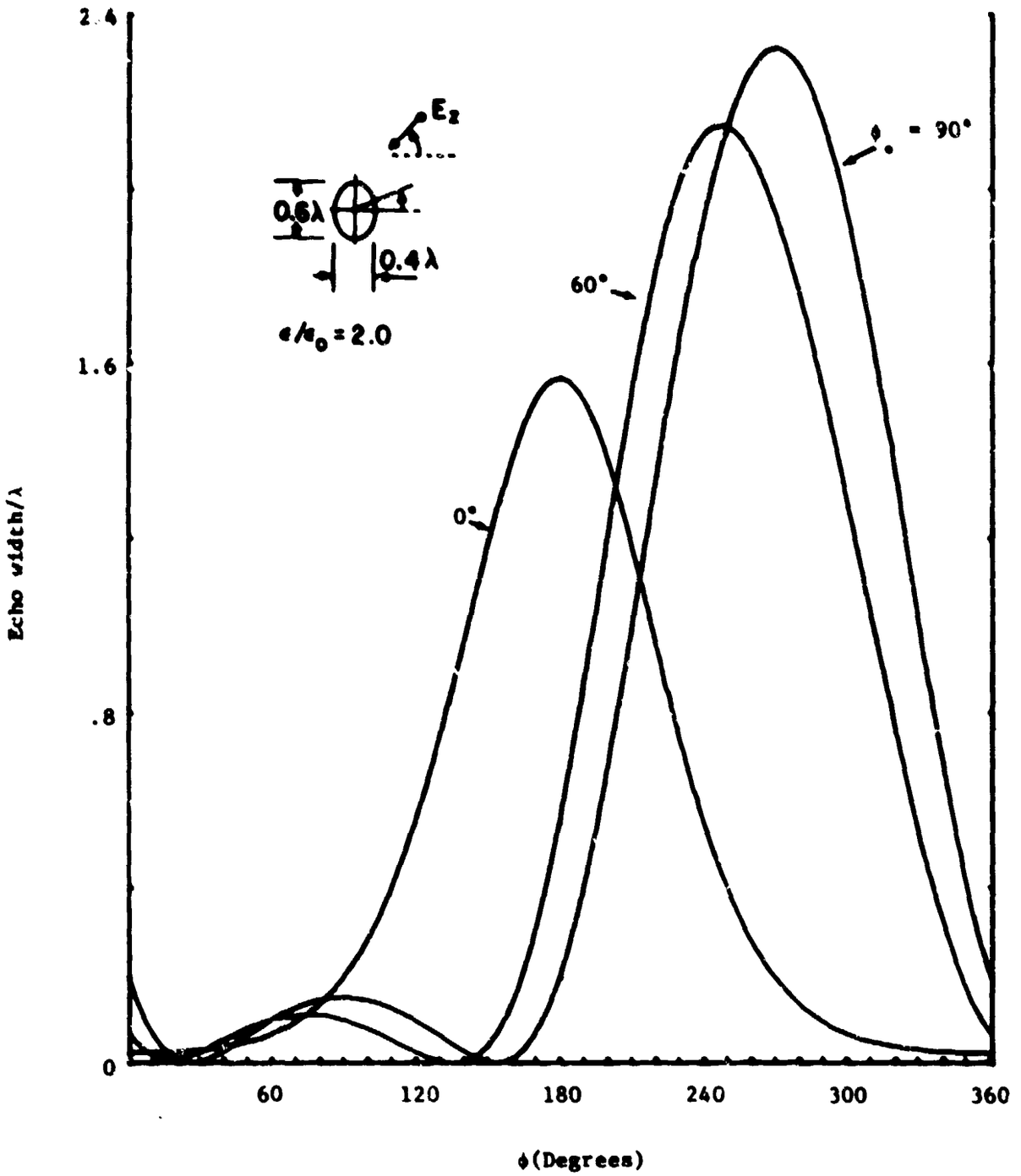

Fig. 12. Scattering by Elliptical Cylinder

References

[1] K. K. Mei, "Uni-moment Method of Solving Antenna and Scattering Problems," to be published.

[2] K. K. Mei and J. G. Van Bladel, "Scattering by Perfectly-Conducting Rectangular Cylinders," IEEE, AP-11, March 1963, p. 185.

[3] J. H. Richmond, "Scattering by a Dielectric Cylinder of Arbitrary Cross Section Shape," IEEE, AP-13, May 1965, p. 344 and AP-14, July 1966, p. 460.

[4] D. R. Wilton and R. Mittra, "A New Numerical Approach to the Calculation of Electromagnetic Scattering Properties of Two-Dimensional Bodies of Arbitrary Cross Section," IEEE, AP-20, May 1972, p. 310.

[5] N. Okamoto, "Matrix Formulation of Scattering by a Homogeneous Gyrotropic Cylinder," IEEE, September 1970, AP-18, p. 642.

[6] T. C. Tong, "Scattering by a Dielectric Rectangular Cylinder," 1973, G-AP International Symposium, p. 79.

[7] P. Silvester, "High-Order Polynomial Triangular Finite Elements For Potential Problems," Int. J. Eng. Sci., 1969, vol. 7. p. 849.

[8] A. Wexler, "Computation of Electromagnetic Fields," IEEE, MTT-17, August 1969, p. 416.

[9] Strang and Fix, "An Analysis of the Finite Element Methods," Prentice Hall, 1973.